Condenser Configuration and Performance Evaluation using Computational Fluid Dynamics

TR-109725

Final Report, April 1998

Prepared for
Electric Power Research Institute
3412 Hillview Avenue
Palo Alto, California 94304

TU Electric
Energy Plaza
1601 Bryan Street, 16th Floor
Dallas, Texas 75201-3411

EPRI Project Manager
J. L. Tsou

DISCLAIMER OF WARRANTIES AND LIMITATION OF LIABILITIES

ORGANIZATION(S) THAT PREPARED THIS REPORT

SEPRIL Services

Heat Exchanger Systems Inc.

Mott MacDonald

ORDERING INFORMATION

Requests for copies of this report should be directed to the EPRI Distribution Center, 207 Coggins Drive, P.O. Box 23205, Pleasant Hill, CA 94523, (510) 934-4212.

REPORT SUMMARY

Modern, three dimensional computational fluid dynamics (CFD) computer programs can model a condenser's thermal dynamics profile, including pressure, temperature, steam flow and concentration. This model can evaluate condenser tube bundle configuration and modifications for performance optimization.

Background

Condenser performance is vital to the performance and heat rate of a power plant. Many older condensers were designed using empirical correlation and resulted in poor steam distribution and excess pressure drop. TU Electric co-funded this project to study three of their condensers (Monticello Unit 1, Martin Lake Unit 2, and Stryker Creek Unit 2) using tailored collaboration.

Objectives

- To identify the main causes for condenser performance deviating from design performance
- To identify potential modifications that can enhance condenser performance

Approach

The project team first gathered the design and operating data for the three condensers. They then modeled the condenser using 3-D CFD code. Results of the computer simulation were used to investigate potential modifications. The modifications were then modeled to confirm the potential performance enhancements. The project team also conducted a cost-to-benefit analysis for the modification.

Results

Results of the computer simulation revealed areas of high pressure drop and non-condensable concentration. Since no retubing is planned for Monticello Unit 1 and Martin Lake Unit 2, no changes are recommended to the condenser configuration. Since retubing is planned for Stryker Creek Unit 2, the CFD model does show that an improvement would be gained by taking out all the baffling after the first support plate from the cooling water inlet end and sealing the hole at the top of the support plate. An improvement of up to about 1.5mbar (0.04 in Hg) was predicted by the model. The estimated cost to remove the baffling is $2,500 and the yearly payback is $228,000. The

model predicted that the addition of fairing to the condenser neck mounted feedwater heater did not improve performance.

EPRI Perspective

CFD is a useful tool for analyzing condenser configuration and performance. The results of CFD models visually reveal the potential trouble spots of high pressure drop and non-condensable concentration. Modifications can then be proposed to eliminate those trouble spots. In addition, the result of the modification can be confirmed using CFD. One draw back of the current CFD model is that the steam entering the condenser from turbine exhaust and the cooling water entering into the tubes are treated uniformly. In reality, considerable turbulence is experienced in those areas. If the condenser model can be coupled with the turbine exhaust model and the cooling water inlet model, the result will be more accurate.

TR-109725

Interest Categories

Fossil steam plant performance optimization
Fossil steam plant O&M cost reduction
Nuclear plant maintenance assistance
Nuclear plant support engineering

Keywords

Condensers
Performance
Heat rate
Computer simulation
Configurations

ACKNOWLEDGMENTS

This report was prepared by SEPRIL Services, Chicago, Illinois.

EPRI wishes to acknowledge the contributions of the authors: J. R. Marasigan of SEPRIL Services, Chicago, Illinois; C. D. Hardy of Heat Exchanger Systems Inc., Boston, Massachusetts; and N. Rhodes of Mott MacDonald, Croydon, United Kingdom.

CONTENTS

LIST OF FIGURES

LIST OF TABLES

1

INTRODUCTION

Scope

Since condenser performance is one of the key factors that directly affects the overall efficiency of a generating unit, optimum condenser performance is imperative. In addition to realizing a savings in fuel cost over the remaining life of a unit, improving the performance of an existing condenser would also result in better deaeration of the condensate, prolonging the life of downstream equipment. Condenser performance is the result of a complex interaction between a condensing two-phase flow and the entire condenser. Most of the condensers in operation in the United States have been designed over twenty years ago based on guidelines whose origins date back to the early 1930's. Improved analysis tools are now available that can be used to model an existing condenser and determine if the condenser configuration can be optimized to improve performance.

In 1933, the Heat Exchange Institute (HEI) was created in the United States to establish order in the condenser manufacturing market. Prior to 1933, each condenser manufacturer had developed their own heat transfer evaluation method, resulting in a wide range of heat transfer rates among the different manufacturers for similar condenser designs. After decades of extensive laboratory tests and correlation of the test results with actual field performance data, the HEI developed the Standards for Steam Surface Condensers (Standards). With the Standards, the HEI provided the condenser manufacturing industry with a consistent means to evaluate condenser thermal performance. In fact, condenser manufacturers in the United States still use these Standards as their guideline to design today's condensers and to estimate their thermal performance.

However, lost in the correlation between laboratory test results and field data are the dynamic effects of condenser geometry, e.g., flow obstructions such as a feedwater heater in the condenser neck, extraction piping, bracing, ... etc., on steam flow distribution. For instance, the Standards assume constant thermal conditions along the tube length and uniform steam distribution around the periphery of the tube bundle. Actually, the pressure drop associated with the condenser configuration results in varying exhaust steam pressures, temperatures, and flows at the tube bundle entrance along the tube length. Although the HEI treats this effect on an empirical basis, the

Standards do not specifically address this dynamic effect on condenser thermal performance.

Whereas the Standards have been the basis for design and performance evaluation for steam surface condensers in the United States, other analysis methods are available and in use in other parts of the world. In Europe, some condenser manufacturers have been using two-dimensional (2-D) computational fluid dynamics (CFD) since the early 1980's to design condensers and analyze their performance. CFD involves the modeling of the entire condenser, including the shell, tube bundle(s), condenser neck (including feedwater heaters if applicable), baffles, and air removal section, as thousands of discrete two or three-dimensional elements and then thermodynamically analyzing each element, taking into consideration the effect of adjacent elements. By using three-dimensional (3-D) CFD analysis on a condenser, the three-dimensional thermodynamic profile, including pressure, temperature and flow, of the condenser can be modeled. The model can then be evaluated to determine if the condenser configuration can be optimized to improve condenser performance.

This report covers the evaluation of three steam surface condensers using CFD. CFD provides an in-depth view of the dynamics inside the condenser, a subject matter not addressed in the HEI Standards. A 3-D CFD model of each condenser will be created and analyzed to determine if any improvements can be made to enhance its performance.

The three steam surface condensers that are modeled are from the following TU Electric generating stations:

- Monticello Unit 1
- Martin Lake Unit 2
- Stryker Creek Unit 2

Monticello is one of TU Electric's lignite-fueled generating stations. Unit 1 is a base-loaded unit, has a capacity of 565 MW, and went into commercial service in 1974. The condenser at Unit 1 is a non-divided, Foster Wheeler MCP type. Two low-pressure extraction feedwater heaters are mounted in the condenser exhaust necks. Table 1-1 lists additional condenser design data for Monticello Unit 1.

Martin Lake is another one of TU Electric's lignite-fueled generating stations. Unit 2 is also a base-loaded unit, has a capacity of 750 MW, and went into commercial service in 1978. The condenser at Unit 2 is a DeLaval, twin-shell, single-pass condenser. Like Monticello, two low-pressure extraction feedwater heaters are mounted in the condenser exhaust necks. Table 1-2 lists additional condenser design data for Martin Lake Unit 2.

Stryker Creek is one of TU Electric's natural gas-fueled generation stations. Unit 2 is a cycling unit, has a capacity of 520 MW, and went into commercial service in 1965. The condenser at Unit 2 is a Worthington, twin-shell, single-pass condenser. This condenser also includes two low-pressure extraction feedwater heaters mounted in the condenser exhaust necks. Table 1-3 lists additional condenser design data for Stryker Creek Unit 2.

Table 1-1
Monticello Unit 1 Condenser Design Data

Parameter	Value	
	SI	English
Type	Double-Flow, Twin-Shell	
Surface Area	19,509.6 m^2	210,000 ft^2
Number of Passes	1	
Tube Material	304 ASTM A-269 SS	
Tube Size	22.2 mm, 22 BWG	0.875 in, 22 BWG
Effective Tube Length	12.19 m	40 ft
Number of Tubes	22,916	
Heat Load	761.57 MW	2,600 E+06 Btu/h
Absolute Pressure	130.35 mbar	3.85 in Hg
Inlet Water Temperature	35.56 °C	96°F
Tube Cleanliness Factor	95%	
Circulating Water Quantity	21.261 m^3/s	337,000 US gpm

Table 1-2
Martin Lake Unit 2 Condenser Design Data

Parameter	Value	
	SI	English
Type	Twin-Shell	
Surface Area	29,264.5 m^2	315,000 ft^2
Number of Passes	1	
Tube Material	304 ASTM A-269 SS	
Tube Size	25.4 mm, 22 BWG	1.000 in, 22 BWG
Effective Tube Length	12.93 m	42.42 ft
Number of Tubes	28,512	
Heat Load	995.90 MW	3,400 E+06 Btu/hr
Absolute Pressure	104.62 mbar	3.09 in Hg
Inlet Water Temperature	32.22 °C	90°F
Tube Cleanliness Factor	95%	
Circulating Water Quantity	30.788 m^3/s	488,000 US gpm

Table 1-3
Stryker Creek Unit 2 Condenser Design Data

Parameter	Value	
	SI	English
Type	Twin-Shell	
Surface Area	17,651.6 m^2	190,000 ft^2
Number of Passes	1	
Tube Material	Admiralty & 304 ASTM A-269 SS	
Tube Size	22.2 mm, 18 BWG	0.875 in, 18 BWG
Effective Tube Length	12.19 m	39.98 ft
Number of Tubes	20,864 (17,512 Admiralty)	
Heat Load	689.51 MW	2,354 E+06 Btu/hr
Absolute Pressure	135.43 mbar	4.0 in Hg
Inlet Water Temperature	35.00 °C	95°F
Tube Cleanliness Factor	85%	
Circulating Water Quantity	14.511 m^3/s	230,000 US gpm

Objectives

The objectives of the analysis are to evaluate current condenser performance, identify overall shell-side behavior and its effect on performance, and explore modifications with the most potential to improve unit performance based on the boundary conditions.

CFD Mathematical Model Description

The evaluation has been performed using a three-dimensional numerical model which utilizes CFD techniques (see Reference 1). This section describes the mathematical basis and the physical models that are utilized.

Governing Differential Equation

Shell-side steam flow is treated as three-dimensional and steady flow. The governing equations are solved on a fixed grid which is distorted to accommodate the features of the condenser. The x and y coordinates are used in the cross section of the condenser, and the z coordinate is used in the direction of the tube axis. The CFD model solves for the following variables:

- Mixture velocities in the x, y, and z directions denoted by u, v, and w, respectively.
- Steam concentration, c.
- Pressure, p.

The equations utilized in the model represent the conservation of momentum, steam concentration, and mass continuity. They can be expressed in the following form:

$$\frac{\partial}{\partial x}(\rho u\phi)+\frac{\partial}{\partial y}(\rho v\phi)+\frac{\partial}{\partial z}(\rho w\phi)-\frac{\partial}{\partial x}(\Gamma_\phi\frac{\partial\phi}{\partial x})-\frac{\partial}{\partial y}(\Gamma_\phi\frac{\partial\phi}{\partial y})-\frac{\partial}{\partial z}(\Gamma_\phi\frac{\partial\phi}{\partial z})=S_\phi \quad \text{(eq. 1-1)}$$

where

ϕ stands for u, v, w, c, or 1, where the latter corresponds to the continuity equation.
ρ is the mixture density.
Γ_ϕ is the diffusion coefficient.
S_ϕ is the source term of per unit volume.

In order to use these equations for the model, the following assumptions have been made:

1. The steam is at saturation temperature corresponding to its local pressure. The pressure in each computational cell is calculated although the solution of the above continuity equation and the local temperature is determined from the steam tables. An enthalpy equation is therefore not required.

2. The condensate is not explicitly modeled. To do this would require the solution of similar equations to those described above but having to account for the momentum and enthalpy of the liquid phase. Such models have been developed (see Reference 2) and utilized to enhance understanding of the detailed mechanisms of heat and mass transfer within the condenser. The effect, such as condensate drainage, is modeled empirically.

The source terms in the equations include the effects of pressure gradient, heat and mass transfer, and frictional pressure drop. These are calculated within each appropriate grid cell and are defined as follows:

Momentum equations:

$$S_u = -\frac{\partial p}{\partial x} V - F_u \qquad \text{(eq. 1-2)}$$

$$S_v = -\frac{\partial p}{\partial y} V - F_v \qquad \text{(eq. 1-3)}$$

$$S_w = -\frac{\partial p}{\partial z} V \qquad \text{(eq. 1-4)}$$

Continuity and steam concentration equations:

$$S = -\dot{m} \qquad \text{(eq. 1-5)}$$

where:

V is the cell volume.
$F_{u,v}$ is the tube friction force.
$\dot{m}$ is the mass condensed in the cell.

Heat and mass transfer is calculated in each cell through an iterative procedure to determine the local temperature difference between vapor and cooling water. It is assumed that the heat flux (q) and mass transfer (m) are related through the latent heat by the following relationship:

$$m = \frac{q}{\lambda} \qquad \text{(eq. 1-6)}$$

The heat flux (q) is a function of the local temperatures of the vapor, condensate, outer tube wall, and cooling water denoted by T_v, T_c, T_w, and T_1, respectively, and the corresponding heat transfer coefficients between cooling water and outer tube wall (a_{w1}), across the condensate film (a_c), and the overall value between vapor and liquid (a_{ov}). The mass transfer can be deduced from the temperature gradient between vapor and condensate surface. Empirical correlations are used to estimate these various heat transfer coefficients using the local flow variables, i.e. velocity and steam/air concentrations. The method is similar to that outlined by Chisholm (see Reference 3).

Tube friction is calculated assuming turbulent cross-flow conditions. The source terms have the following form:

$$F = 2uf\rho N \qquad \text{(eq. 1-7)}$$

where

$$f = (0.23 + \frac{0.11}{(P/d_o - 1)^{1.08}})\,\mathrm{Re}^{-0.15} \qquad \text{(eq. 1-8)}$$

and N is the number of tube rows per cell.

2

BASE CASE EVALUATION

For each condenser evaluated, only one-quarter of the whole condenser has been modeled as illustrated in Figures 2-1 and 2-2. Each model incorporates all the main features, including the tube-support plates, tube bundle regions, air-offtake section, baffles, exhaust neck and feedwater heater shell. For each case, the water at the bottom of the condenser is assumed to be at the normal level indicated on the design drawings.

Monticello Unit 1

Geometry

The Monticello tube bundle is shown in Figure 2-3. An upside down U-shaped hood runs along the length of the condenser above the air-cooler section. At the top right of the hood is another baffle, consisting of two horizontal plates joined by a vertical plate near the end. This also runs along the length of the condenser. At the air-offtake, a pipe of rectangular cross-section is connected to the hood. Two of these pipes, one from each side of the shell, join to form a single pipe at the centerline of the shell. This pipe then carries the air up and out of the shell. Monticello consists of 2 shells, identified as sections A and B on the drawings. The CFD model is one-half of a single shell or one-quarter of the whole condenser.

The CFD model of the condenser model is shown in Figure 2-4, which also depicts the hood and air-offtake pipe. Figure 2-5 shows the computational grid used for the calculations. Approximately 75,000 total number of cells have been used for the simulations. The feedwater heater shell was modeled as a solid region along the length of the condenser. A solid region was also used to represent the air-offtake pipe.

The physical properties of the condenser tubes are summarized below:

Parameter	Value	
	SI	English
Number of tubes	5,729 (22,916 whole condenser)	
Tube diameter	22.2 mm	7/8 in
Tube pitch	30.16 mm	1.188 in
Tube orientation angle	60	
Tube thickness	0.71 mm	0.028 in (22 BWG)
Effective tube length	11.77 m	38.625 ft
Thermal conductivity (SS)	14.884 W/m-°K	8.6 Btu/h-ft-°F
Tube Cleanliness	95%	

Boundary Conditions

For each CFD simulation, or run, the boundary conditions have to be applied to the model. At the top of the exhaust neck, a constant velocity is imposed which is calculated from the area of the exhaust neck and the inlet mass flow of steam, obtained from the given heat load of the condenser. A constant pressure value is set at the air-offtake point, and all other pressures in the domain are calculated with reference to this fixed pressure. The temperature of the steam is determined based on the pressure using the steam tables.

A constant cooling or circulating water (CW) flow rate and temperature is set, and the inlet water temperature is assumed to be constant across the array of tubes. In addition to the mass flow of steam into the condenser, it is necessary to specify the air in-leakage which determines the inlet concentration of the steam. For each simulation, the air in-leakage was assigned a value of 10 kg/h (22.2 lb/h).

The three cases examined were design conditions, typical summer conditions, and typical winter conditions (see Reference 4). The table below shows the data used for the typical summer case:

Parameter	Value	
	SI	English
Cold Water Flow Rate	17.224 m^3/s	273,000 US gpm
Cold Water Inlet Temperature	31.89°C	89.4°F
Condenser Heat Load	816.59 MW	2786.9 E+06 Btu/h
Measured Condenser Pressure	120.89 mbar	3.57 in Hg
Measured CW Outlet Temp	43.23°C	109.8°F

Note that the values in the table are for the whole condenser.

Discussion of Results

Since no measured pressures were available for the air-offtake, a number of 2-D parametric studies were performed to determine the most suitable air-offtake pressure to use in the 3-D model. For the 2-D simulations, the air-offtake pressure was varied over a range of values, and the predicted condenser pressure was compared with the measured value. The most comparable offtake pressure was then used in the 3-D model, corresponding to an offtake steam concentration of about 0.7, which is an ideal value. The result for the 3-D summer case simulation is tabulated below:

Table 2-1
Monticello Model - Summer Case

Air Offtake Pressure	Predicted Condenser Pressure	Measured Condenser Pressure
80 mbar (2.36 in Hg)	138.9 mbar (4.1 in Hg)	120.9 mbar (3.57 in Hg)

Based on the results shown in Table 2-1, it is clear that the predicted condenser pressure is much higher than the measured value.

A possible reason for the high condenser pressure predicted is the use of too low a value of cooling water flow rate. The calculated value of flow rate given could be too low if there was either an error in the measurement of the outlet cooling water

temperature (a degree or two would make a significant difference) or if the quoted heat load was incorrect. The cooling water flow was therefore increased to the design value of 21.261 m^3/s (337,000 US gpm) and the flow calculation performed again. A condenser pressure of 129.7 mbar (3.83 in Hg) was predicted, about 9 mbar (0.27 in Hg) lower than for the first simulation but still about 9 mbar (0.27 in Hg) higher than the measured value.

It is interesting to note that the parametric 2-D runs provided condenser pressures which were much lower than the 3-D runs. For the design cooling water flowrate, the measured condenser pressure was well predicted by the 2-D model. This suggests that the differences between the 3-D and 2-D results are due to the geometrical details of the model.

Not all of the geometrical features are represented in the 2-D model, such as the slope of the exhaust region and the baffle plate in the air-offtake section which prevents steam by-passing to the air pumps. This latter feature was thought to be an important factor in the discrepancy between the 2-D and 3-D calculations and indicates that the differences in the predicted condenser pressure may be due to plant variations from the design drawings.

The results from the 3-D simulation (original CW flow rate) are shown in Figures 2-6 through 2-21. Contours of steam concentration through selected planes are provided, followed by pressure contours, cooling water temperature rise contours, and velocity vectors.

Figures 2-6 through 2-11 show the steam concentrations at various planes. Figures 2-6 and 2-7 are 3-D views of the concentration of steam at cross-sectional and longitudinal planes along the condenser. Figures 2-8 through 2-11 are enlarged views of the steam concentration at various cross-sectional planes. The figures clearly reveal the presence of air-bubbles on the left and right sides of the hood and in the top part of the hood next to the air-offtake point.

Contours of steam pressure are shown in Figures 2-12 through 2-18. The contour values are given in inches of mercury (in Hg). The air-offtake pressure is 80 mbar (2.36 in Hg). Figure 2-13 shows that there is a much higher pressure drop across the tubes in the air-offtake section than across the rest of the bundle. Two sets of contours at the air-offtake point are given in Figures 2-14 and 2-15. In Figure 2-14, contours are given at 1.69 mbar (0.05 in Hg) intervals, and show the drop in pressure across the main part of the bundle. Figure 2-15 gives contours at 6.77 mbar (0.2 in Hg) intervals, revealing the large drop in pressure up towards the air-offtake point. It is believed that this large pressure gradient at the air-offtake is what gives rise to the over-predicted condenser pressures for the 3-D simulations. An examination of the pressure field shows that the presence of the small plate behind the air-offtake point accounted in part for the difference between the 3-D result and the measured value of condenser pressure.

Another 3-D run was undertaken with this plate removed. The predicted condenser pressure fell by about 5 mbar (0.15 in Hg). The importance of the geometry is therefore clearly seen, and it may be the case that the geometry of the condenser is different in the air-offtake area to what is shown on the design drawings.

The other pressure drop contours are given for cross-sectional planes at 3m (9.8 ft), 6m (19.7 ft), and 9m (29.5 ft) from the CW inlet end of the condenser, similar to the concentration plots. There is a much smaller pressure loss across the tubes in the cooler section at these planes than for the air-offtake plane.

In Figure 2-19 cooling water temperature rise contours are plotted. The greatest increase in cooling water temperature is in the top part of the bundle and below the baffles to the right of the hood. As the velocity vector plots show (Figures 2-20 and 2-21), the increase in cooling water temperature to the right of the hood is a result of the increased flow of steam into this part of the bundle. Figure 2-21 shows steam flowing around the outside of the bundle and up towards the air-offtake pipe. The downward flow meets the upward flow at this point, where the steam then enters into the right side of the bundle. The figures also indicate a recirculation region underneath the feedwater heater shell that extends to the top of the tube bundle.

The pressure contours in Figure 2-16 show regions of lower pressure on the left and right sides of the tube bundle that are also apparent in the other figures. The reason for this is the higher flow velocities in these regions. Outside the tube bundle region, there is little friction along the streamlines of the flow, so the Bernoulli energy conservation equation applies. A lower static pressure implies a higher flow velocity, and vice versa.

Martin Lake Unit 2

Geometry

The Martin Lake tube bundle is shown in Figure 2-22. The tube bundles are symmetrical about the center of each support plate, with the air-offtake section situated between the tube bundles. Two vertical baffles are located at the center of each tube bundle, which run along the length of the condenser. There is also a small horizontal baffle on each side, where a gap appears between this baffle and the top of the vertical baffles. At the air-offtake point, a horizontal pipe runs from the center of each tube bundle (fixed to the innermost vertical baffle) towards the center of the support plate (between the bundles). The pipes join to form a vertical pipe leading up and away from the air-offtake point.

The CFD model of the condenser is shown in Figure 2-23. The air-offtake pipe and feedwater heater shell are also shown. Figures 2-24 and 2-25 show the computational grid used for the calculations. Approximately 95,000 total number of cells have been

used for the simulations. The feedwater heater shell was modeled as a solid region along the length of the condenser. A solid region was also used to represent the air-offtake pipe.

The physical properties of the condenser tubes are summarized below:

Parameter	Value	
	SI	English
Number of tubes	7,128 (28,512 whole condenser)	
Tube diameter	25.4 mm	1.000 in
Tube pitch	31.75 mm	1.021 in
Tube orientation angle	60	
Tube thickness	0.71 m	0.028 in (22 BWG)
Effective tube length	12.84 m	42.146 ft
Thermal conductivity (A304 Stainless Steel)	15.4 W/m-°K	8.9 Btu/h-ft-°F
Tube cleanliness	90%	

Boundary Conditions

The two cases examined were design conditions and typical summer conditions. The summer case data (see Reference 4) is summarized in the table below:

Parameter	Value	
	SI	English
Cold Water Flow Rate	27.64 m^3/s	438,116 US gpm
Cold Water Inlet Temperature	29.04°C	84.0°F
Condenser Heat Load	997.73 MW	3405.07 E+06 Btu/h
Measured Condenser Pressure	114.8 mbar	3.39 in Hg
Measured CW Outlet Temp	37.68°C	99.55°F

The tabulated data is for the whole condenser. The appropriate values used in the CFD model are only one-quarter of the values shown.

Discussion of Results

The result for the 3-D summer case simulation is provided below:

Table 2-2
Martin Lake Model - Summer Case

Air Offtake Pressure	Predicted Condenser Pressure	Measured Condenser Pressure
99.8 mbar (2.95 in Hg)	112.4 mbar (3.32 in Hg)	114.8 mbar (3.39 in Hg)

As Table 2-2 shows, the measured condenser pressure was closely predicted by the simulation. An identical result could have been obtained by increasing the air-offtake pressure by a small amount. The result indicates a pressure drop across the bundle of about 12.6 mbar (0.37 in Hg), which is much less than the pressure drop for the other two condensers.

Another 3-D simulation was made with the air-offtake pipe modeled as circular, rather than the square approximation in the first simulation. This virtually made no difference to the condenser pressure.

The results from the 3-D simulation are shown in Figures 2-26 through 2-40. Contours of steam concentration through selected planes are provided, followed by pressure contours, CW temperature rise contours, and velocity vectors. Figures 2-26 and 2-27 show 3-D views of the steam concentration along the length of the condenser. The air bubbles increase in size towards the air-offtake point, with a larger air bubble appearing in the right-hand bundle. These bubbles are shown in more detail in Figures 2-28 through 2-31.

Figures 2-28 through 2-31 show cross-sectional views of the steam concentration at selected planes through the condenser. The most significant feature of these plots is the region of low steam concentration in the inner side of the right-hand bundle. This feature occurs along the whole length of the condenser. There is a lesser marked tendency for this behavior to also occur in the left-hand bundle (refer to Figure 2-29). However, the dimensions of the air bubble do not reach the same proportions as on the right-hand side.

The pressure distribution in the condenser is shown in Figures 2-32 through 2-37. These figures also show a broadly similar behavior along the length of the condenser.

Note that in Figure 2-36, which depicts the central plane, the pressure gradients along the left-hand wall and central lane show a similar fall of pressure, from 111.7mbar (3.3 in Hg) to 108.3mbar (3.2 in Hg) and then a recovery to 111.7mbar (3.3 in Hg), as the velocities are reduced in the lower half of the condenser and pressure recovers. In the right-hand lane, the pressure is more uniform. This is due to a convergence of the steam flow from above and below, as illustrated in Figure 2-40 which shows steam flowing down the left-hand lane, passing along the bottom of the shell, and then turning upward into the right-hand lane. This upward flow meets the downward flow, and the higher pressure in this lane turns the flow into the tube nest.

The pressure between the tube bundles is lowest in the region of the air off-take baffles, and there is a region of nearly uniform pressure coincident with the region of low steam concentration. The plot of cooling water outlet temperature shown on Figure 2-38 illustrates a low value in this region. The difference in performance between the inner sections of the tube nests is thought to be due to the overall flow distribution in the condenser and the effect that this has on the balance of the offtake pressures. There is a tendency for the steam to rotate in a counter-clockwise direction, as viewed in the figures. This increases the load on the right-hand bundle, increasing the pressure in the air offtake region, which further unbalances the flow behavior.

It is interesting to compare the upper and inner regions of the tube nests, where the right-hand nest has a slightly higher pressure (0.34 mbar [~0.01 in Hg]) and a lower steam concentration than the corresponding left-hand nest. This effect is caused by the very low flow velocities in the right-hand nest, where consequently all the steam is condensed. In the left-hand bundle, the offtake pressure is lower, thus reducing the overall pressure near the offtake section and inducing more direct steam flow into this region.

Velocity vectors are shown in Figures 2-39 and 2-40. The flow field around the tube bundles varies along the length of the condenser. Behind the feedwater heater shell, a region of recirculation appears. As for the other two condensers, there is an upflow of steam to the right of the right-hand bundle, which meets downward flowing steam.

Stryker Creek Unit 2

Geometry

The Stryker Creek tube bundle is shown in Figure 2-41. The tube bundle is symmetrical about the centerline, with the air-offtake situated in the center above the cooler section. Each support plate has a square hole cut in it just above the top row of

tubes in the middle section, allowing steam to flow along the length of the condenser towards the air-offtake. Like the other condensers analyzed, there is also a feedwater heater that runs above the support plates. The center section of tubes is shielded from the main tube region by vertical baffles which run along the length of the condenser between the support plates.

The CFD condenser model is shown in Figure 2-42. The rectangular hood and air-offtake point are shown. Figure 2-43 shows the computational grid used for the calculations. Similar to Monticello, about 75,000 grid cells have been used for the simulations. The feedwater heater shell was modeled as a solid region along the length of the condenser.

The physical properties of the tubes are provided below:

Parameter	Value	
	SI	English
Number of tubes	5,216 (20,864 whole condenser)	
Tube diameter	22.2 mm	0.875 in
Tube pitch	28.6 mm	1.010 in
Tube orientation angle	60	
Tube thickness	1.22 mm	0.049 in (18 BWG)
Effective tube length	12.12 m	39.771 ft
Thermal conductivity (Admiralty)	110.765 W/m-°K	64 Btu/h-ft-°F
Tube Cleanliness	85%	

Boundary Conditions

Three cases examined were design conditions, typical summer conditions, and typical winter conditions. The summer case data (see Reference 4) is summarized in the table below:

Parameter	Value	
	SI	English
Cold Water Flow Rate	9.61 m^3/s	152,360 US gpm
Cold Water Inlet Temperature	22.74°C	72.94°F
Condenser Heat Load	694.46 MW	2370.09 E+06 Btu/h
Measured Condenser Pressure	107.35 mbar	3.17 in Hg
Measured CW Outlet Temp	40.03°C	104.05°F

The above data is for the whole condenser. Only one-quarter of the appropriate values above have been used in the CFD model.

Discussion of Results

A number of 2-D parametric studies for the summer case were performed to determine the most suitable air-offtake pressure to use in the 3-D model. An air-offtake pressure of about 80 mbar (2.36 in Hg) was indicated. The following table shows the result for the 3-D simulation:

Table 2-3
Stryker Creek Model - Summer Case

Air Offtake Pressure	Predicted Condenser Pressure	Measured Condenser Pressure
80 mbar (2.36 in Hg)	107.6 mbar (3.18 in Hg)	107.3 mbar (3.17 in Hg)

As Table 2-3 shows, the measured condenser pressure was closely predicted by the simulation. A comparison of the 2-D result to the 3-D result showed that they were almost identical.

Applying the 2-D model to the design data for the condenser showed that the design value of condenser pressure could not be obtained. A condenser pressure value of about 8 mbar (0.24 in Hg) above design was predicted (Note that the design condenser pressure is 135.4 mbar [4 in Hg]).

The results from the 3-D simulation are shown in Figures 2-44 through 2-60. Contours of steam concentration through selected planes are given, followed by pressure contours, CW temperature rise contours, and velocity vectors. Figure 2-45 shows the steam concentration contours at a plane along the length of the condenser. An air bubble forms towards the air-offtake point, with larger bubbles forming at the air-offtake end. Note that this differs from the Monticello results, where the bubbles are of similar size along the whole length of the condenser. The figures reveal smaller air bubbles than those for Monticello, appearing on the left and right sides of the bundle outside the vertical baffles and near the top of the air cooler section.

Contours of steam pressure are shown in Figures 2-50 through 2-55. As for Monticello, the contour values are given in inches of mercury, with the air-offtake pressure at a value of 80 mbar (2.36 in Hg). The figures reveal a fairly even fall of pressure across both sides of the bundle.

Figure 2-56 shows the CW temperature rise near the outlet end of the condenser. Increases in CW temperature are greatest in the top-half of the bundle, with smaller increases occurring in the region of the air-bubbles, as expected. The contour pattern is similar at each cross-sectional plane shown.

Figures 2-57 and 2-58 illustrate the predicted velocity field. A recirculation region forms behind the feedwater heater shell. Steam flows around the left side of the tube bundle, along the bottom and up towards the downward flow on the other side. The upward and downward flows on the right side of the bundle meet and enter the tube bundle, much like the Monticello steam flow pattern. In regions of higher static pressure around the outside of the bundle (see Figure 2-54 for example), the flow velocities are lower. Like Monticello, the explanation lies in the very low friction outside the bundle, where the flow follows the Bernoulli equation.

Stainless Steel Tube Analysis

The Stryker Creek Condenser is due to be re-tubed with stainless steel tubes (0.71 mm [22 BWG]) rather than the original Admiralty type. The thermal conductivity for stainless steel tubes, approximately 14.884 W/m-°K (8.6 Btu/h-ft-°F) , is much lower than Admiralty. A number of simulations were made with the new tubes to ascertain the effect on condenser pressure. The stainless steel tube analysis results, compared to the results for the Admiralty tubes, suggest an increase in condenser pressure of up to 8 mbar (0.24 in Hg) for the same CW flow rate, inlet CW temperature, and heat load.

Effect of Design Cooling Water Temperature

With the Admiralty tubes in place, the ability of the condenser to achieve the measured summer case condenser pressure of 107.35 mbar (3.17 in Hg) can be attributed to the

lower cooling water temperature of 22.8°C (73°F) rather than 35.0°C (95°F). The cooling water flowrate for the summer simulations was less than design, 9.615 m^3/s (152,000 US gpm) compared to 14.511 m^3/s (230,000 US gpm). It would be expected, however, that the lower cooling water temperature would be the significant factor.

The following table summarizes the results of the simulations:

Table 2-4
Effect of Increasing CW Flowrate and Temperature

	SUMMER CW FLOWRATE 9.615 m^3/s (152,400 US gpm)	**DESIGN CW FLOWRATE 14.511 m^3/s (230,000 US gpm)**
Admiralty Tubing:		
Summer CW Temp 22.8°C (73°F)	107.6 mbar (3.18 in Hg)	
Design CW Temp 35.0°C (95°F)		143 mbar (4.22 in Hg)
Stainless Steel Tubing:		
Summer CW Temp 22.8°C (73°F)	115 mbar (3.40 in Hg)	

Smaller CW flowrates will give rise to higher condenser pressures, as will higher CW temperatures. The effect of the stainless steel tubing will be to increase the condenser pressure. As the condenser pressure design value of 135.43 mbar (4.0 in Hg) could not be obtained by the model for the Admiralty tubing, the effect of the stainless steel tubing will be to increase the condenser pressure even further above the design value.

Due to the inability of the condenser to achieve the design condenser pressure value, it has been concluded that with the stainless steel tubes in place, inlet cooling water temperatures approaching 35.0°C (95°F) would require a cooling water flowrate at the highest possible level to help keep condenser pressures down.

Part Load Conditions

Simulations were performed for the Admiralty tubes in place, with 25% load conditions. Simulations were made for the design CW flowrate and the summer case flowrate. The inlet CW temperature was 35.0°C (95°F).

Some parametric runs were made to establish the most suitable air-offtake pressure to use. For the design cooling water flowrate with an air-offtake pressure of 74.7 mbar (2.21 in Hg), the predicted condenser pressure was 77 mbar (2.27 in Hg), compared to the quoted heat balance value of 50.8 mbar (1.5 in Hg - see Reference 5).

For the CW flowrate at the summer case value of 9.615 m^3/s (152,400 US gpm), the condenser pressure predicted was about 81.3 mbar (2.4 in Hg) with a corresponding air-offtake pressure of 77.5 mbar (2.29 in Hg). Thus, for the 25% load condition with an inlet CW temperature of 35.0°C (95°F), the results are summarized below:

Table 2-5
Stryker Creek Model - 25% Load

CW Flowrate	Predicted Minimum Condenser Pressure
DESIGN	77.0 mbar (2.27 in Hg)
SUMMER CASE	81.3 mbar (2.40 in Hg)

For the stainless steel tubes, predicted condenser pressures are expected to be about 5 to 8 mbar (up to 0.24 in Hg) higher than shown on the table. It is important for the air extraction system to be able to maintain low enough values of air-offtake pressure, around 75 mbar (2.21 in Hg), in order to achieve this level of operation. Note that for both the design and summer values of cooling water flowrate with an inlet CW temperature of 35.0°C (95°F), the predicted condenser pressures are as much as 30 mbar (0.9 in Hg) higher than the design value quoted on the 25% load heat balance, although it is not certain if the CW temperature for the heat balance is 35.0°C (95°F) or at a lower value.

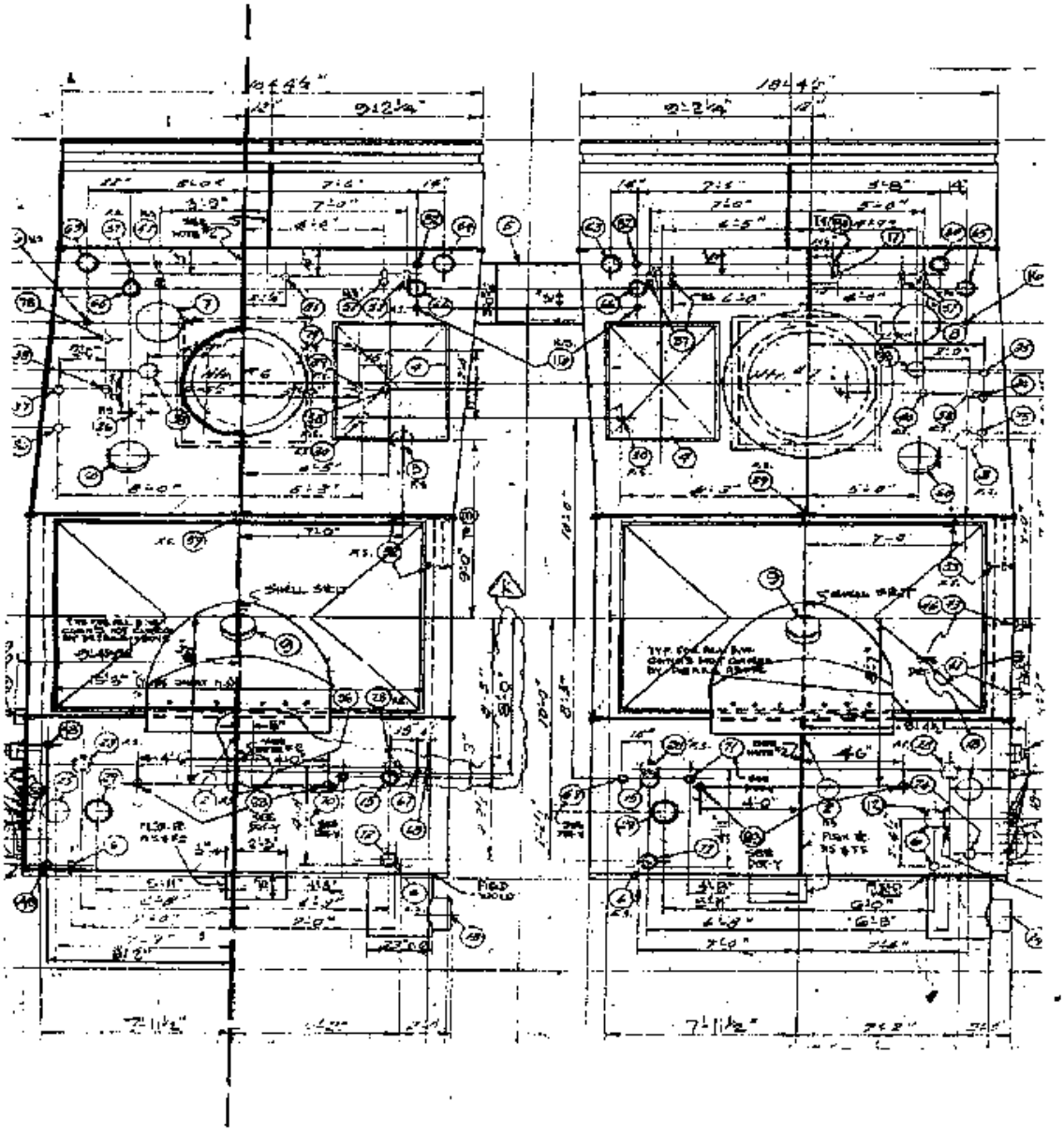

Figure 2-1
Typical Condenser Design - Cross Section

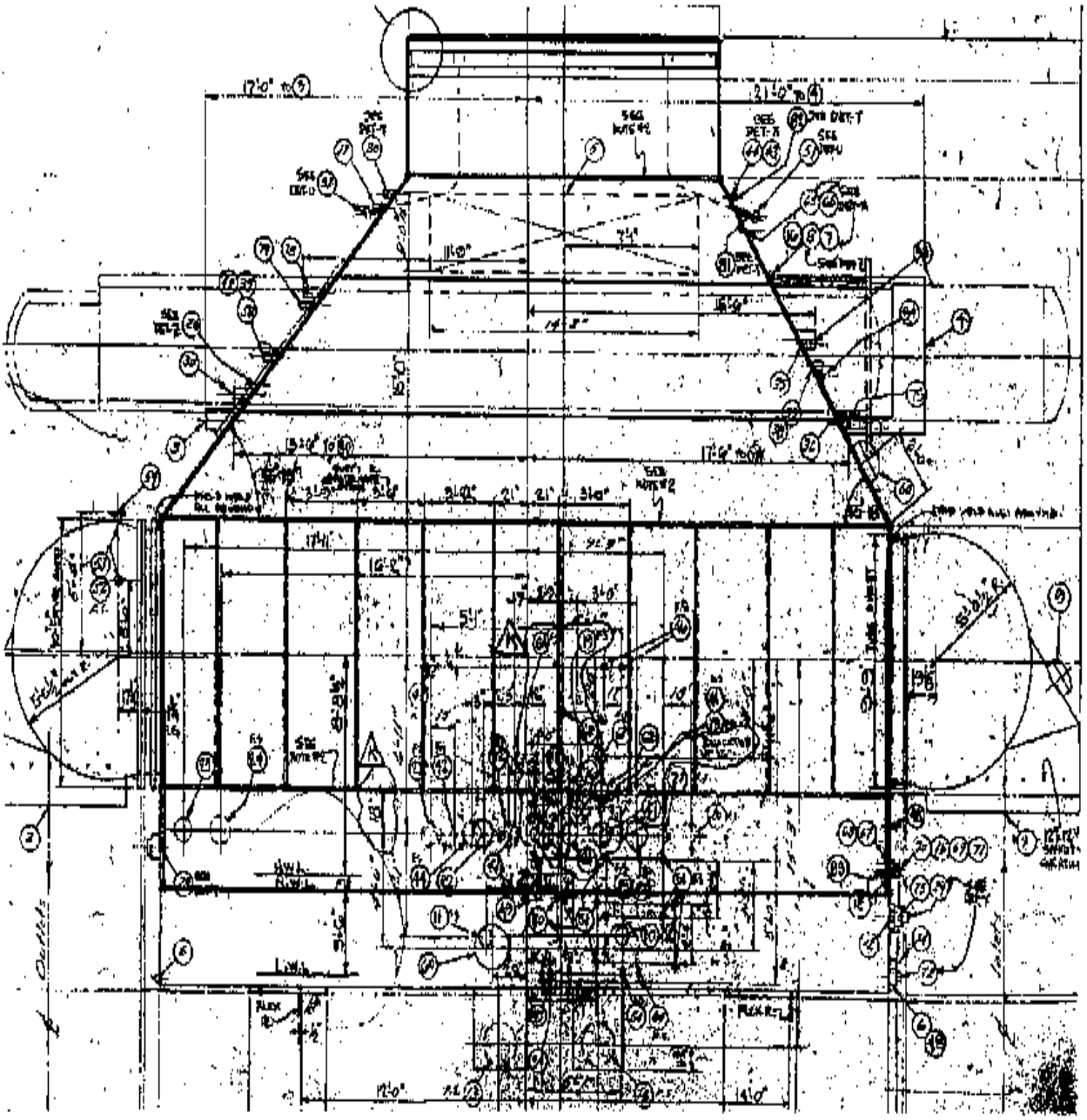

Longitudinal View

Figure 2-2
Typical Condenser Design - Longitudinal

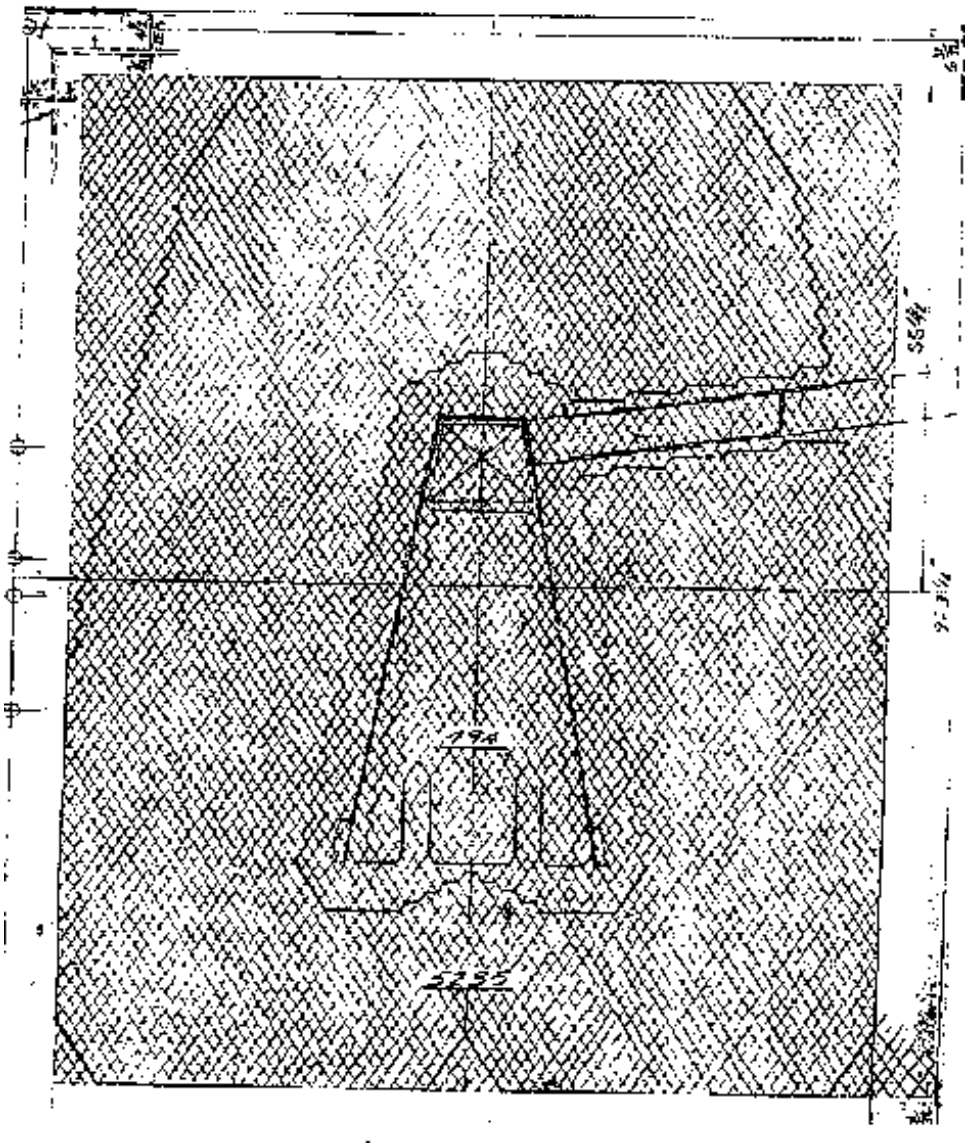

Figure 2-3
Monticello Tube Nest

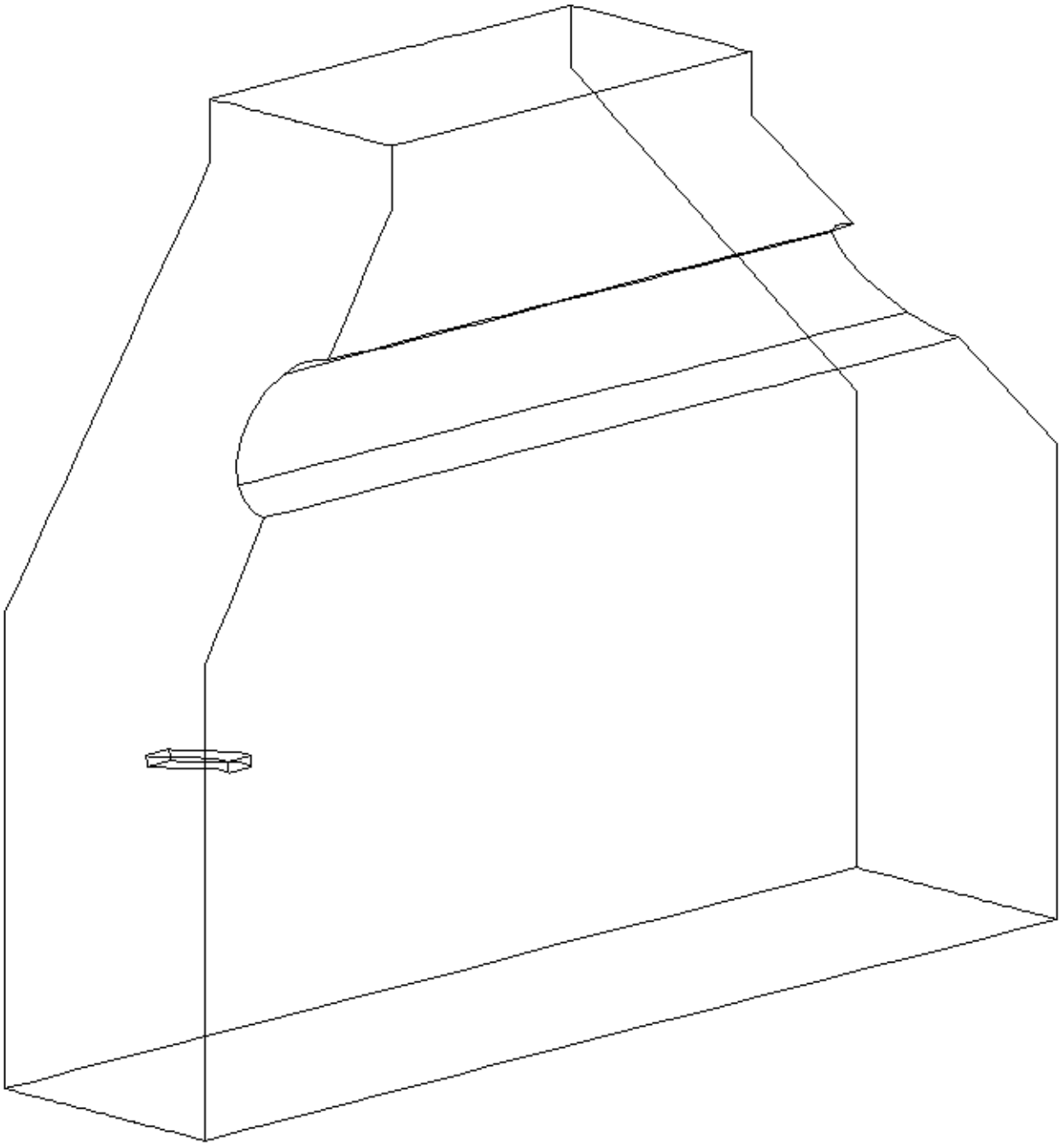

Figure 2-4
Monticello Condenser 3-D View

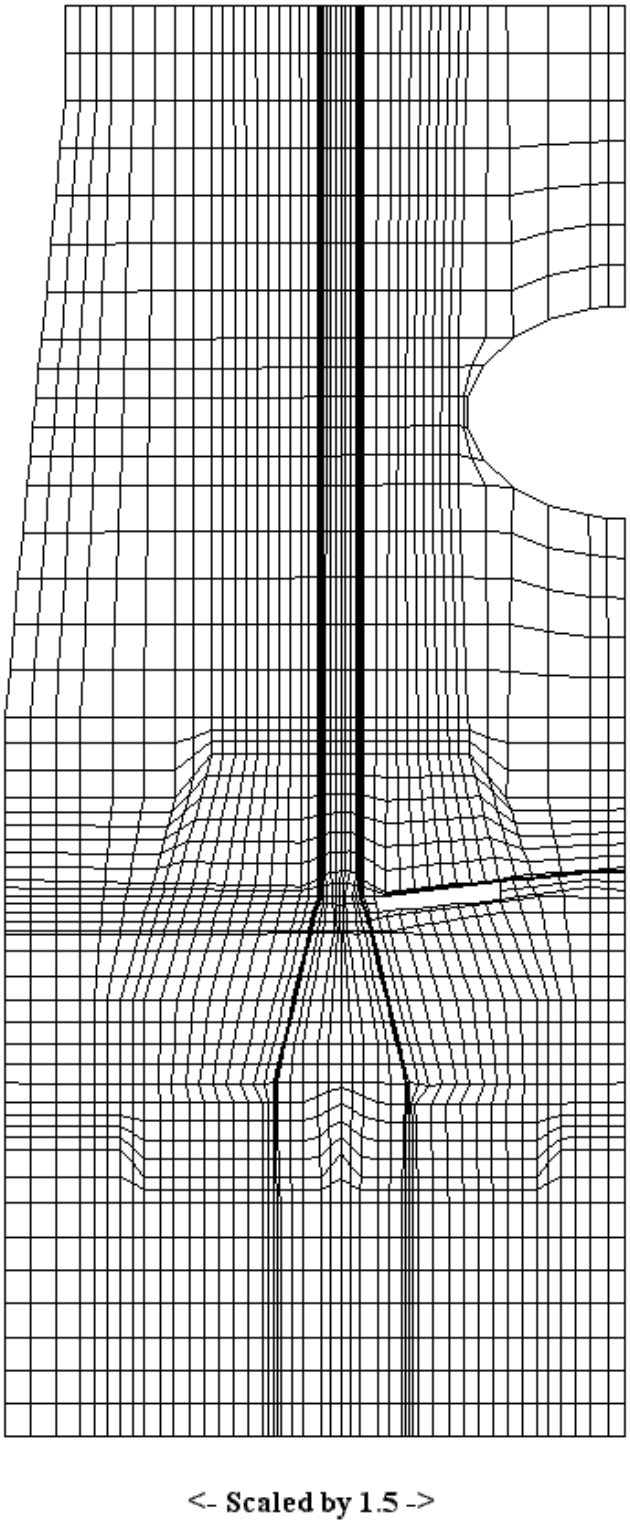

Figure 2-5
Monticello Grid

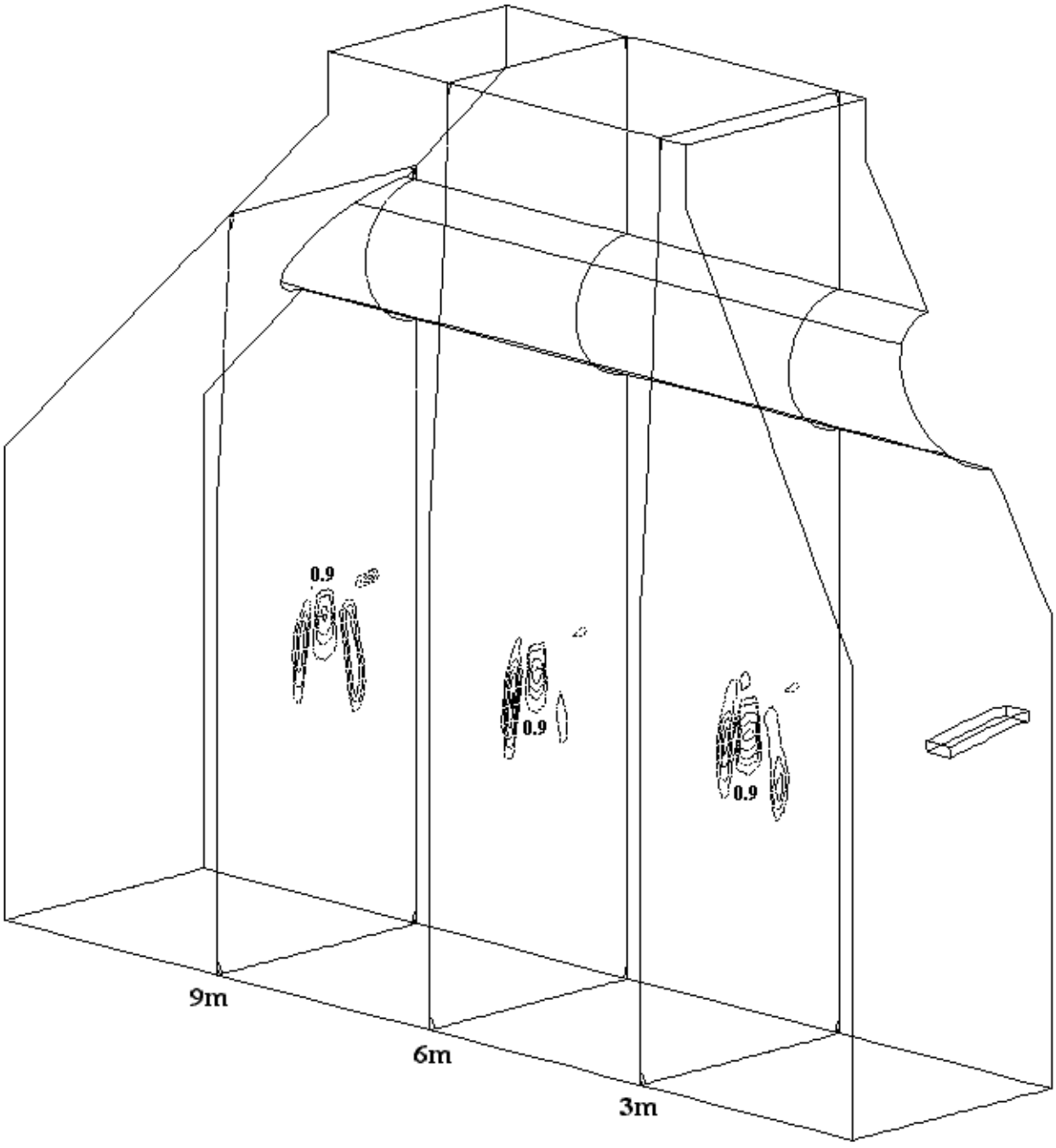

Figure 2-6
Monticello Steam Concentration (%) 3-D View

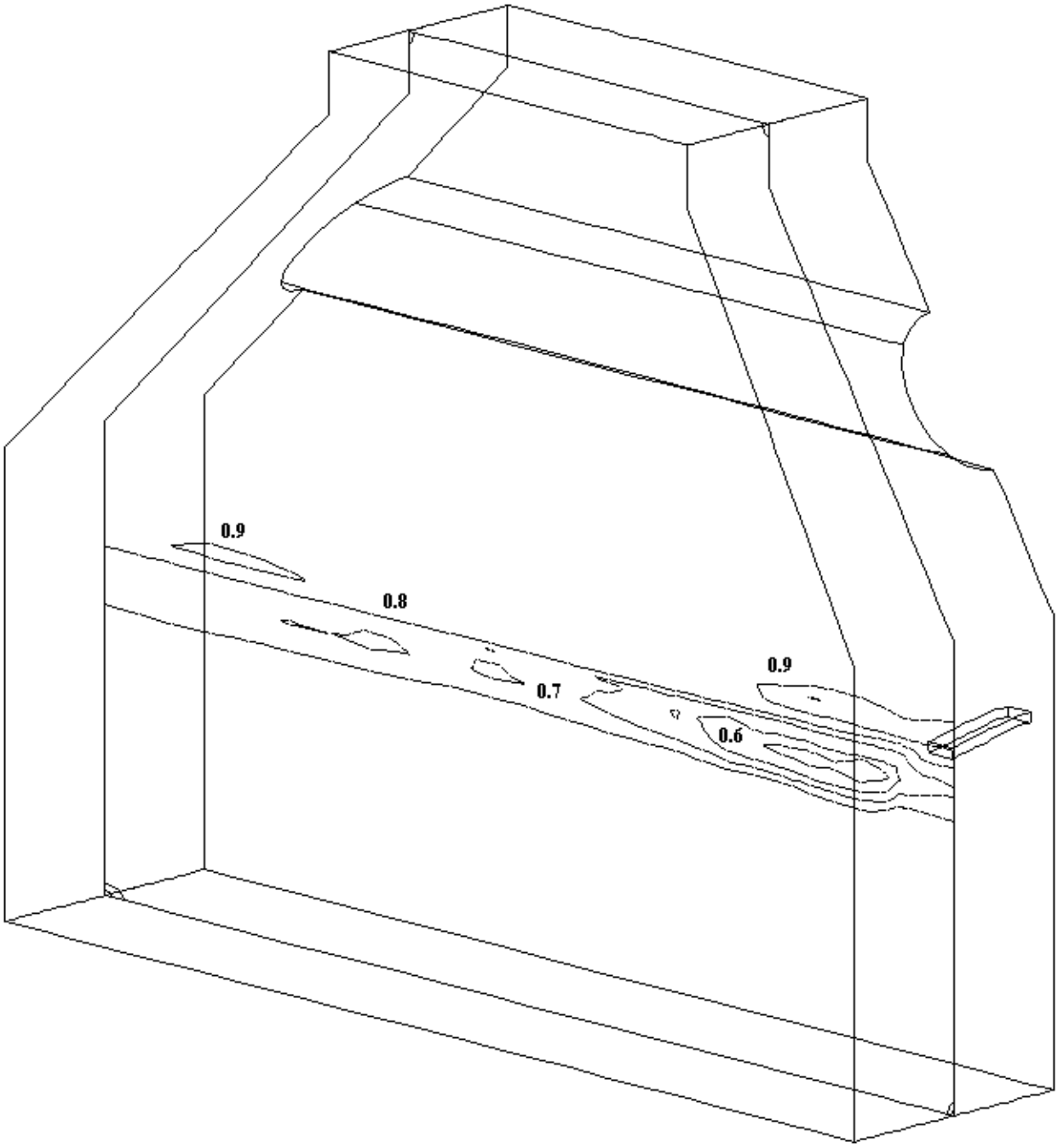

Figure 2-7
Monticello Steam Concentration (%) 3-D View

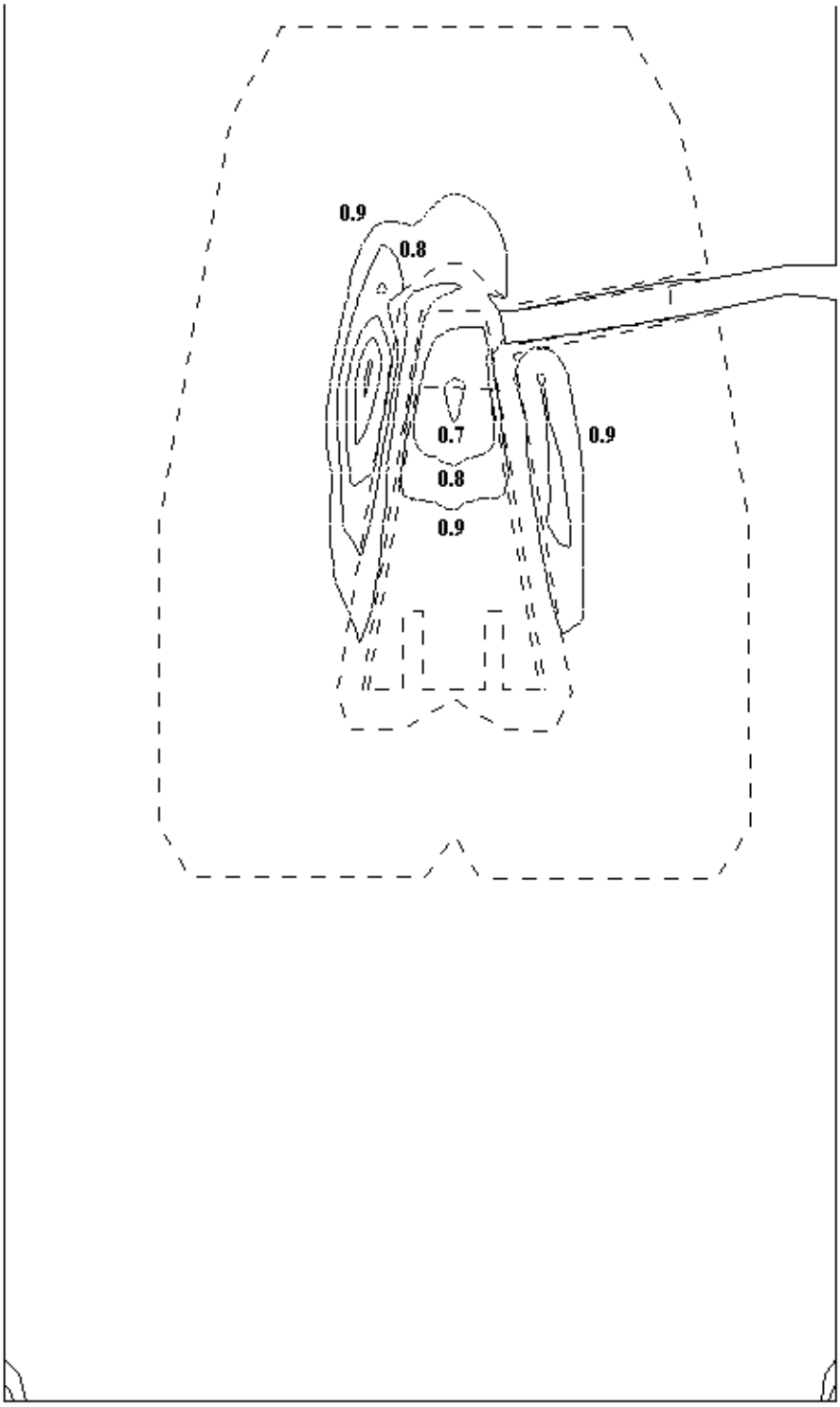

Figure 2-8
Monticello Steam Concentration (%) at Air Offtake

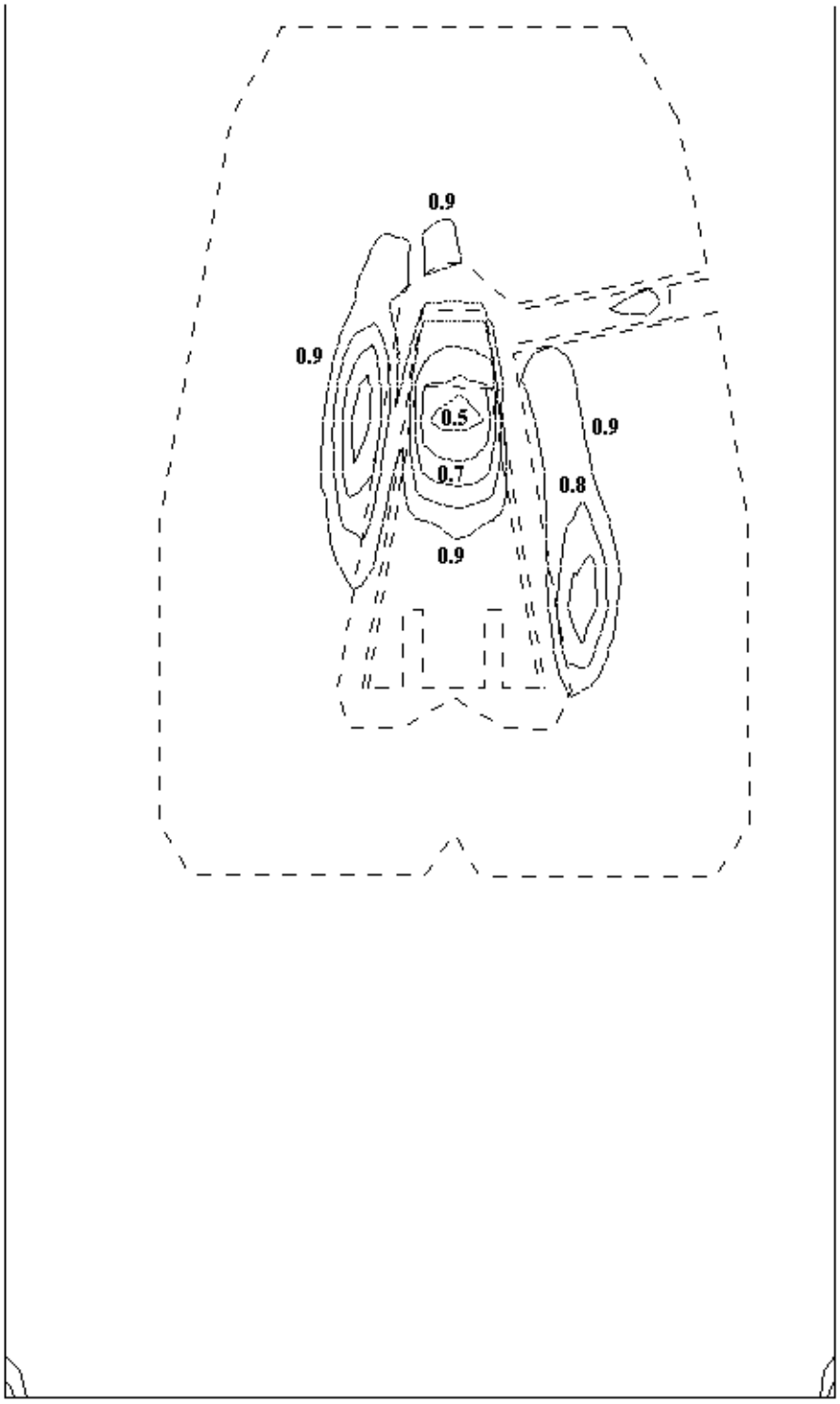

Figure 2-9
Monticello Steam Concentration (%) at Z = 3m (9.8 ft)

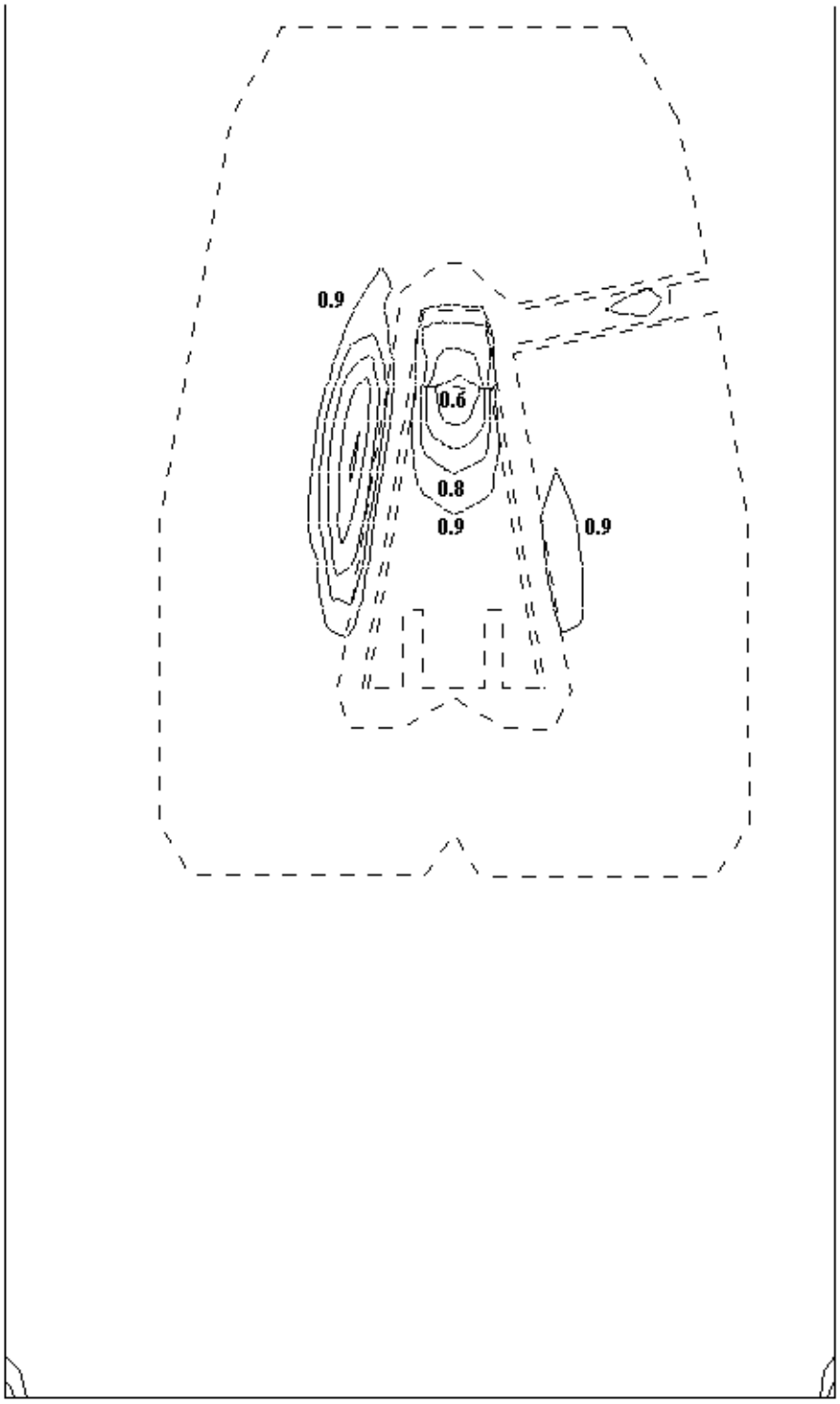

Figure 2-10
Monticello Steam Concentration (%) at Z = 6m (19.7 ft)

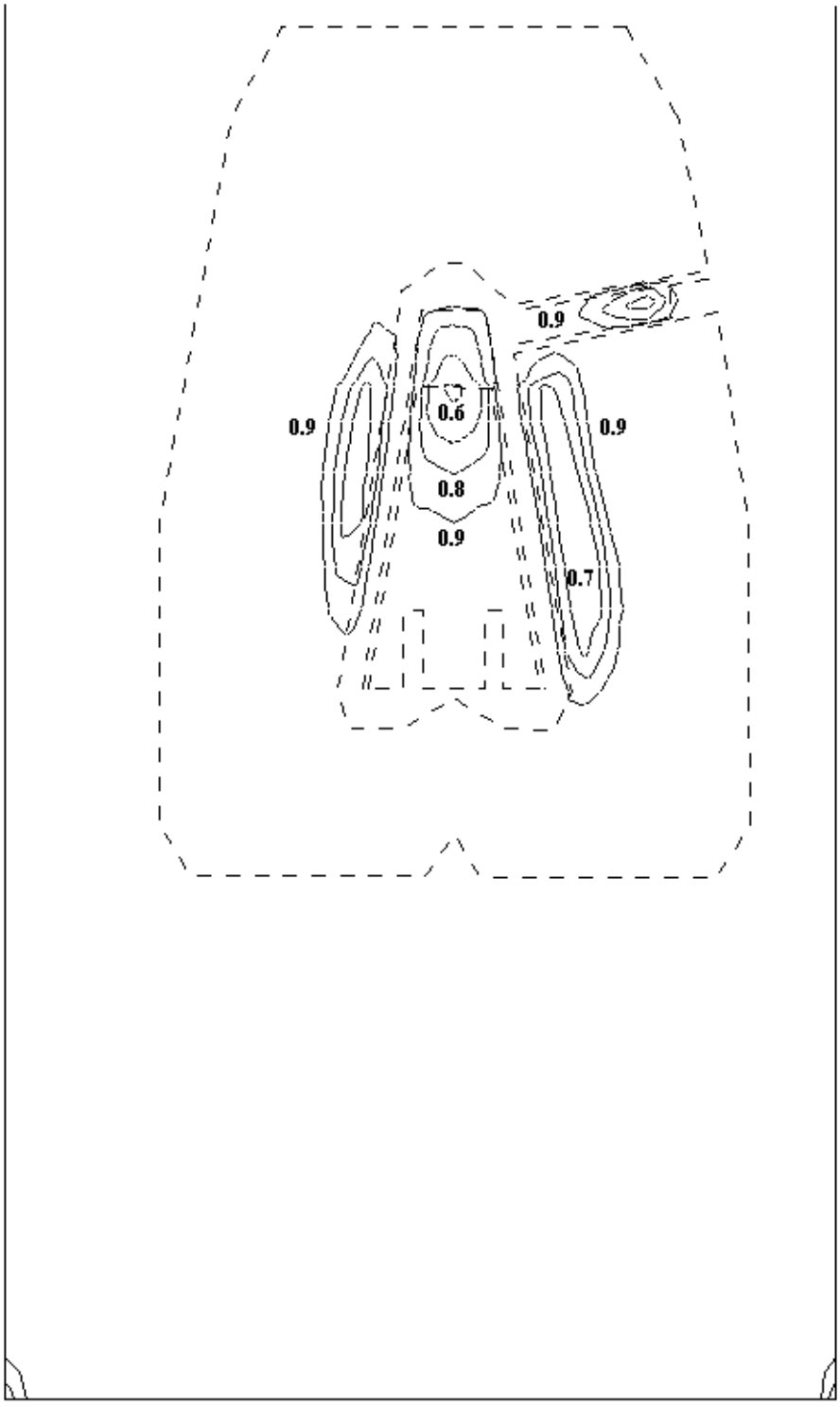

Figure 2-11
Monticello Steam Concentration (%) at Z = 9m (29.5 ft)

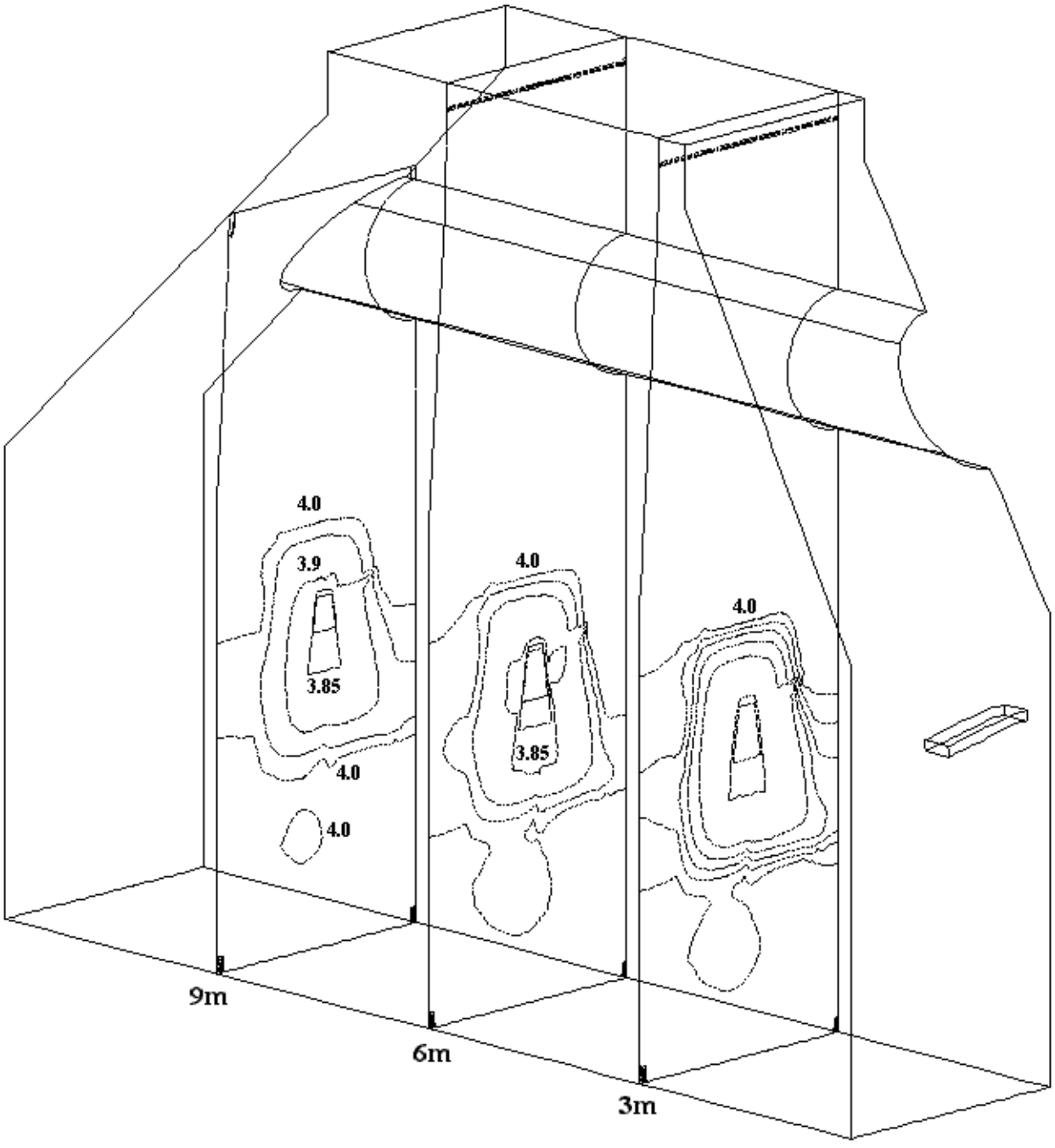

Figure 2-12
Monticello Steam Pressures (in Hg) 3-D View

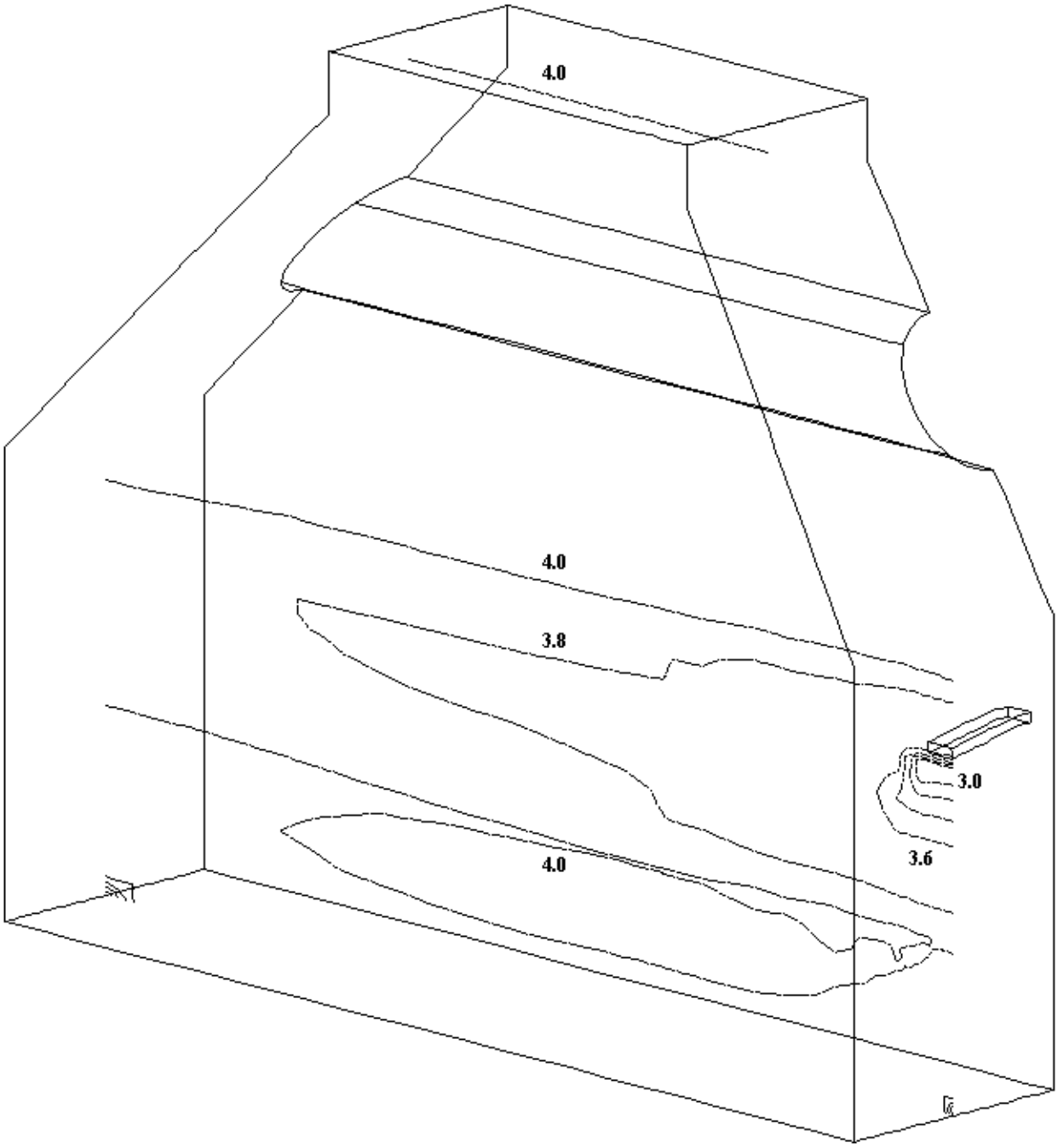

Figure 2-13
Monticello Steam Pressures (in Hg) 3-D View

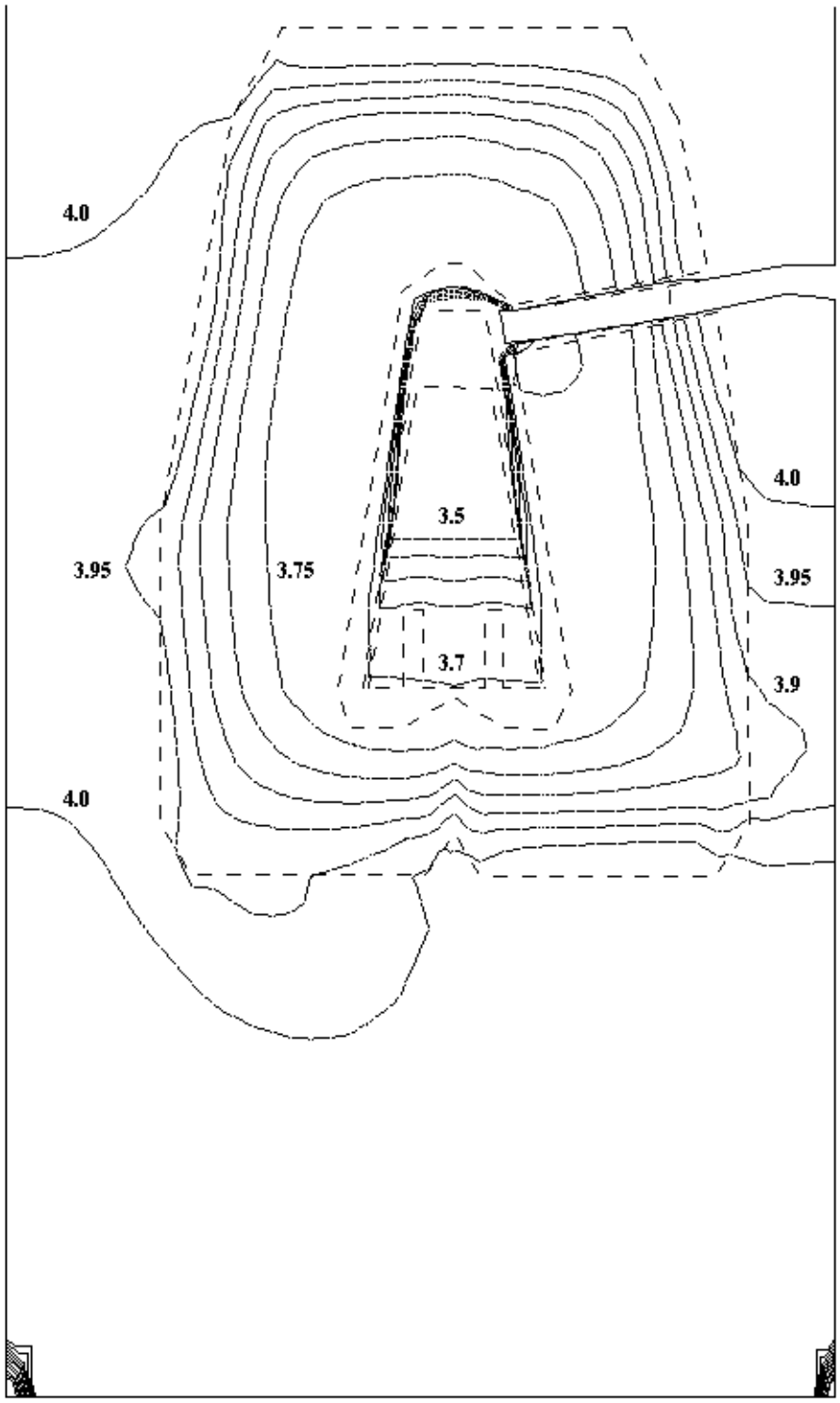

Figure 2-14
Monticello Steam Pressures (in Hg) at Air Offtake

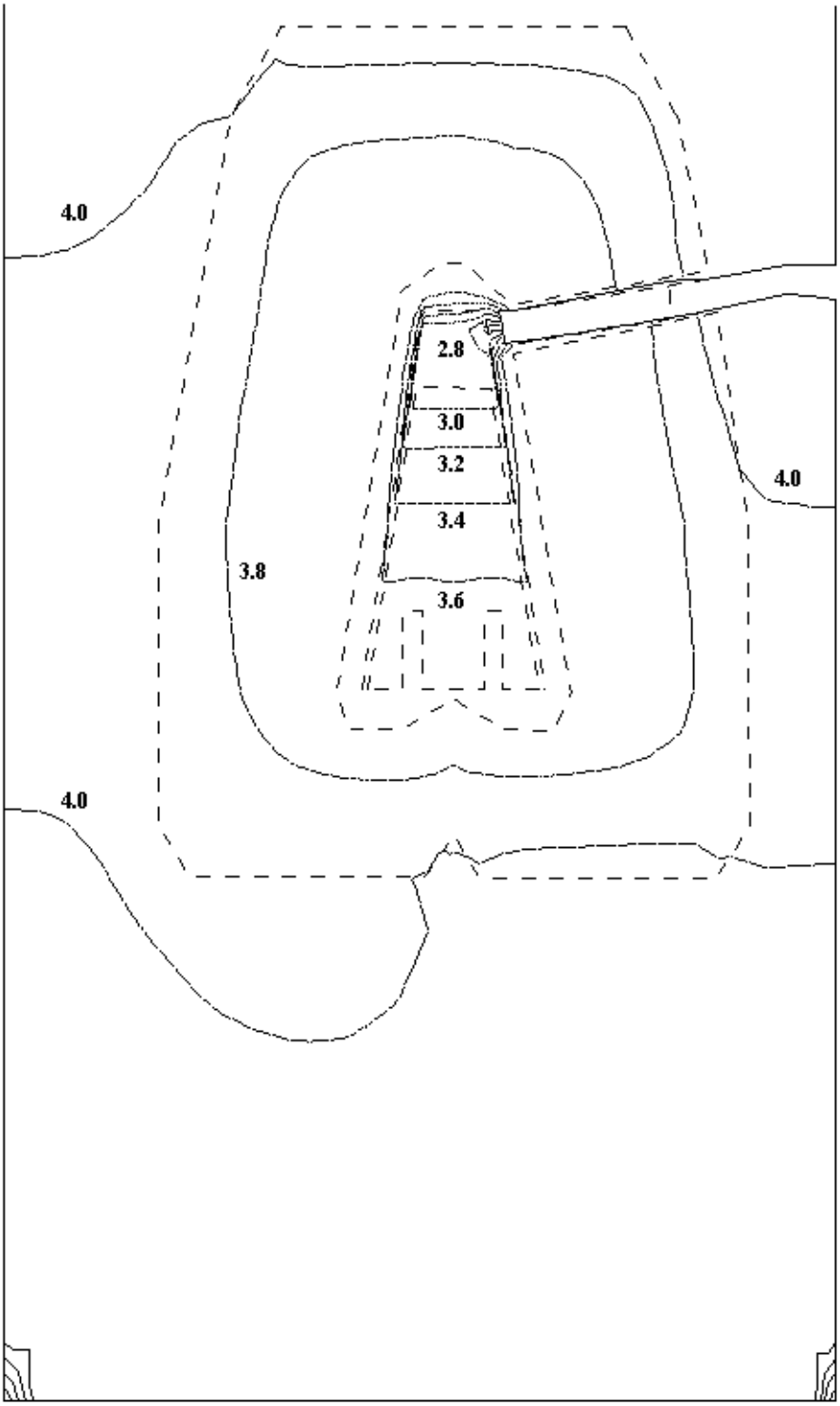

Figure 2-15
Monticello Steam Pressures (in Hg) at Air Offtake

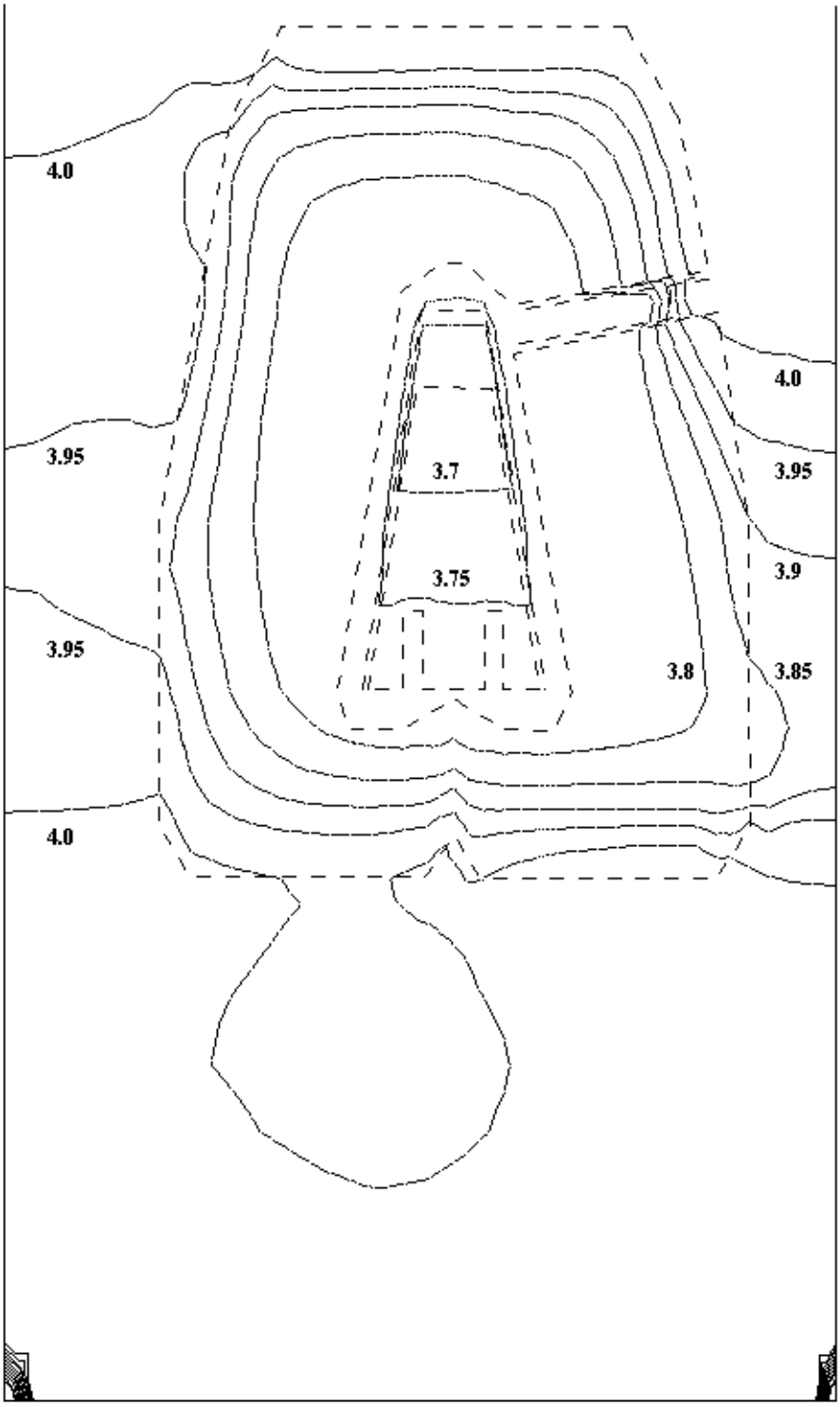

Figure 2-16
Monticello Steam Pressures (in Hg) at Z = 3m (9.8 ft)

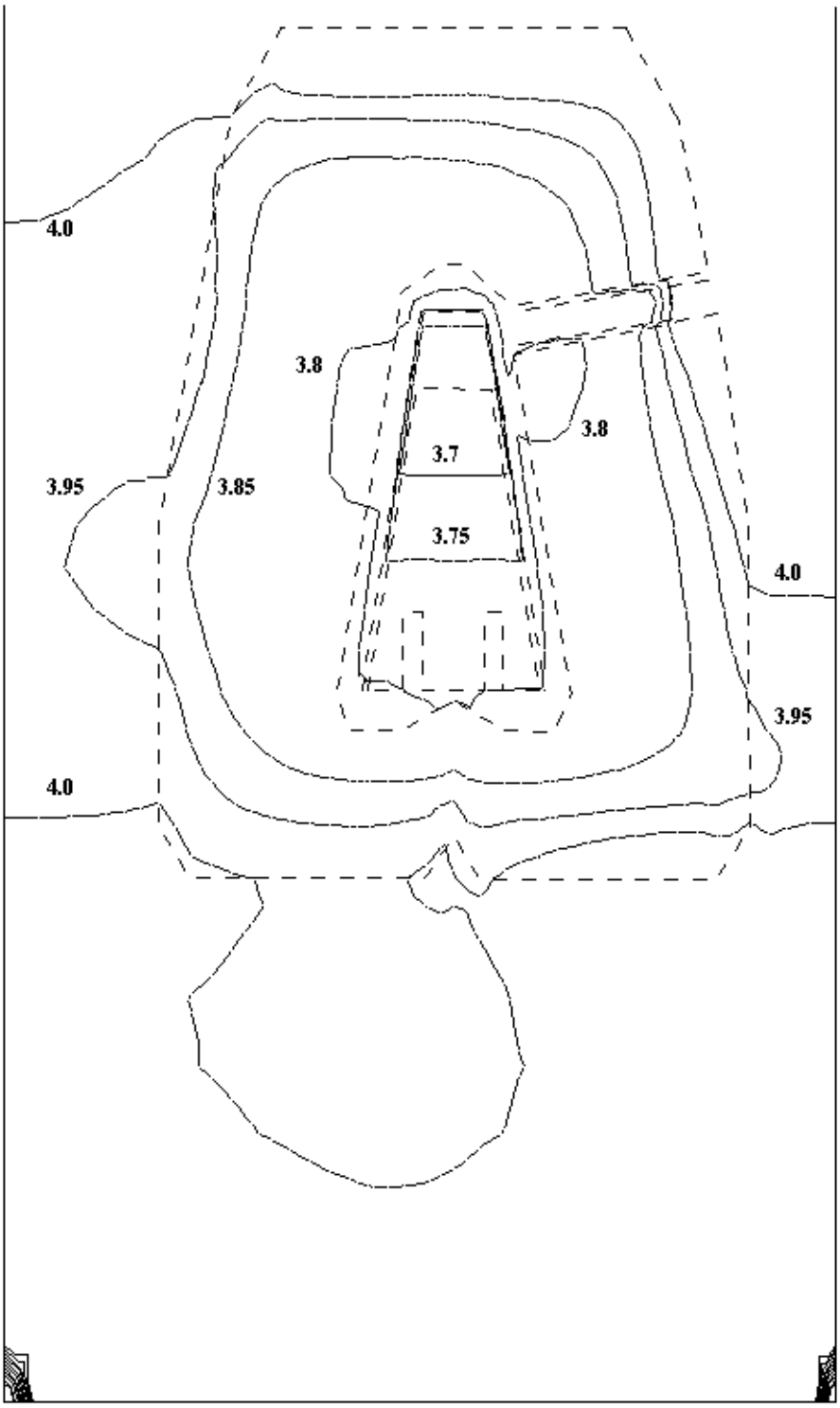

Figure 2-17
Monticello Steam Pressures (in Hg) at Z = 6m (19.7 ft)

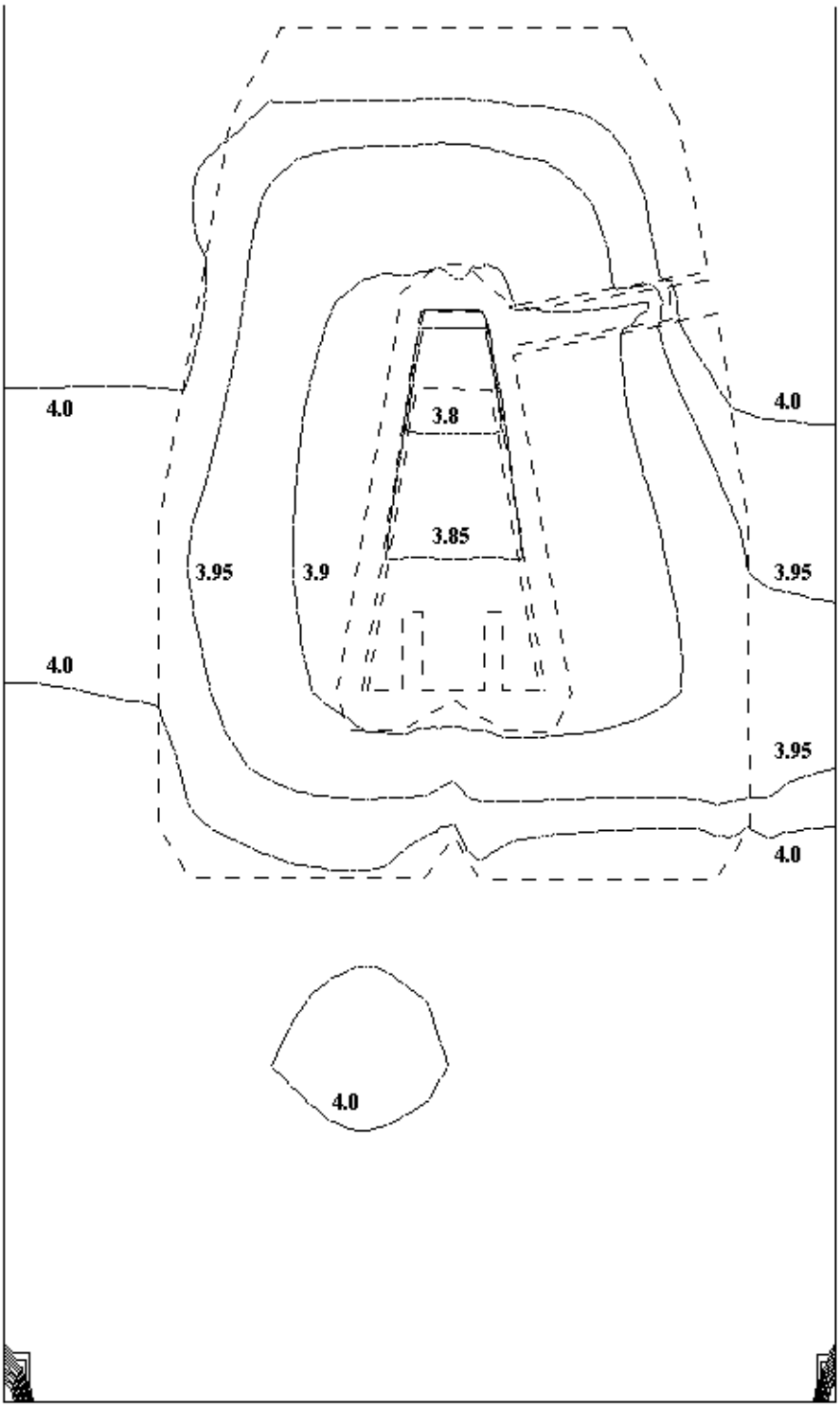

Figure 2-18
Monticello Steam Pressures (in Hg) at Z = 9m (29.5 ft)

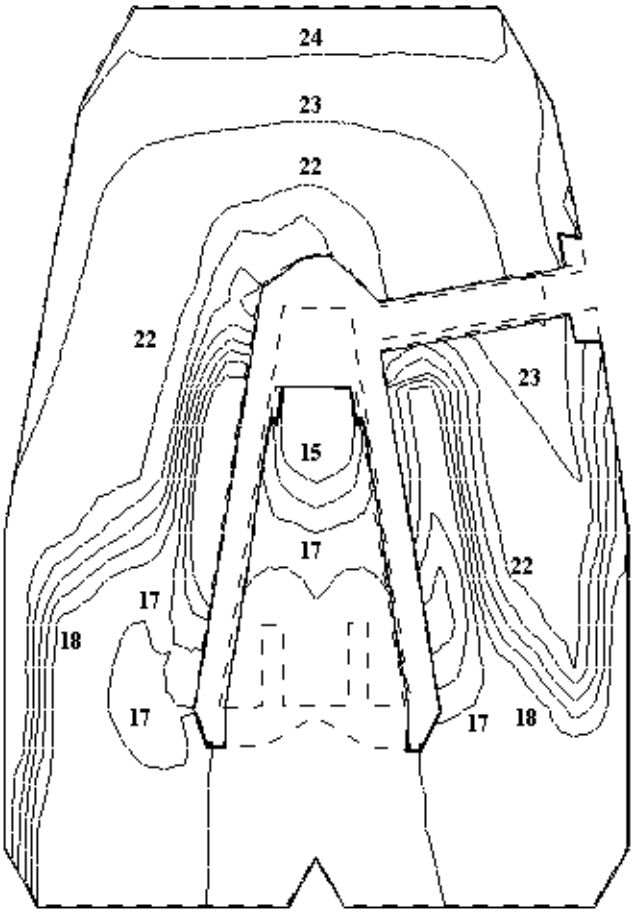

Figure 2-19
Monticello Cooling Water Temperature Rise (°F) at Z = 11.5m (37.7 ft)

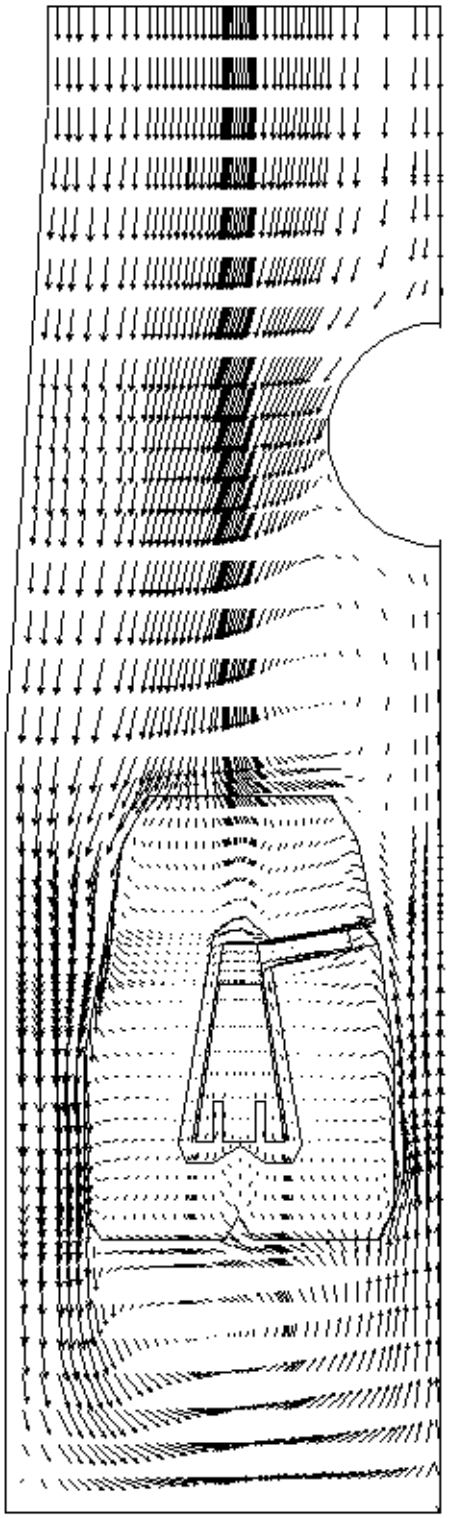

Figure 2-20
Monticello Velocity Vectors at Z = 6m (19.7 ft)

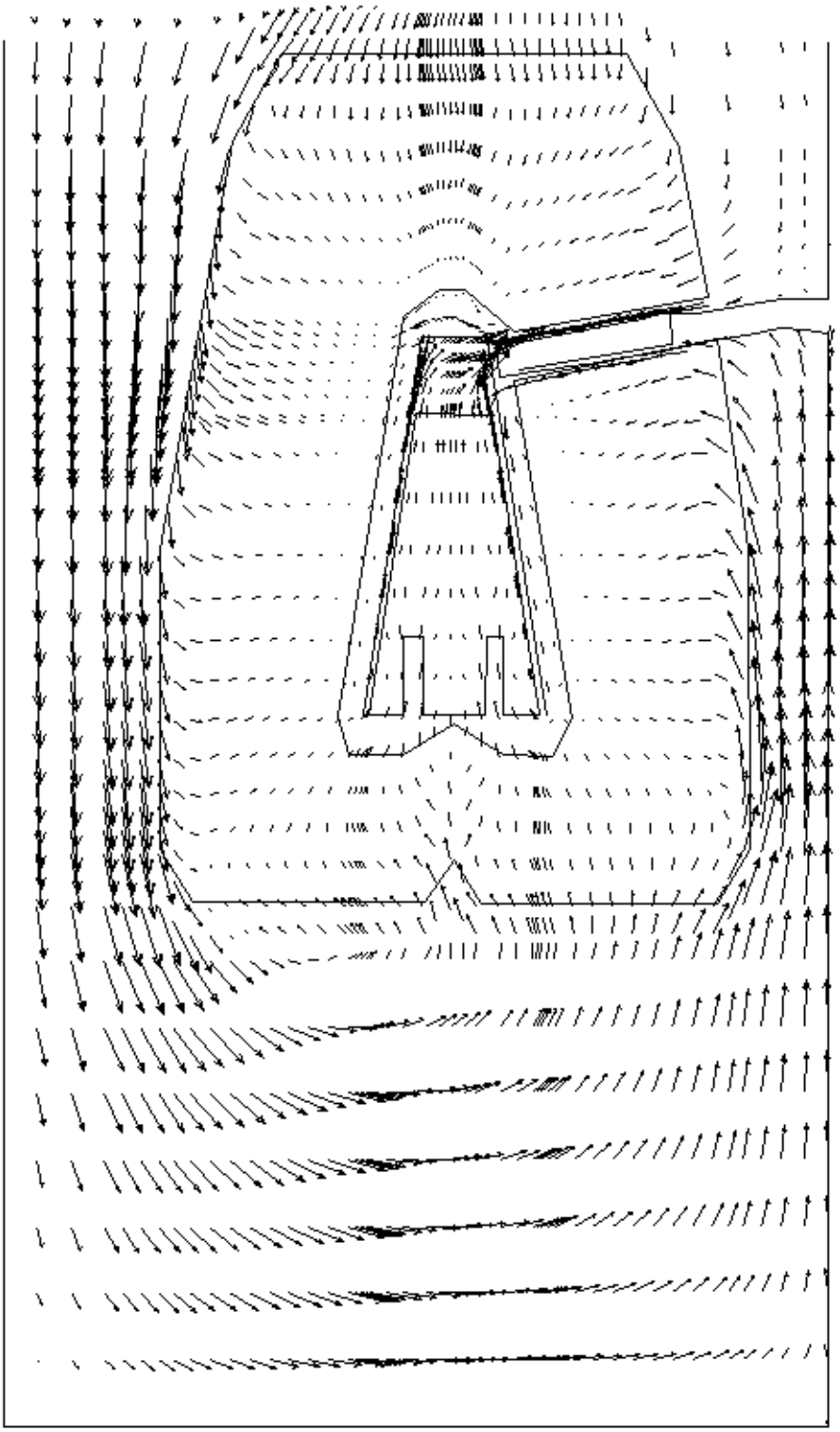

Figure 2-21
Monticello Velocity Vectors at Air Offtake

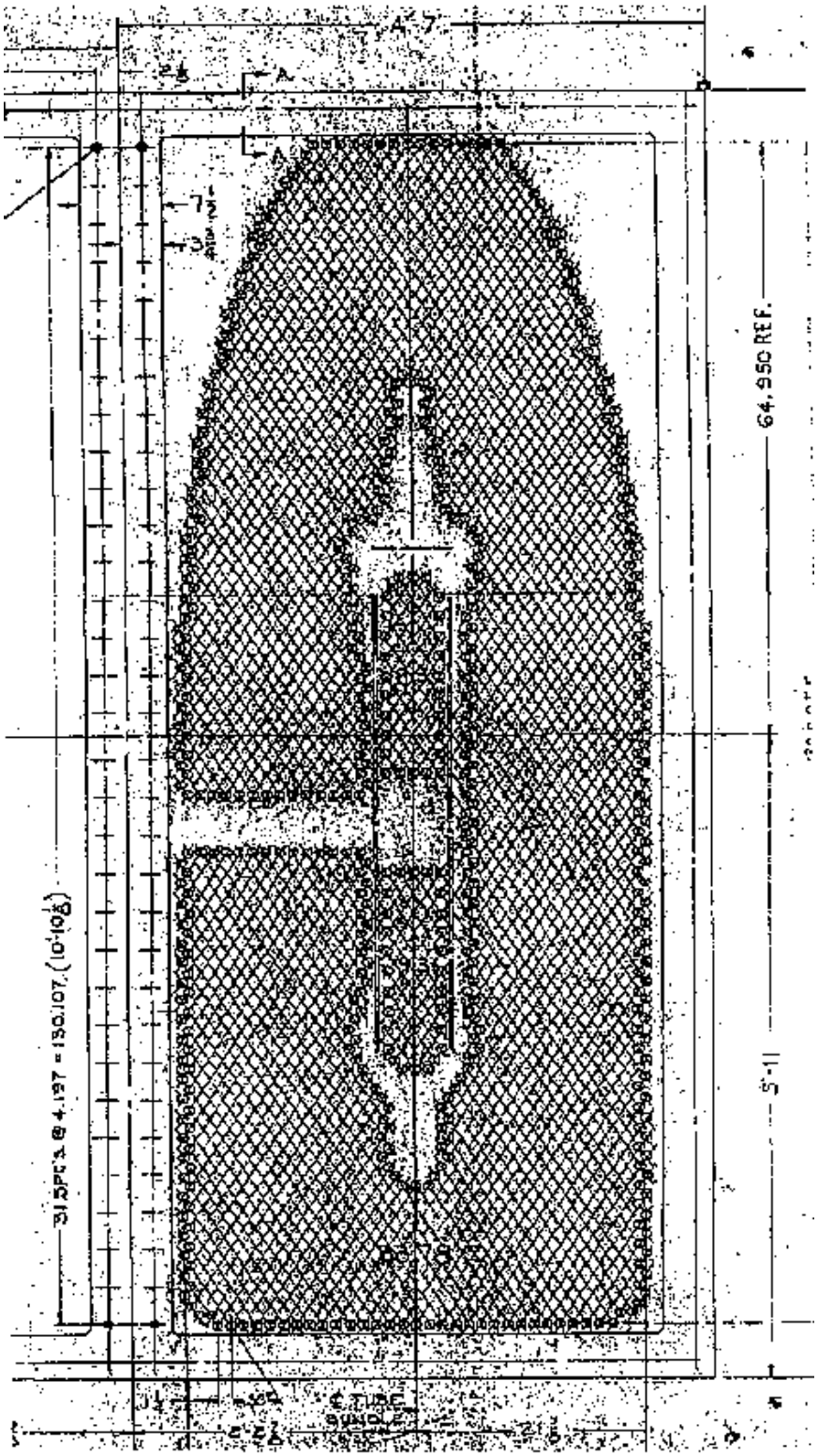

Figure 2-22
Martin Lake Tube Nest

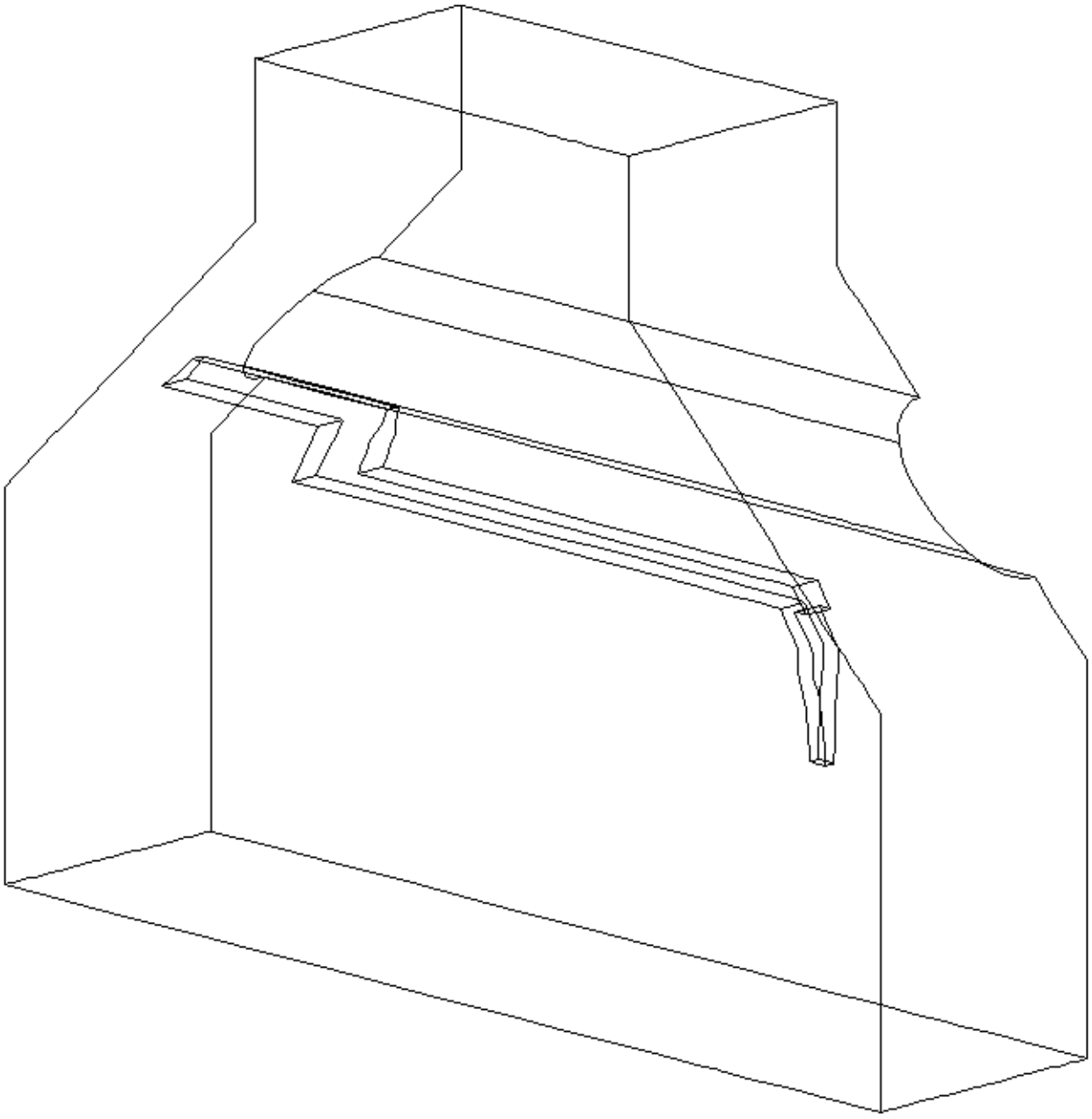

Figure 2-23
Martin Lake Condenser 3-D View

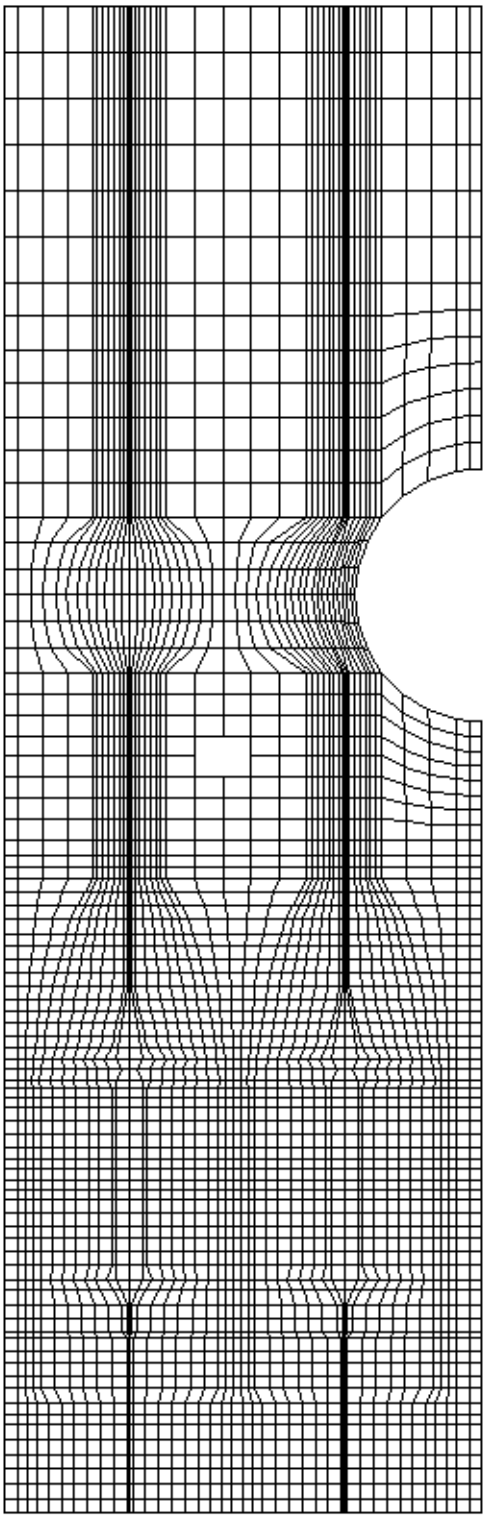

Figure 2-24
Martin Lake Grid at Z = 6.4m (21 ft)

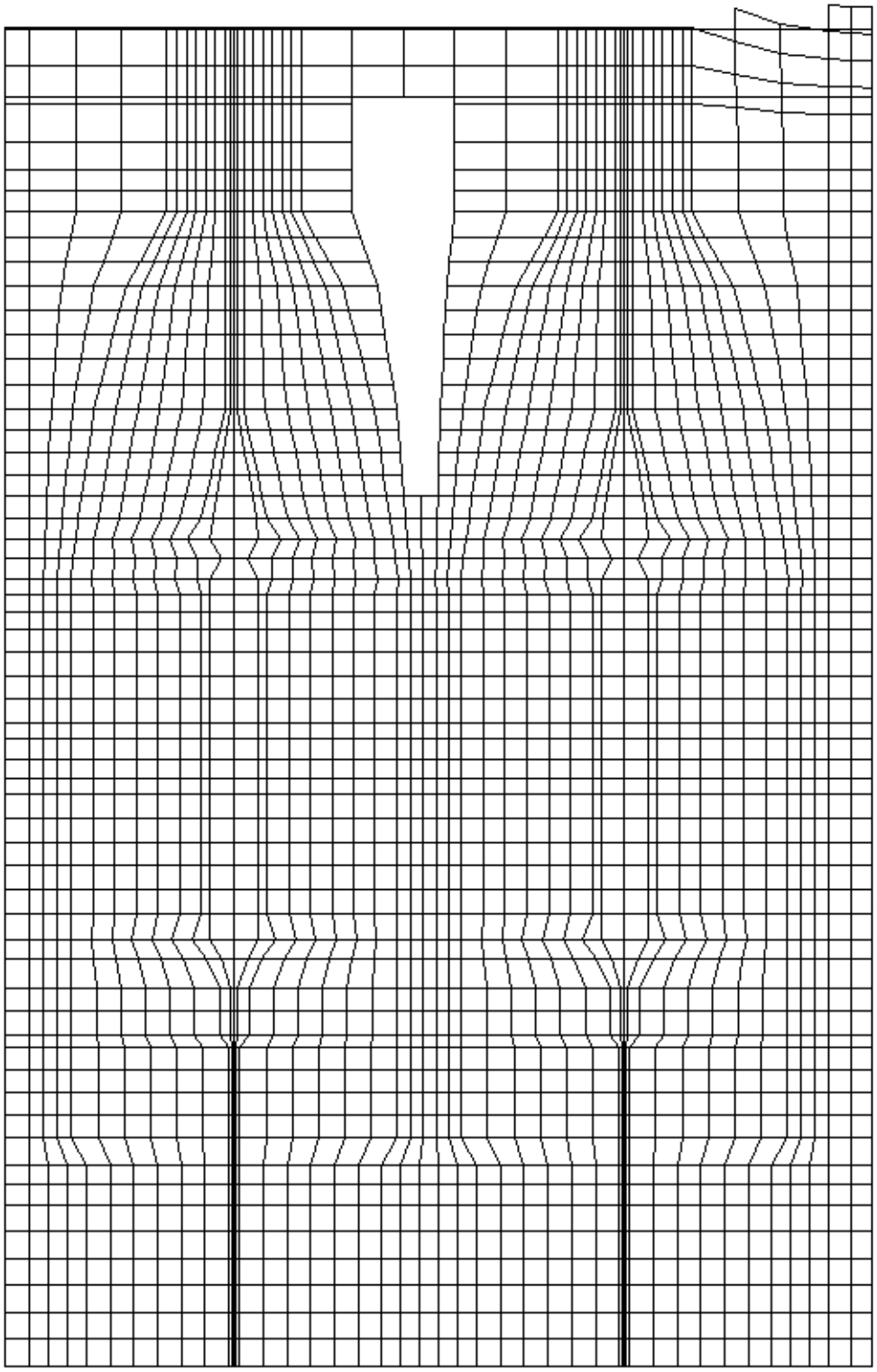

Figure 2-25
Martin Lake Grid at Air Offtake Plane

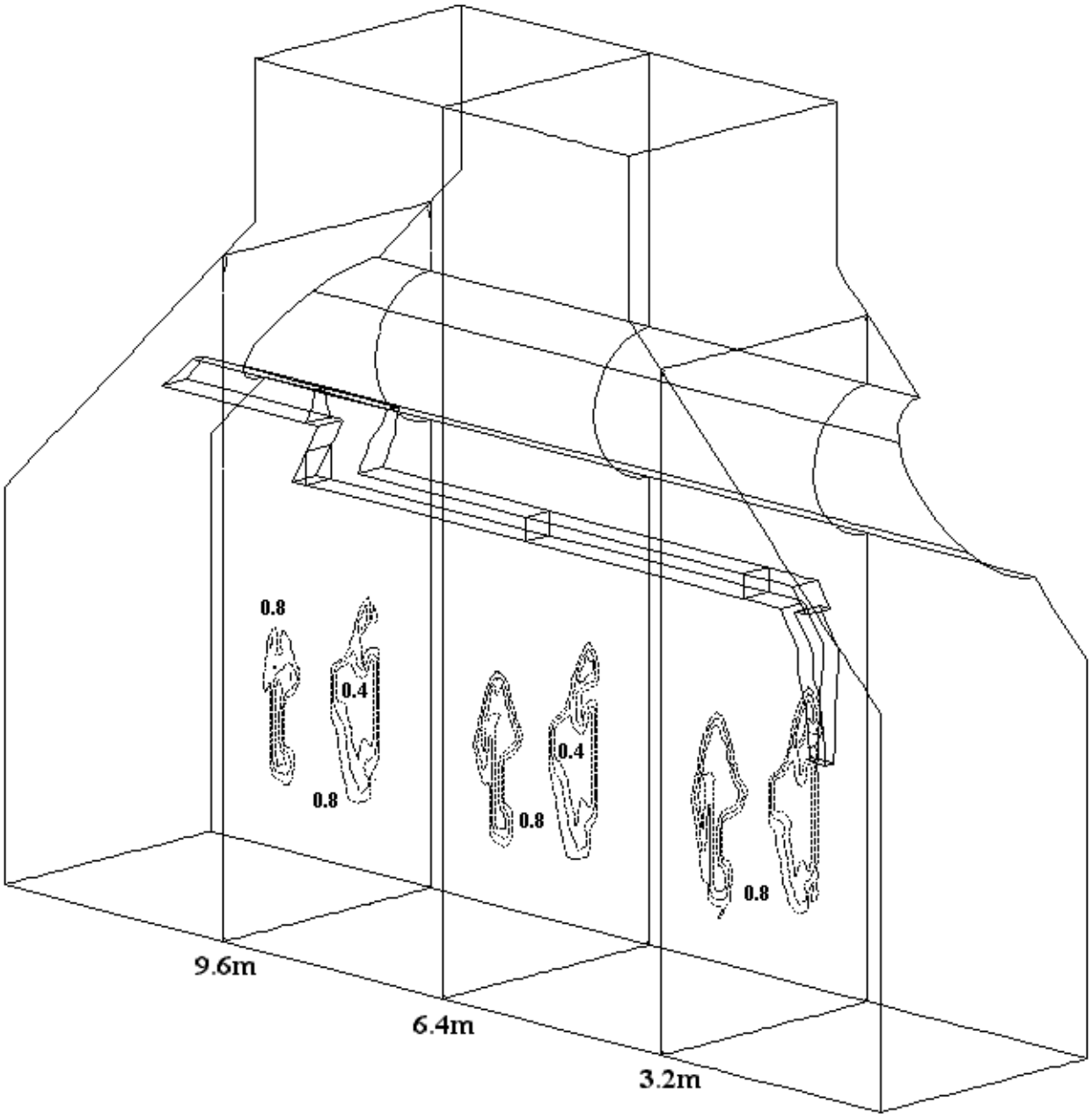

Figure 2-26
Martin Lake Steam Concentration (%) 3-D View

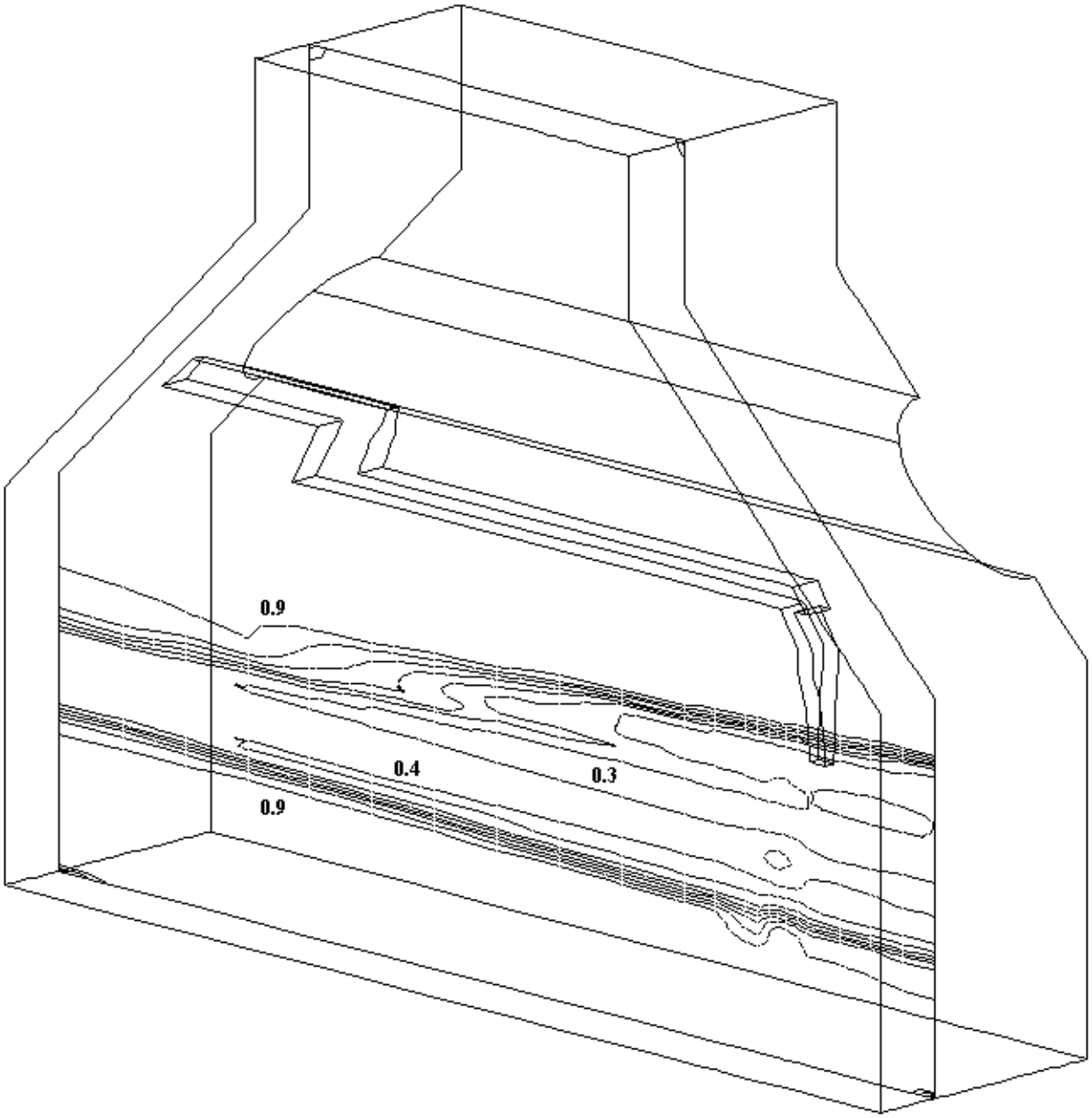

Figure 2-27
Martin Lake Steam Concentration (%) 3-D View

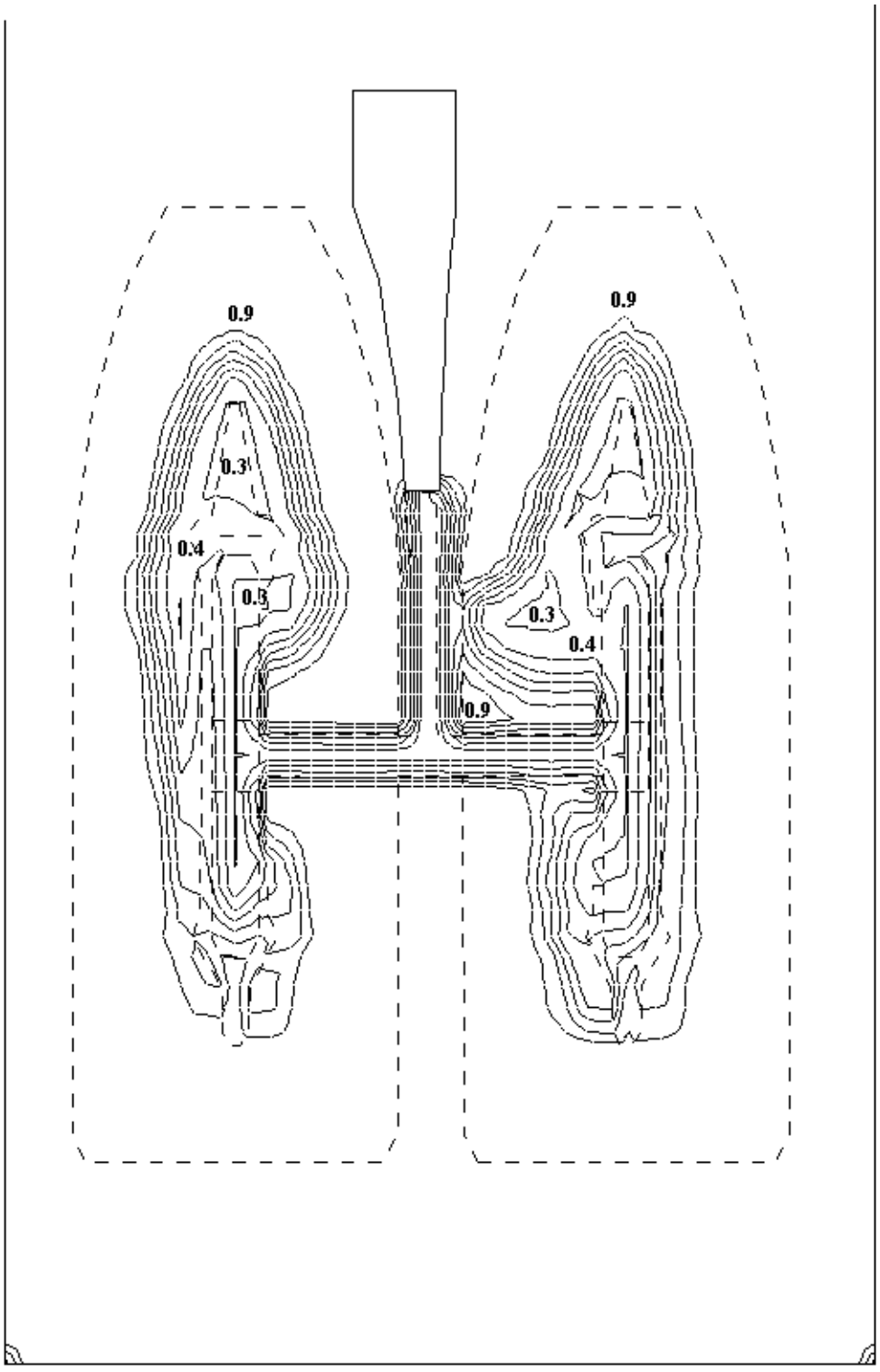

Figure 2-28
Martin Lake Steam Concentration (%) at Air Offtake

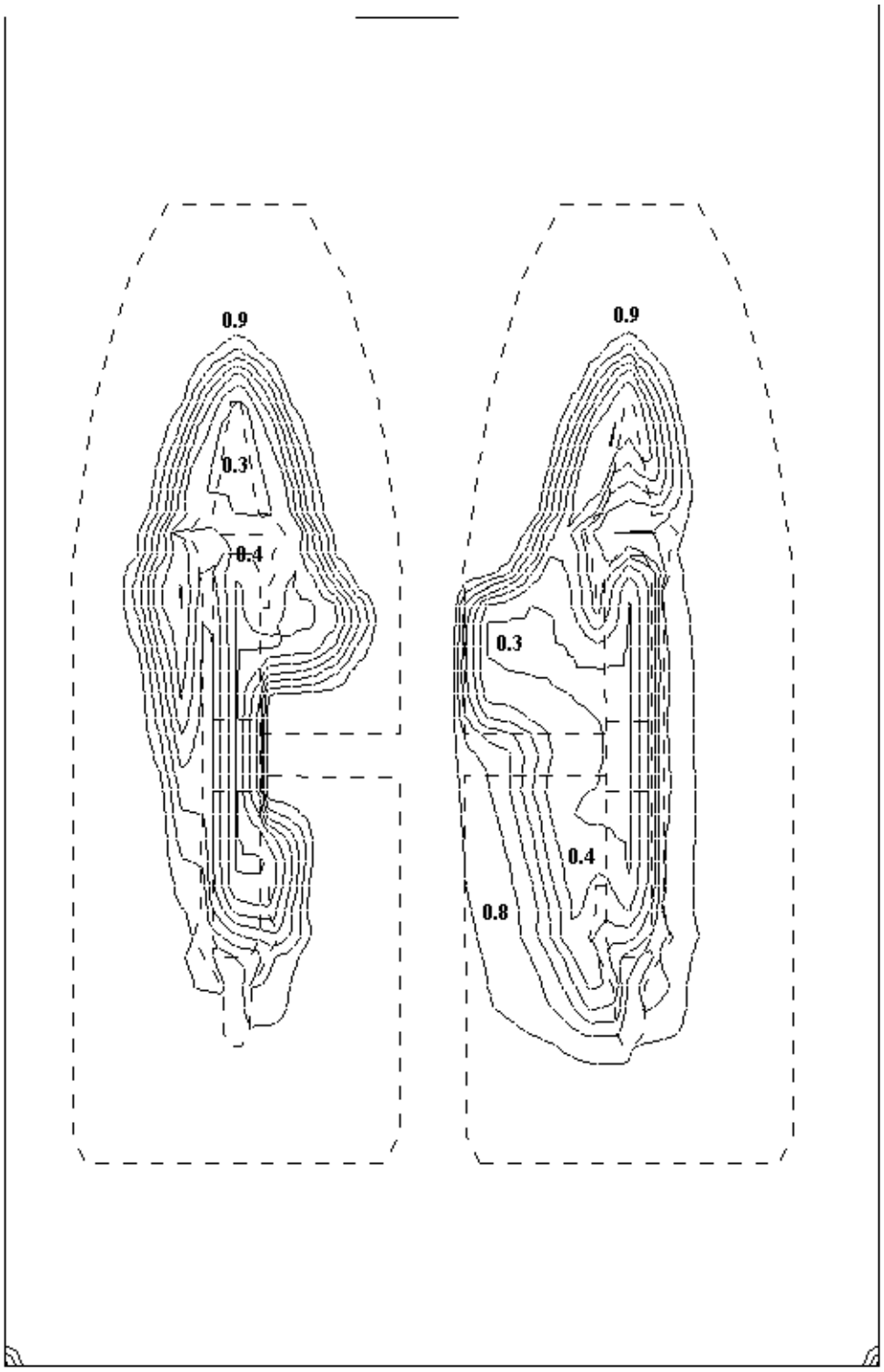

Figure 2-29
Martin Lake Steam Concentration (%) at Z = 3.2m (10.5 ft)

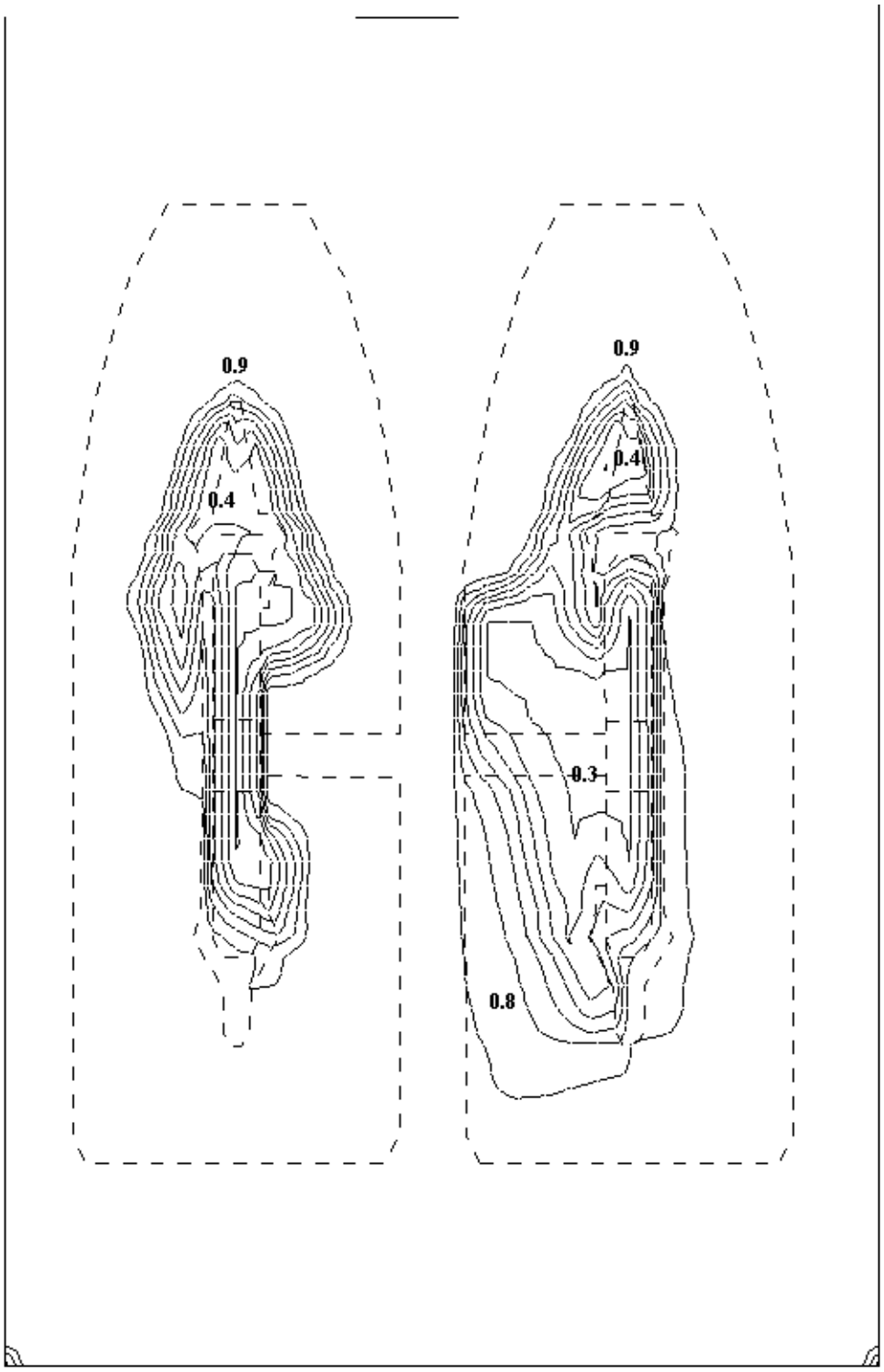

Figure 2-30
Martin Lake Steam Concentration (%) at Z = 6.4m (21 ft)

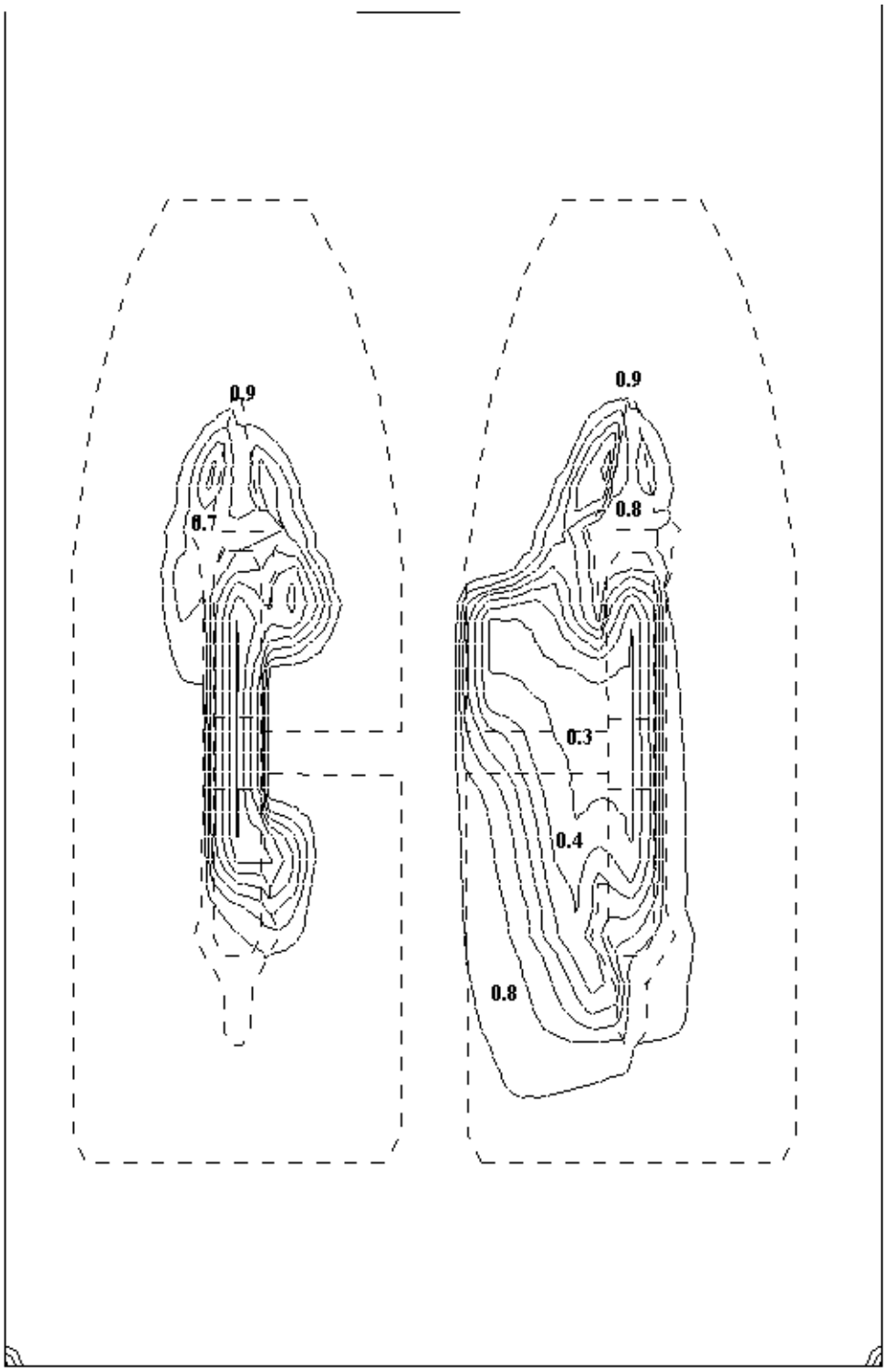

Figure 2-31
Martin Lake Steam Concentration (%) at Z = 9.6m (31.5 ft)

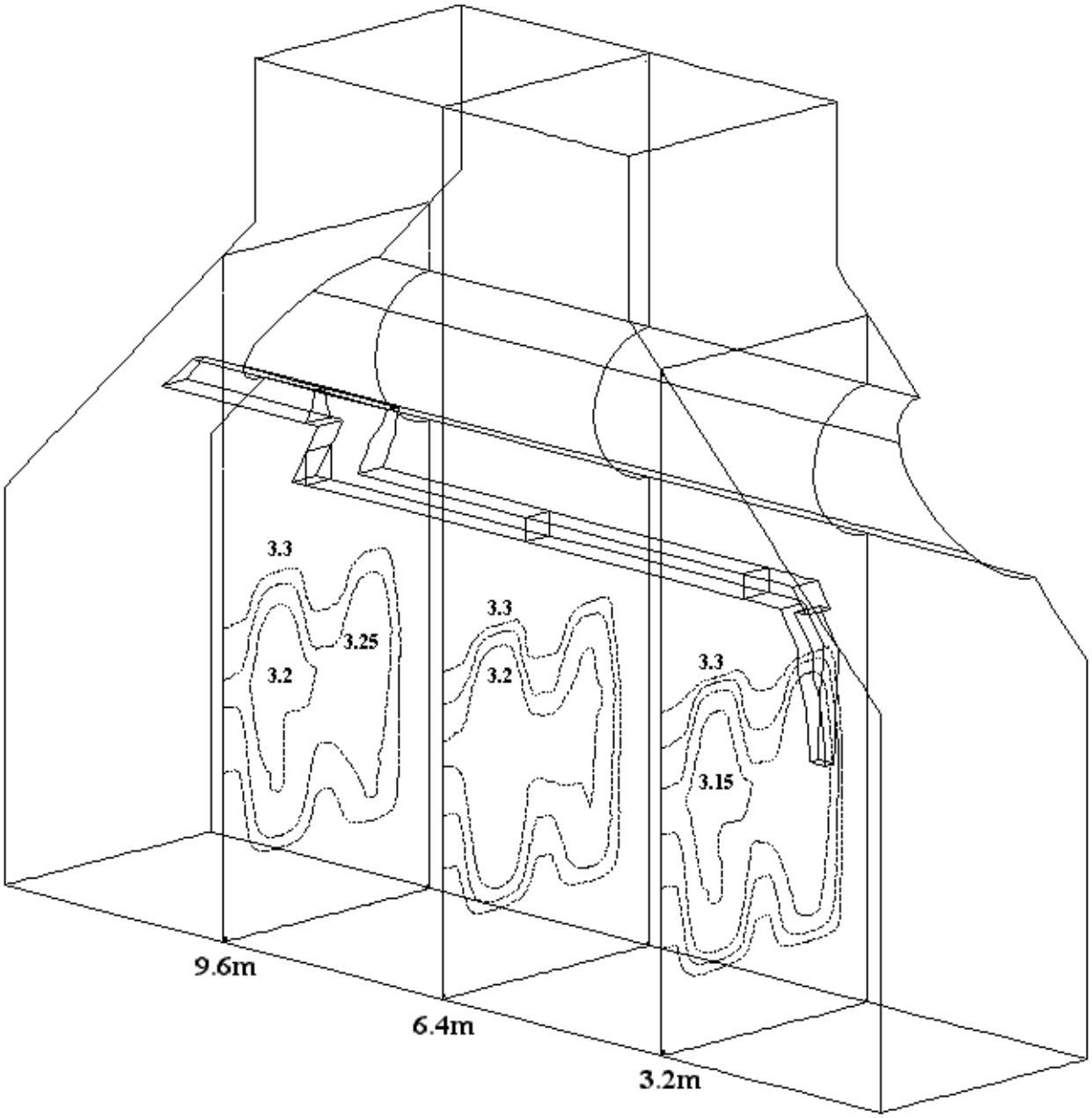

Figure 2-32
Martin Lake Steam Pressures (in Hg) 3-D View

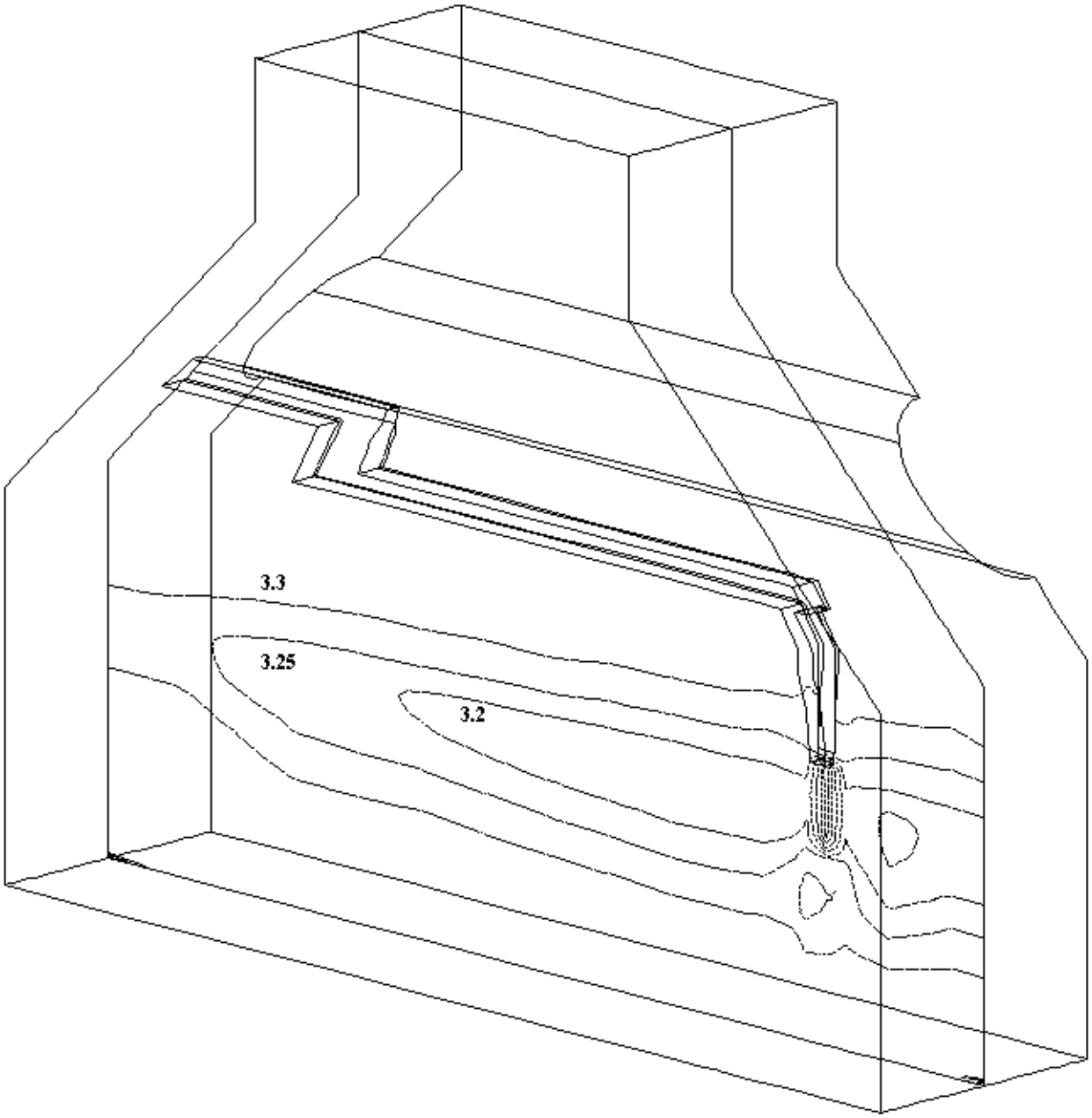

Figure 2-33
Martin Lake Steam Pressures (in Hg) 3-D View

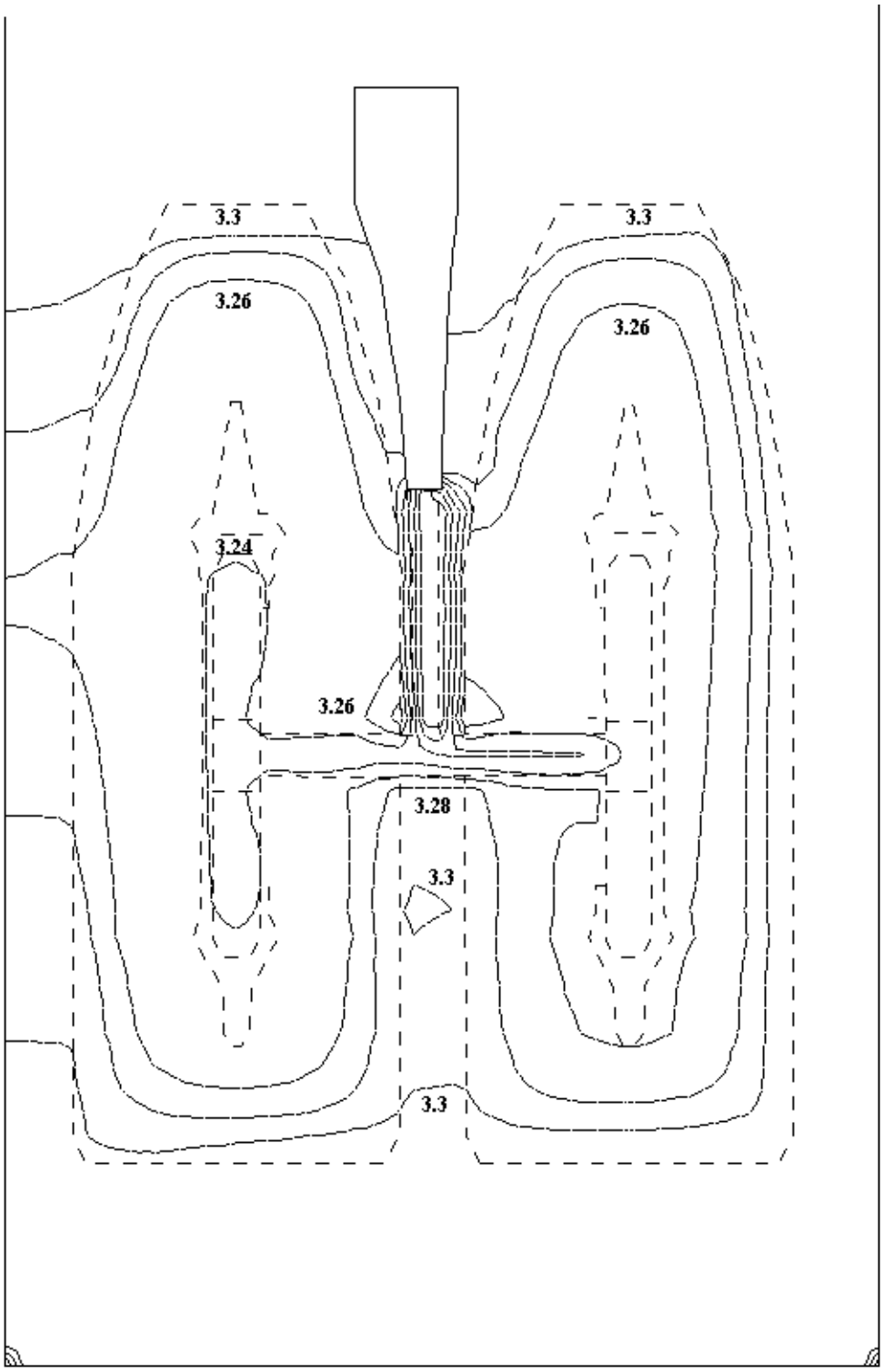

Figure 2-34
Martin Lake Steam Pressures (in Hg) at Air Offtake

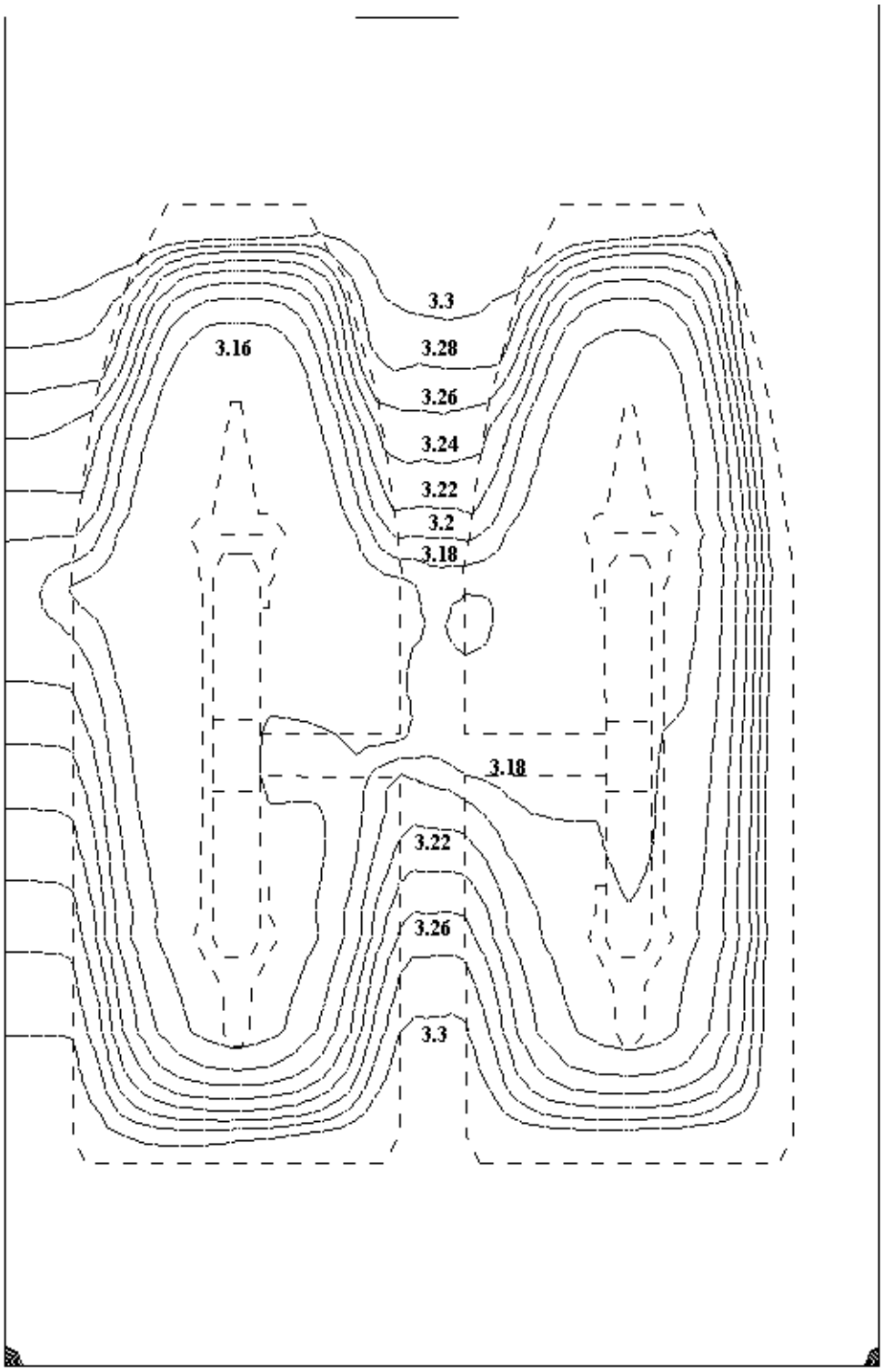

Figure 2-35
Martin Lake Steam Pressures (in Hg) at Z = 3.2m (10.5 ft)

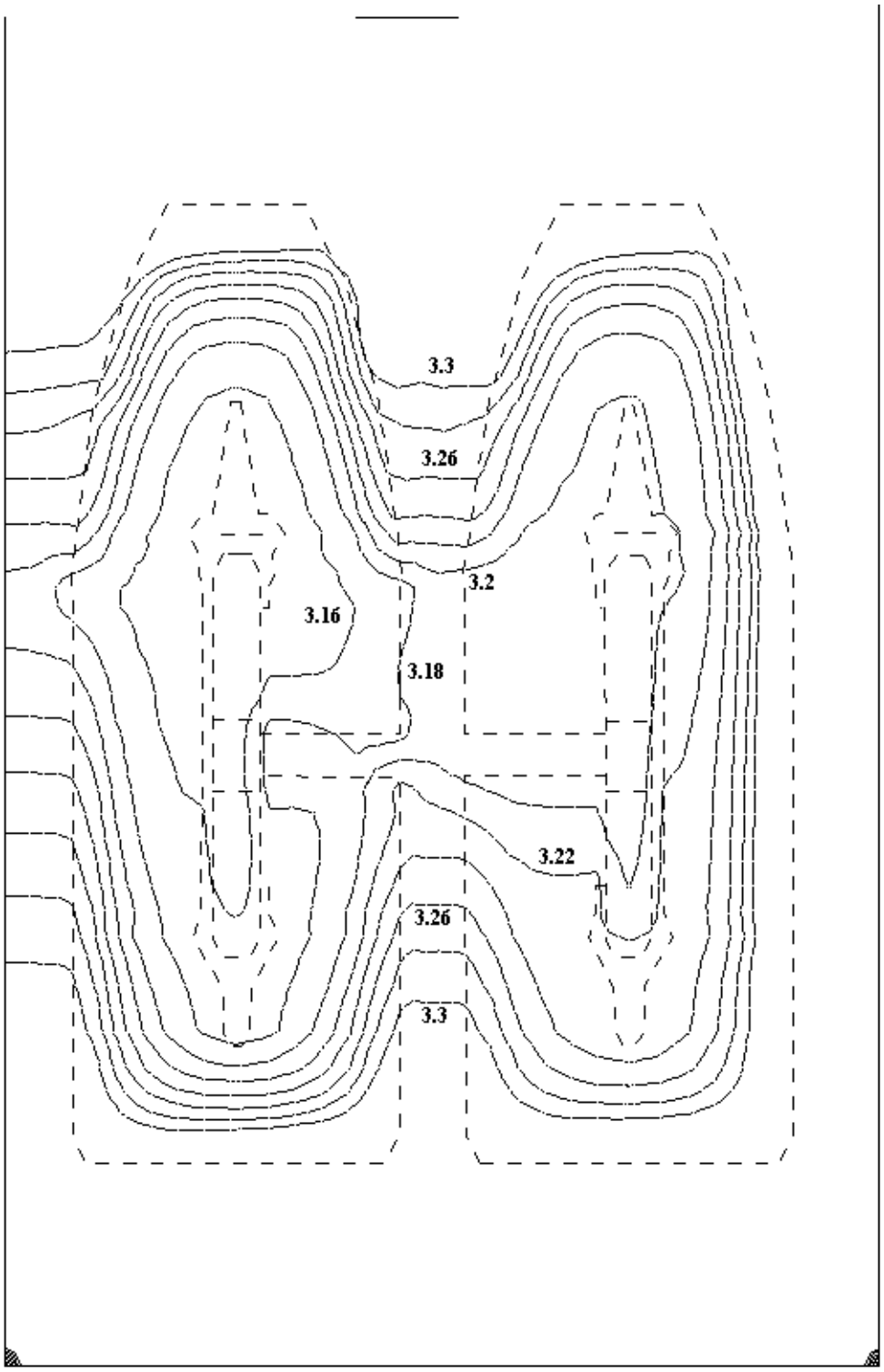

Figure 2-36
Martin Lake Steam Pressures (in Hg) at Z = 6.4m (21 ft)

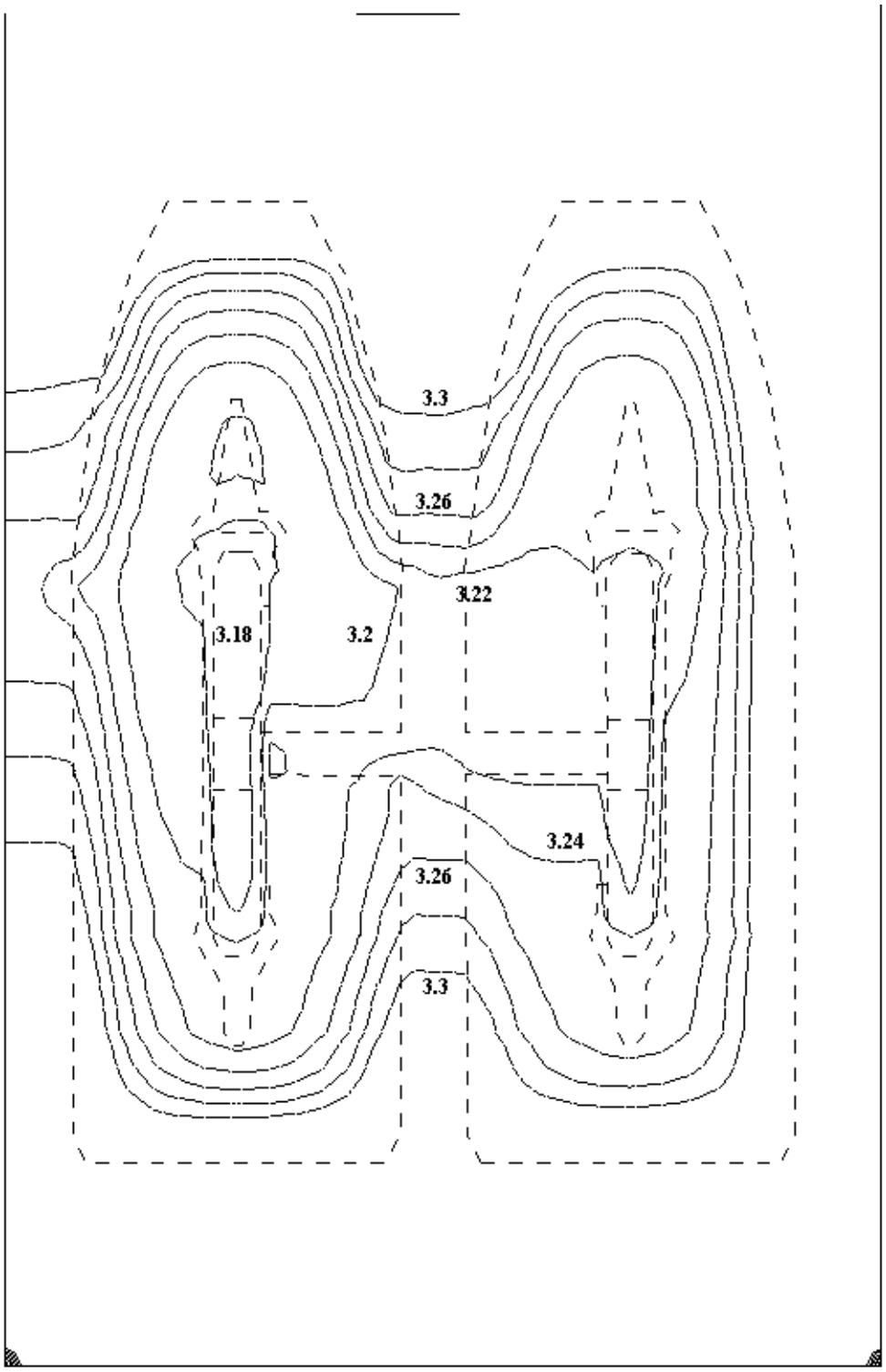

Figure 2-37
Martin Lake Steam Pressures (in Hg) at Z = 9.6m (31.5 ft)

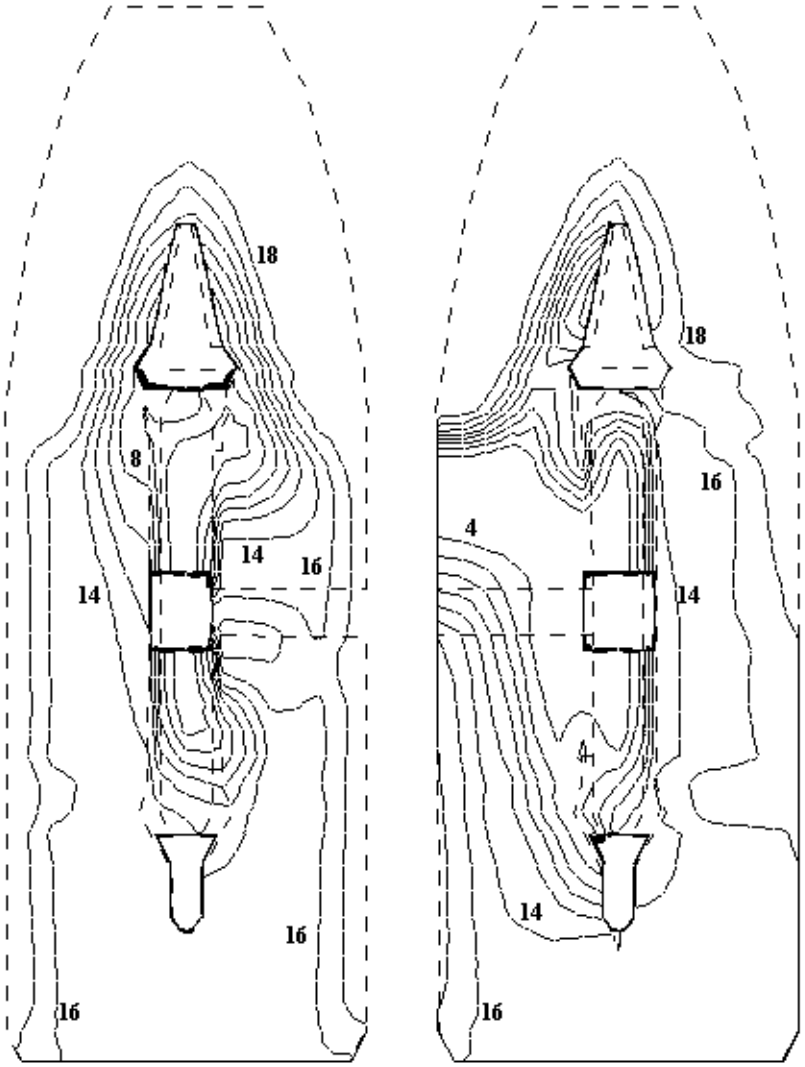

Figure 2-38
Martin Lake Cooling Water Temperature Rise (°F) at Z = 11.75m (38.5 ft)

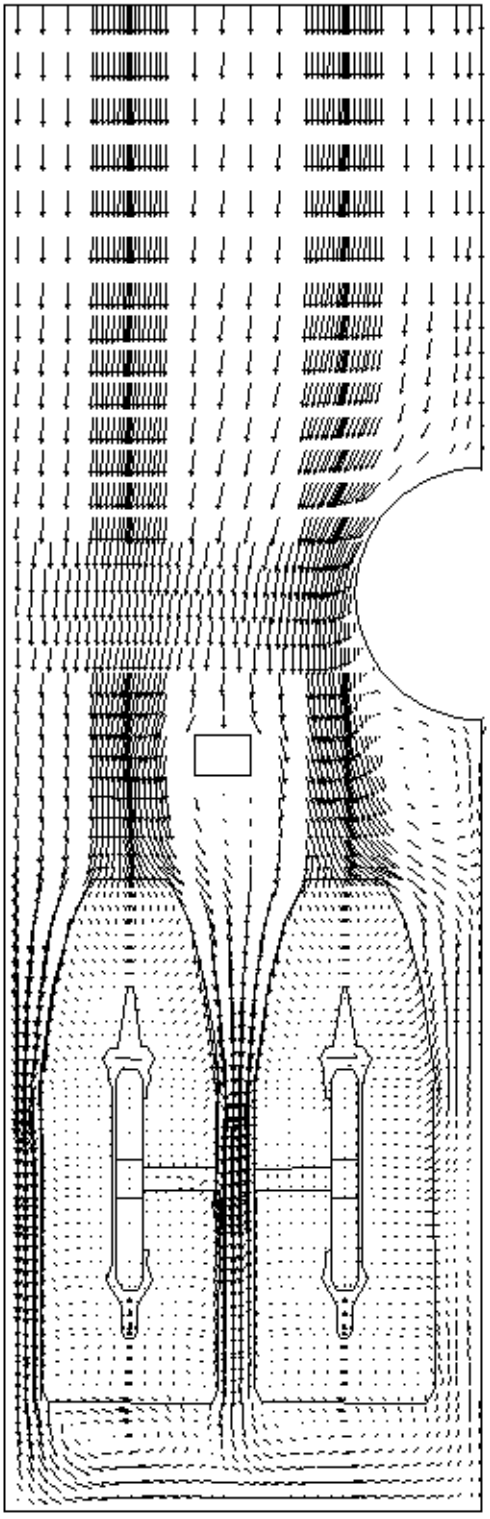

Figure 2-39
Martin Lake Velocity Vectors at Z = 6.4m (21 ft)

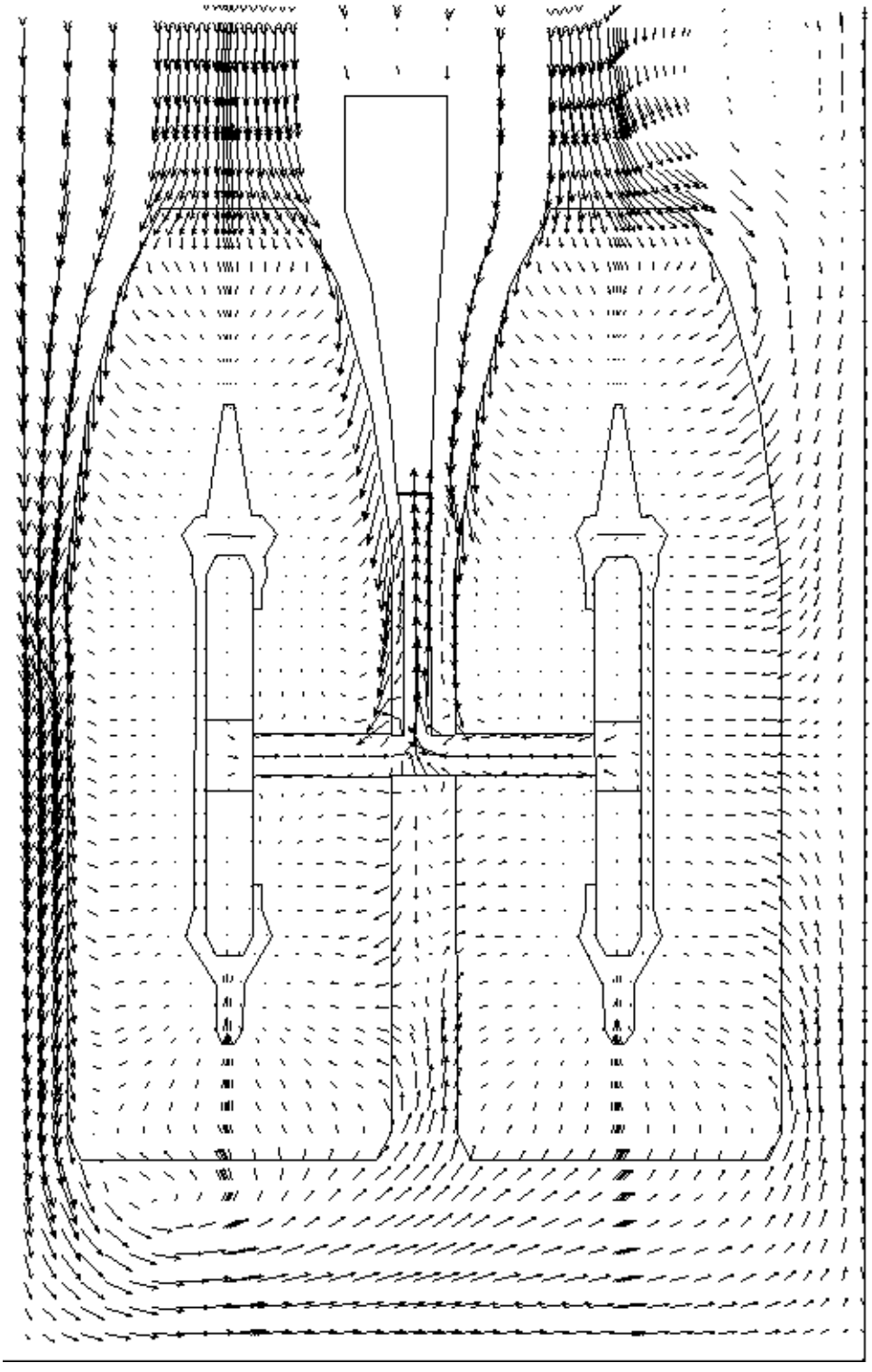

Figure 2-40
Martin Lake Velocity Vectors at Air Offtake

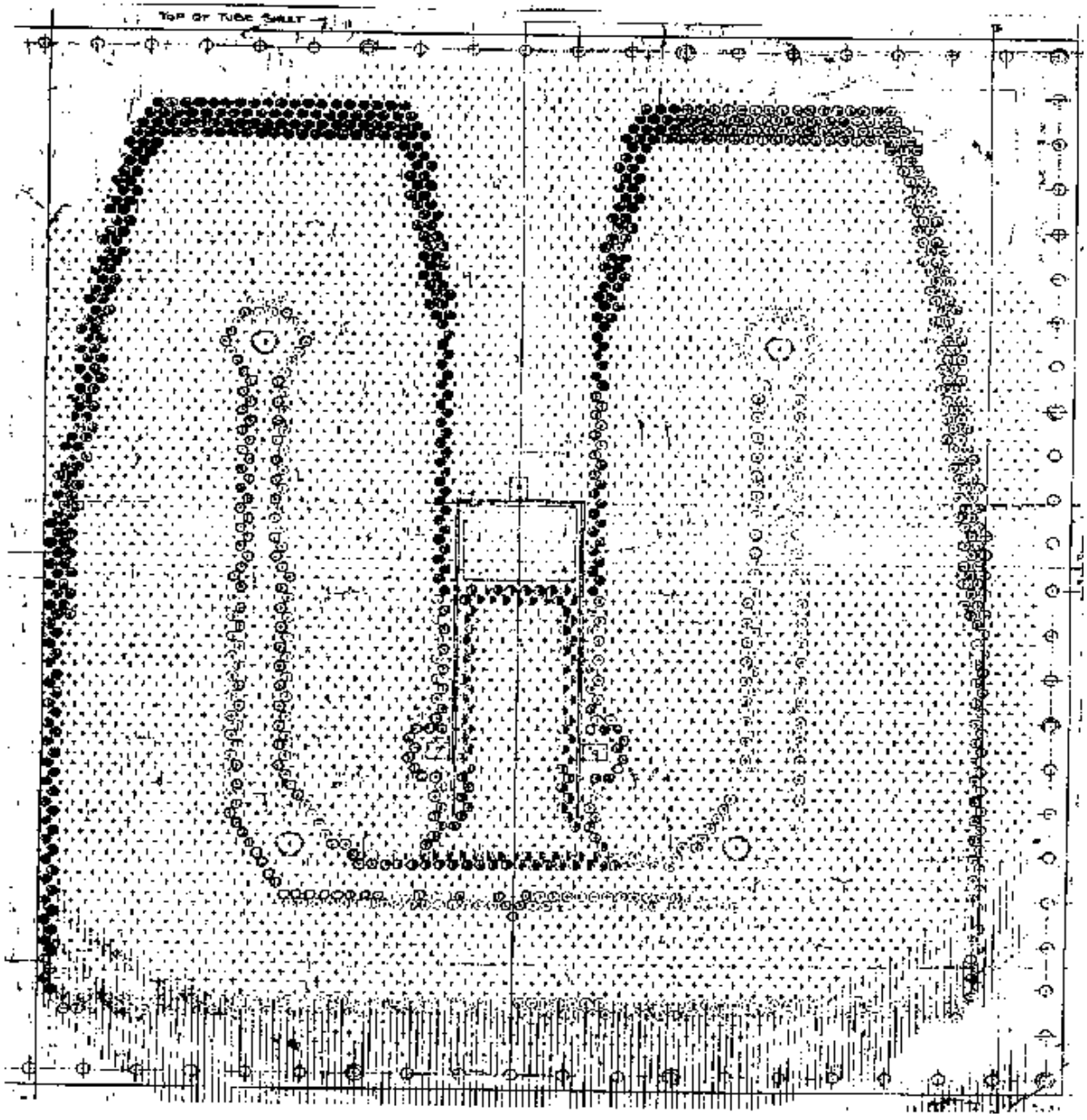

Figure 2-41
Stryker Creek Tube Nest

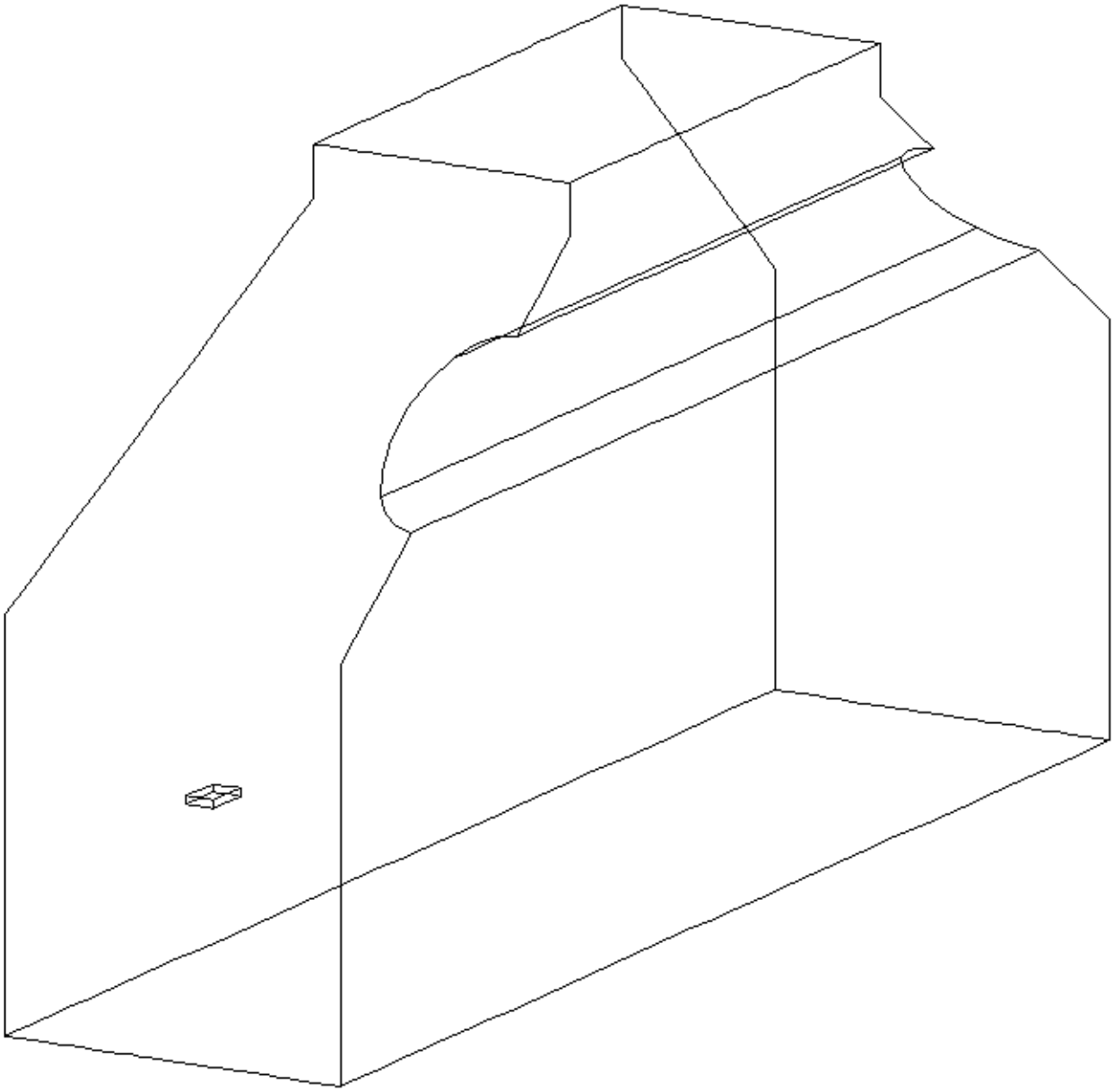

Figure 2-42
Stryker Creek Condenser 3-D View

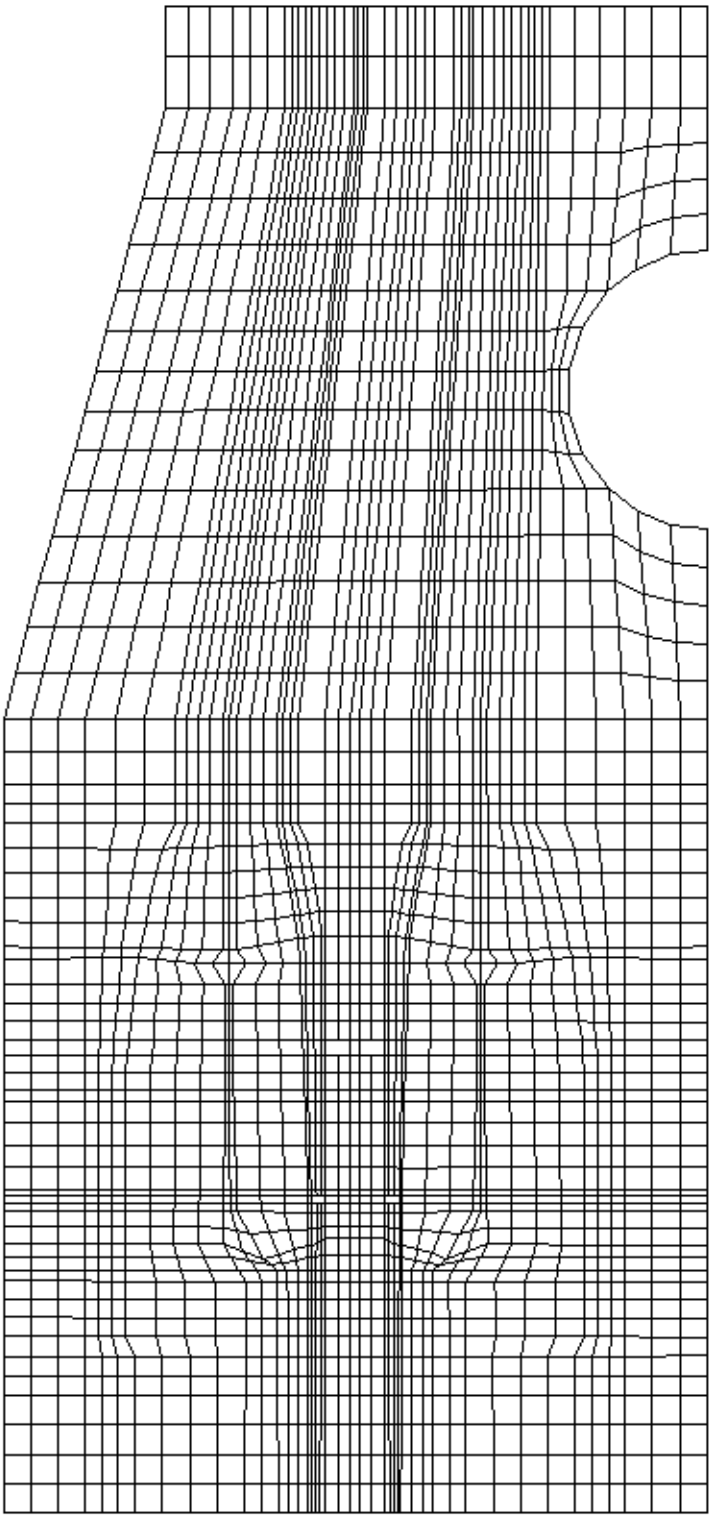

Figure 2-43
Stryker Creek Grid

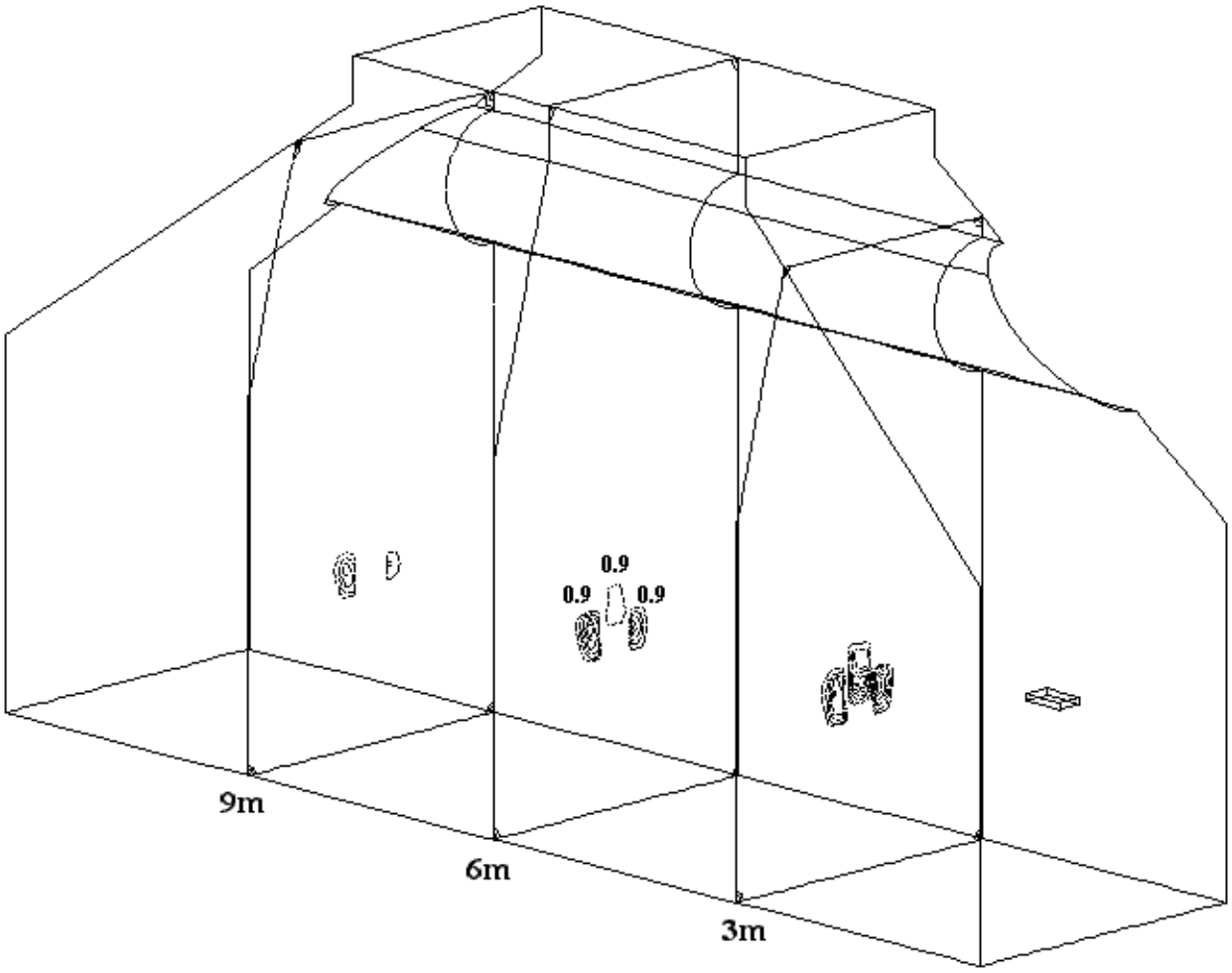

Figure 2-44
Stryker Creek Steam Concentration (%) 3-D View

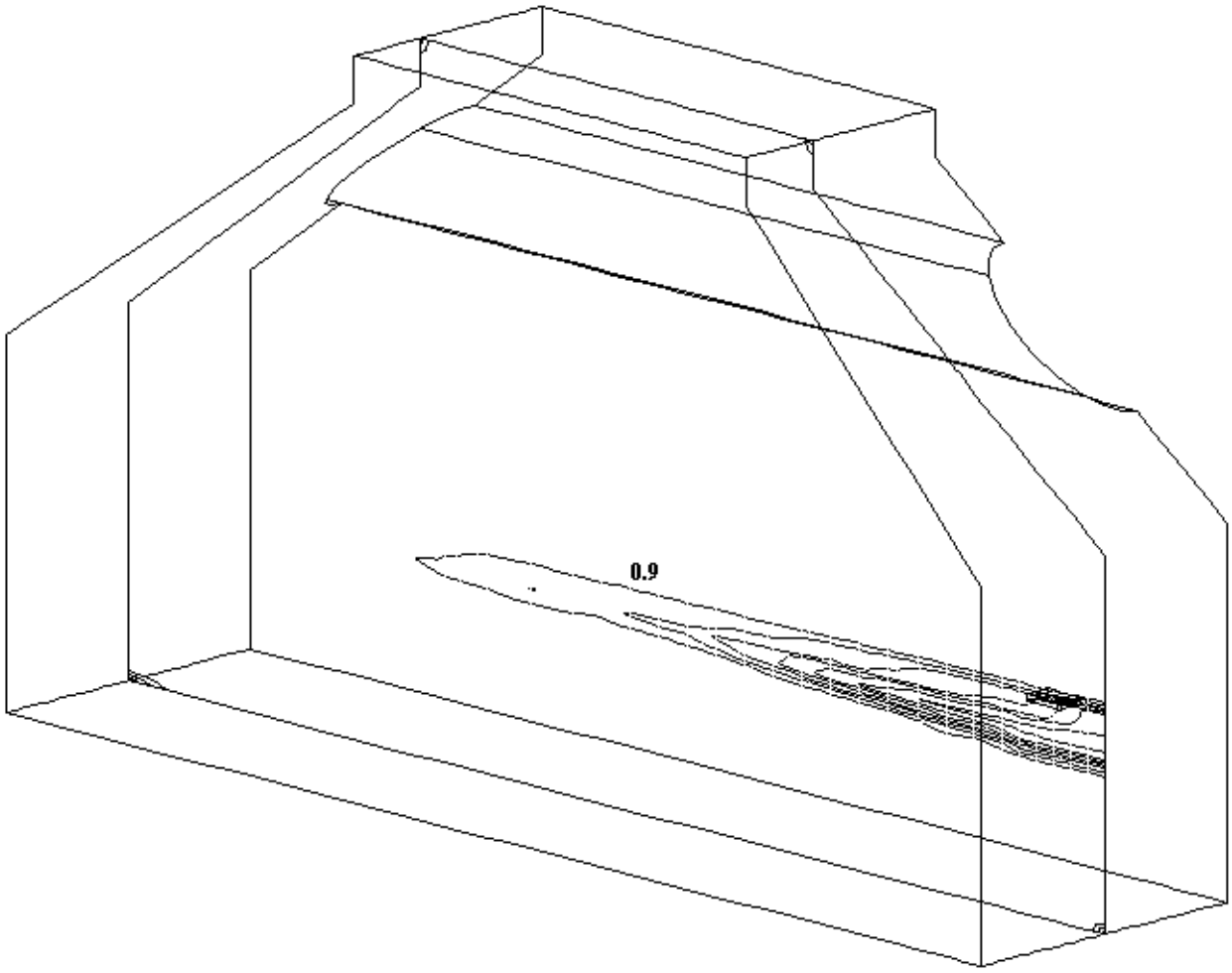

Figure 2-45
Stryker Creek Steam Concentration (%) 3-D View

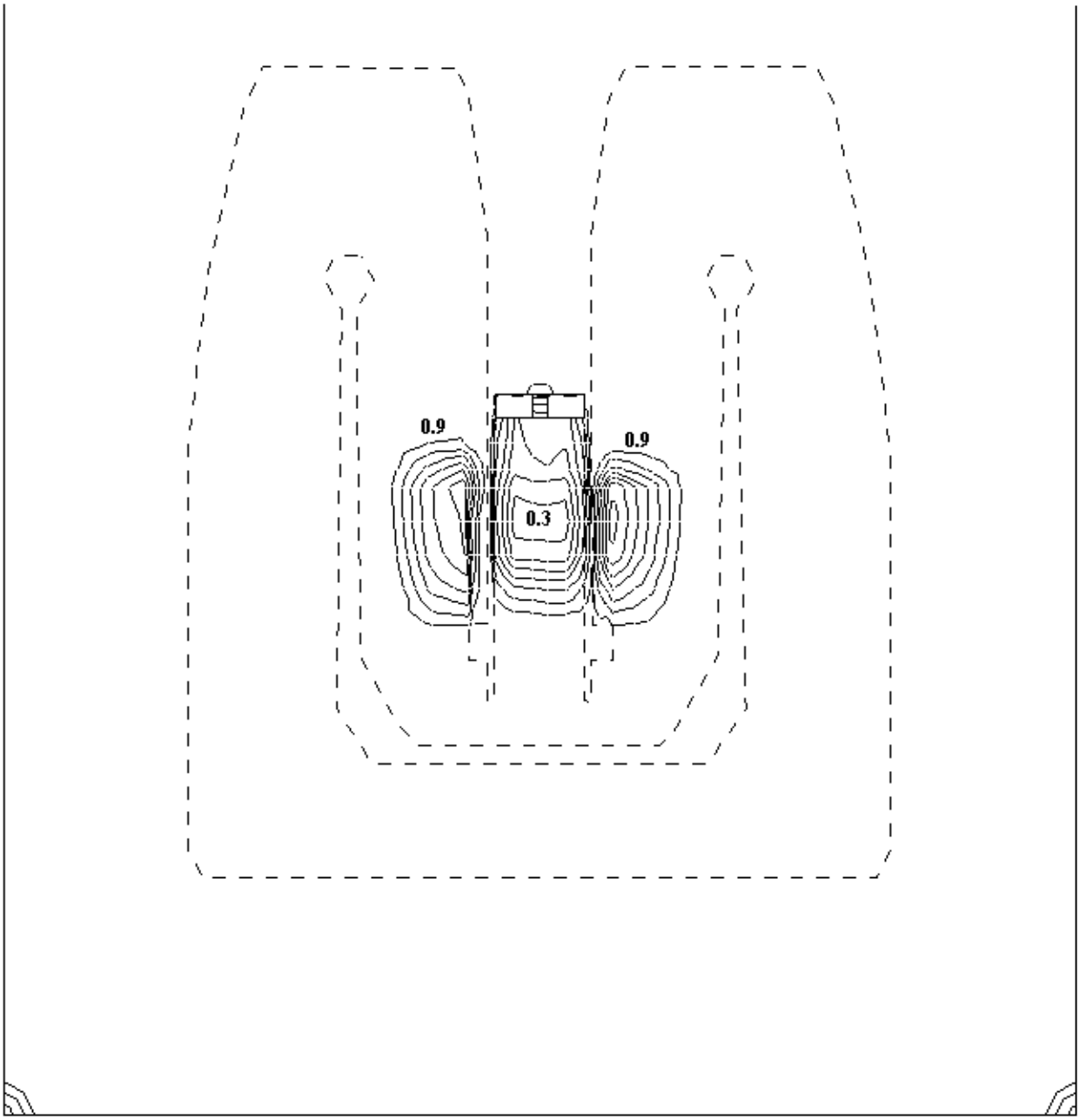

Figure 2-46
Stryker Creek Steam Concentration (%) at Air Offtake

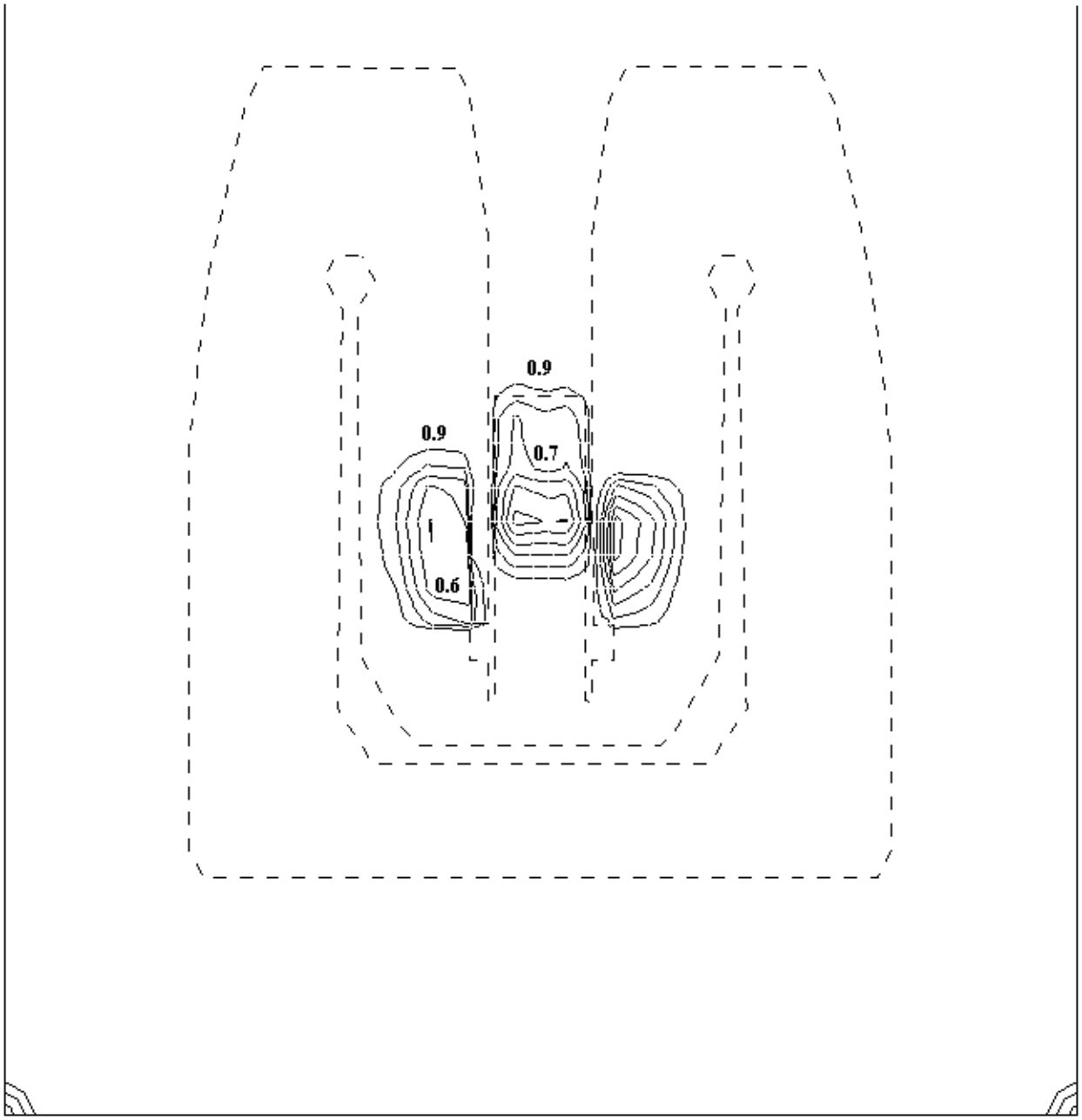

Figure 2-47
Stryker Creek Steam Concentration (%) at Z = 3m (9.8 ft)

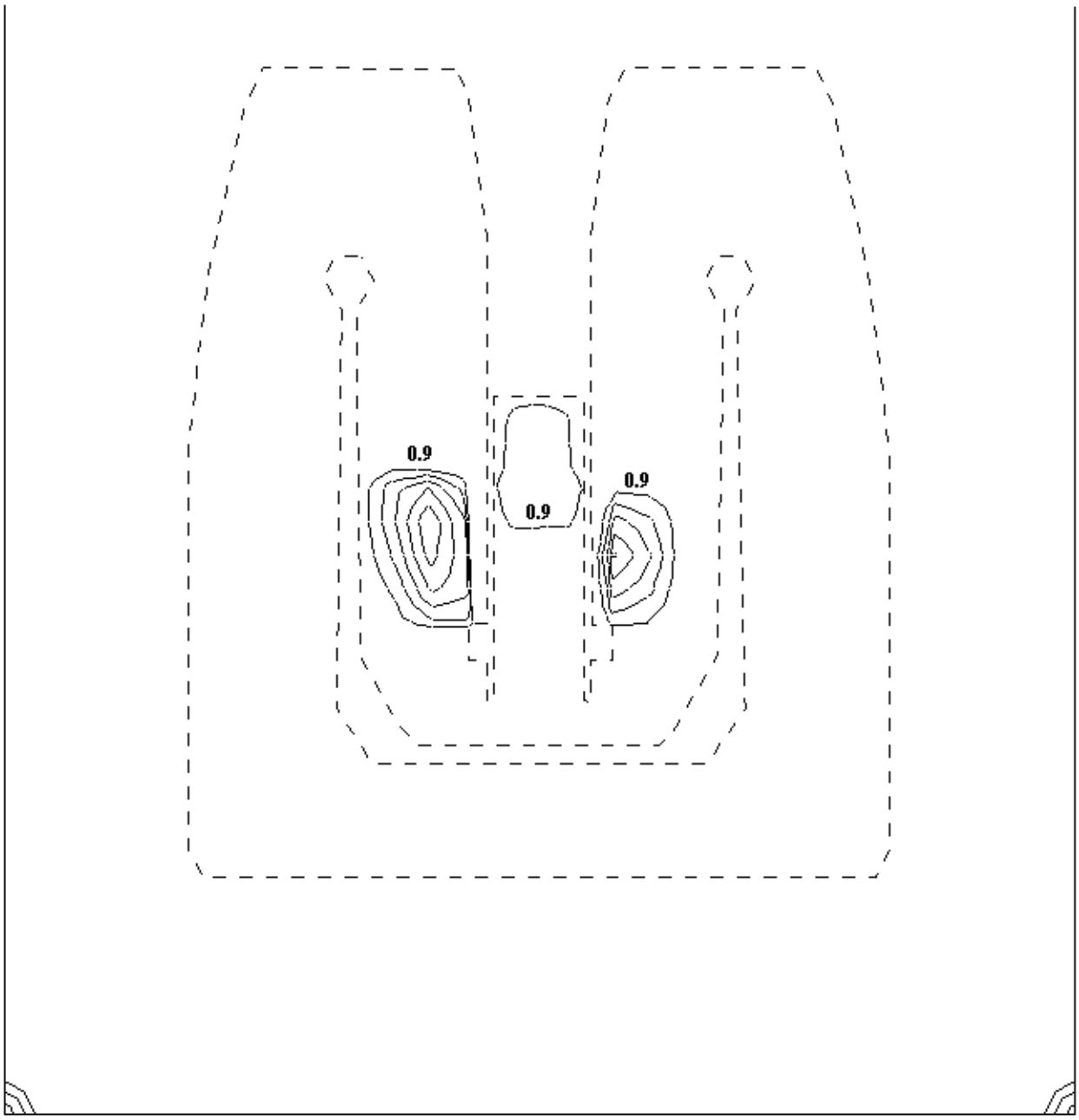

Figure 2-48
Stryker Creek Steam Concentration (%) at Z = 6m (19.7 ft)

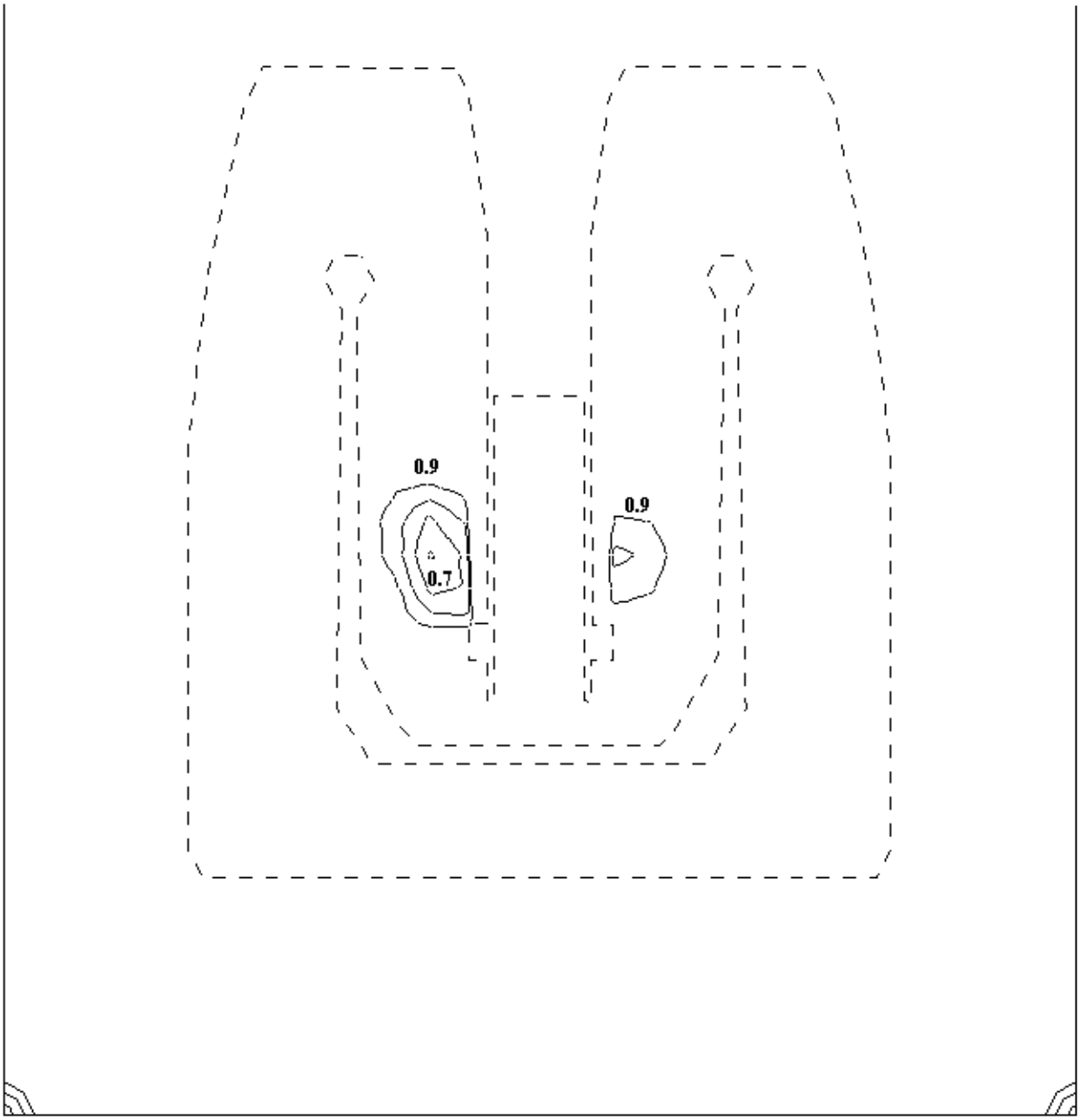

Figure 2-49
Stryker Creek Steam Concentration (%) at Z = 9m (29.5 ft)

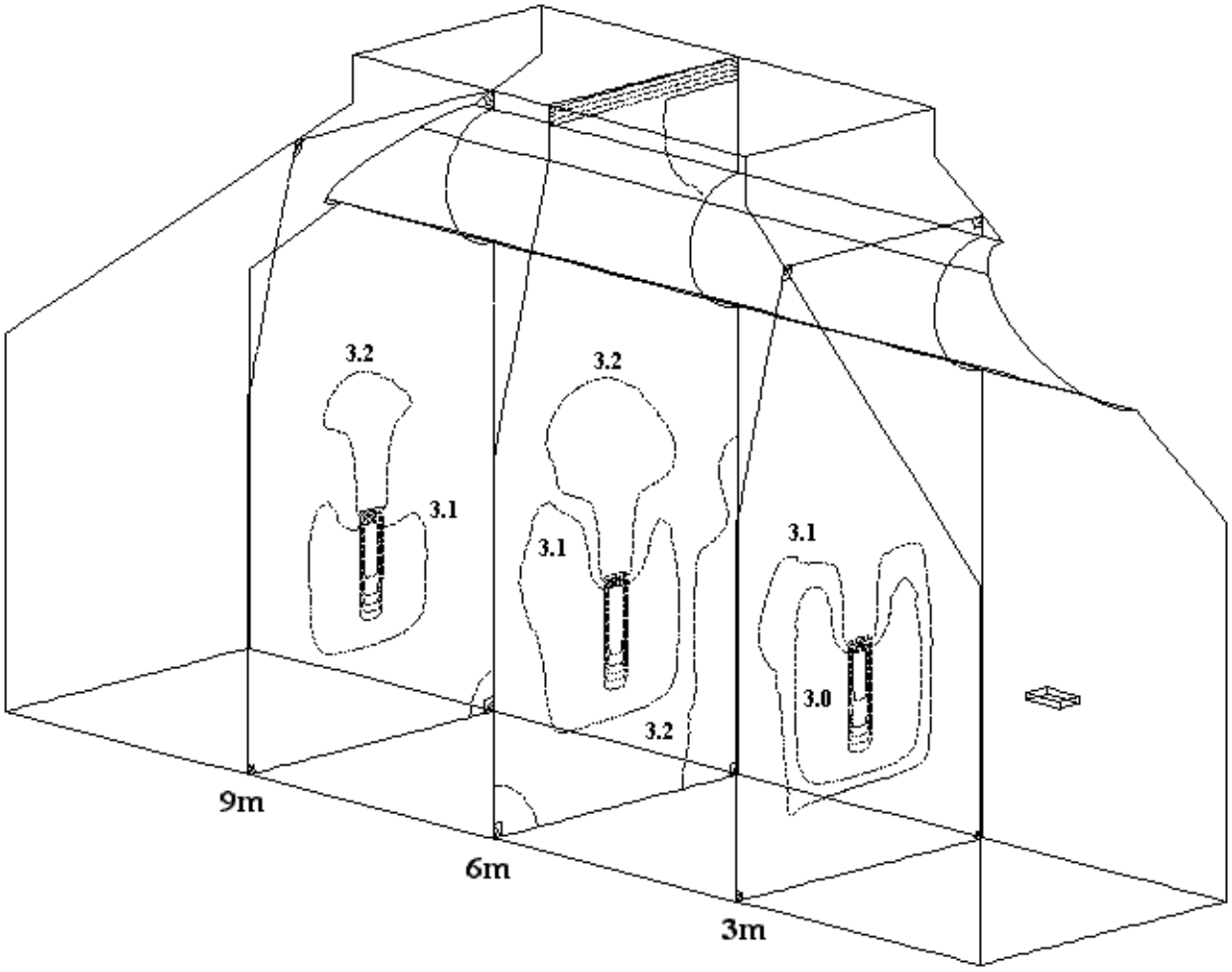

Figure 2-50
Stryker Creek Steam Pressures (in Hg) 3-D View

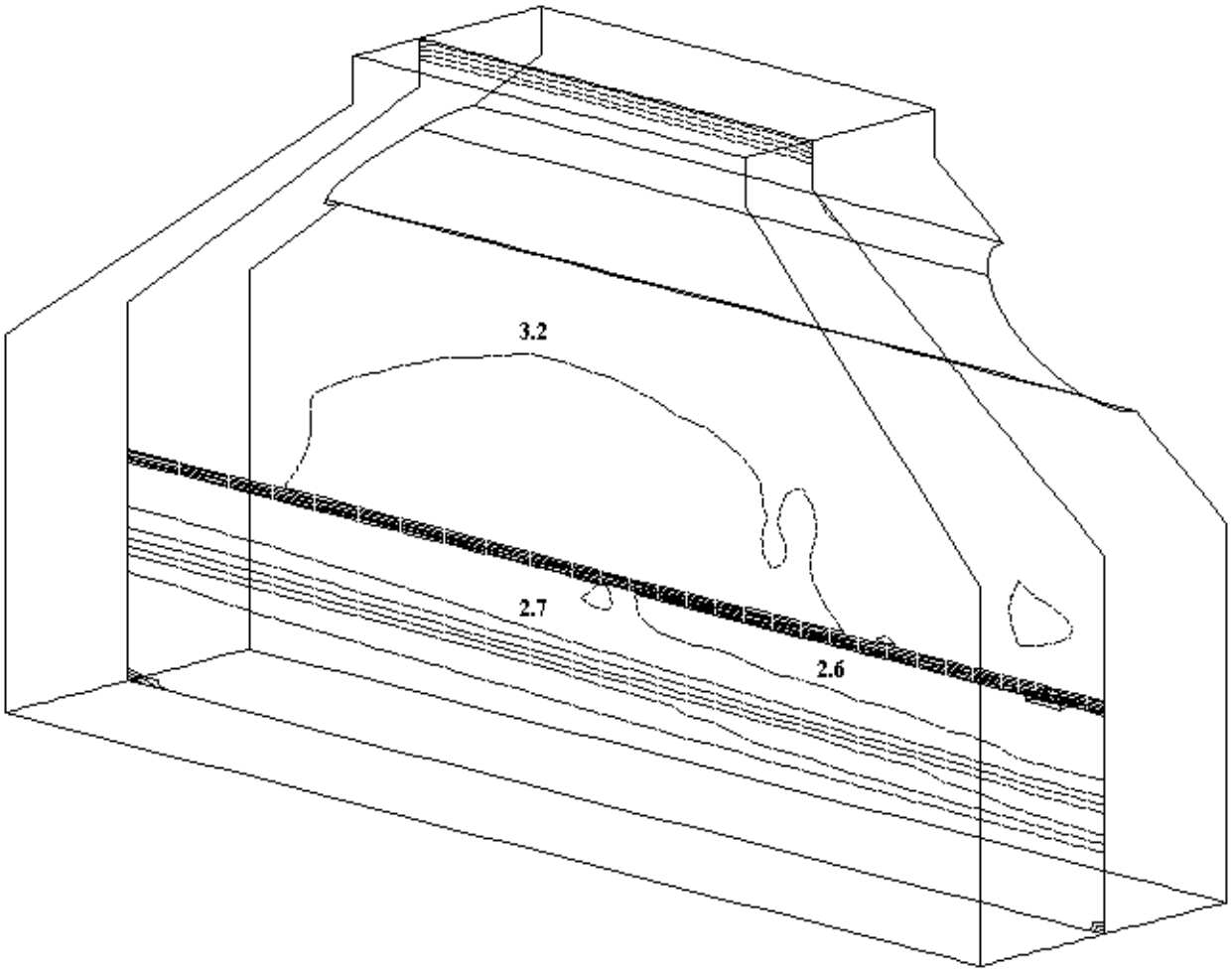

Figure 2-51
Stryker Creek Steam Pressures (in Hg) 3-D View

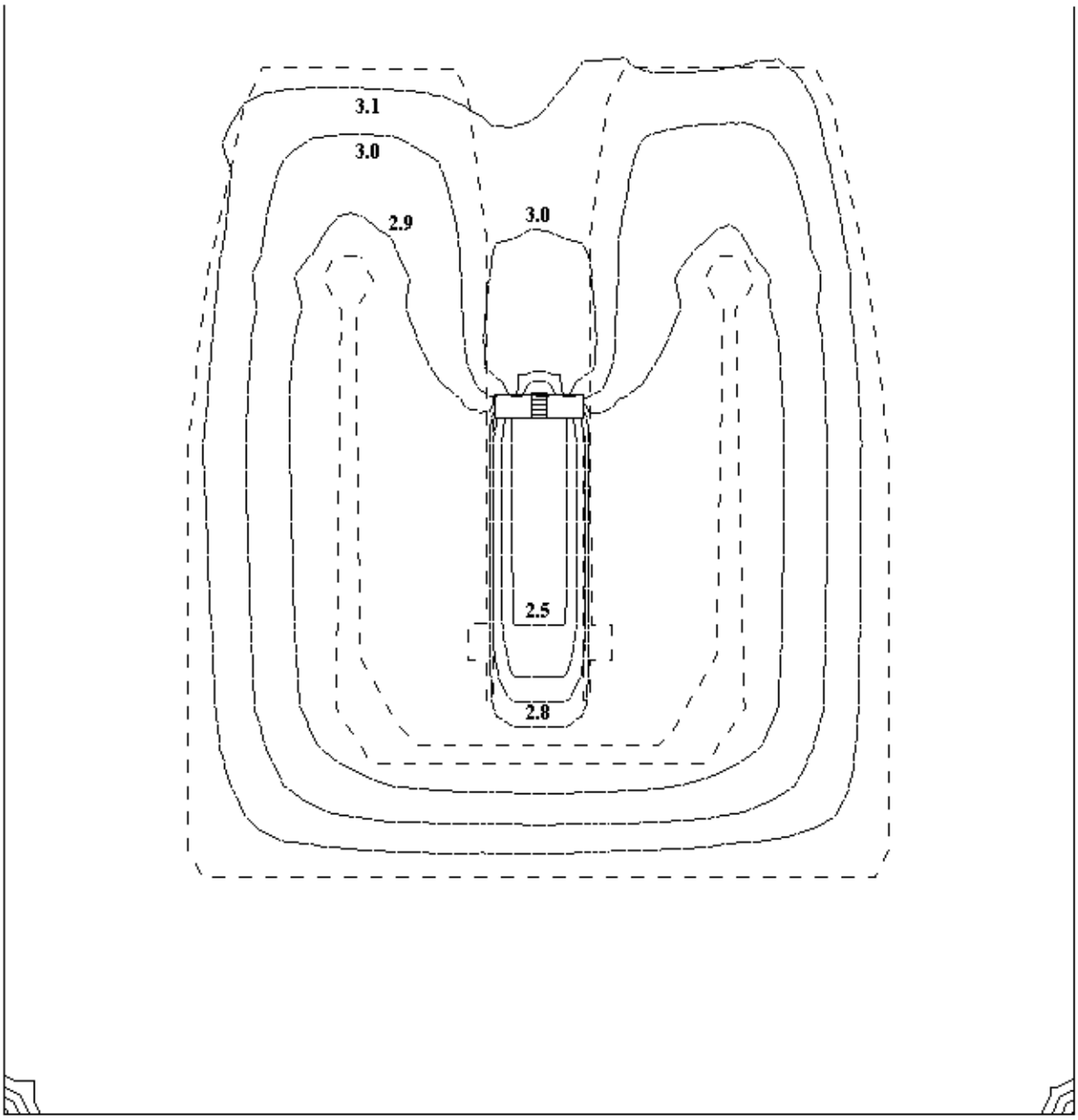

Figure 2-52
Stryker Creek Steam Pressures (in Hg) at Air Offtake

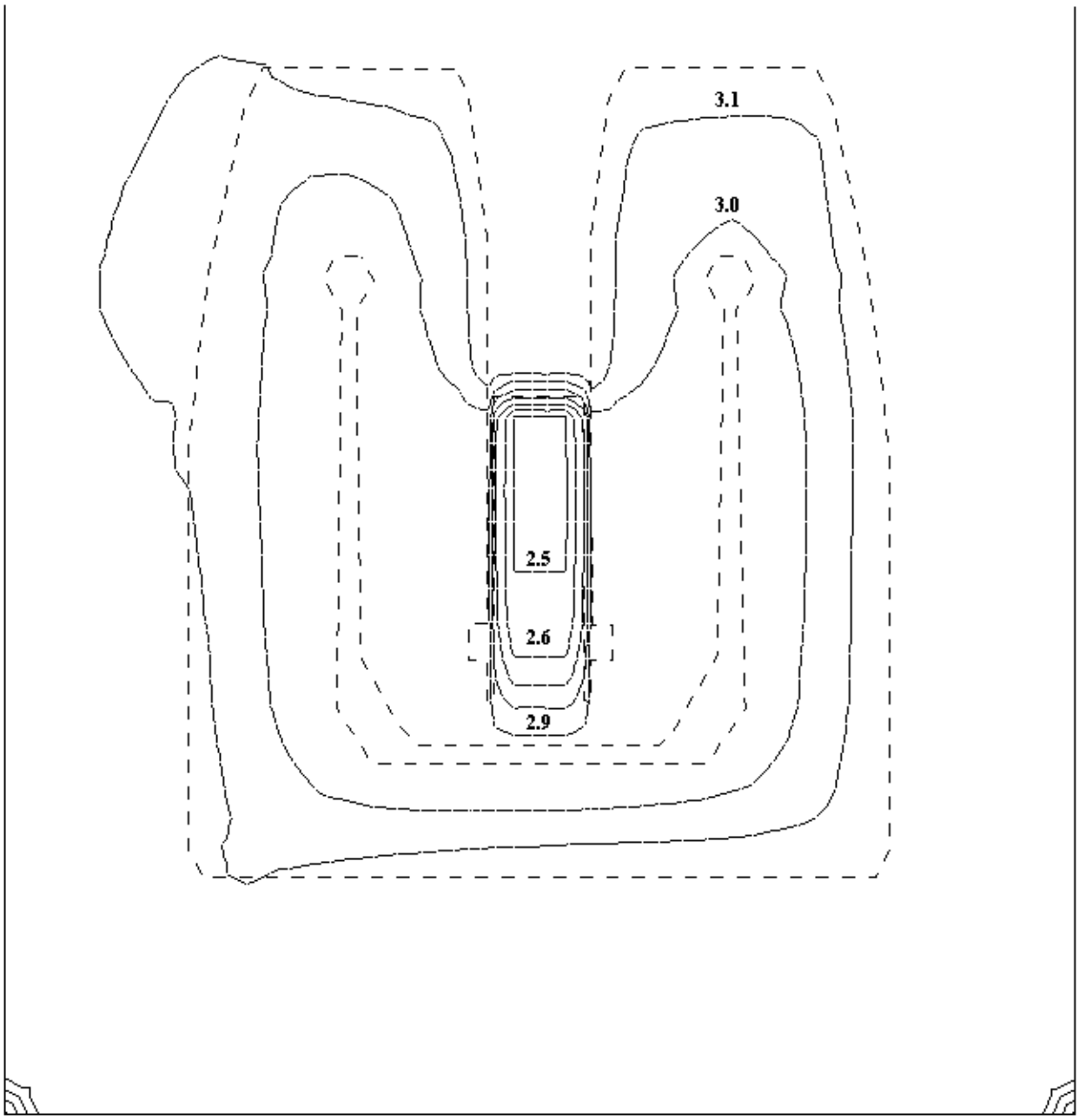

Figure 2-53
Stryker Creek Steam Pressures (in Hg) at Z = 3m (9.8 ft)

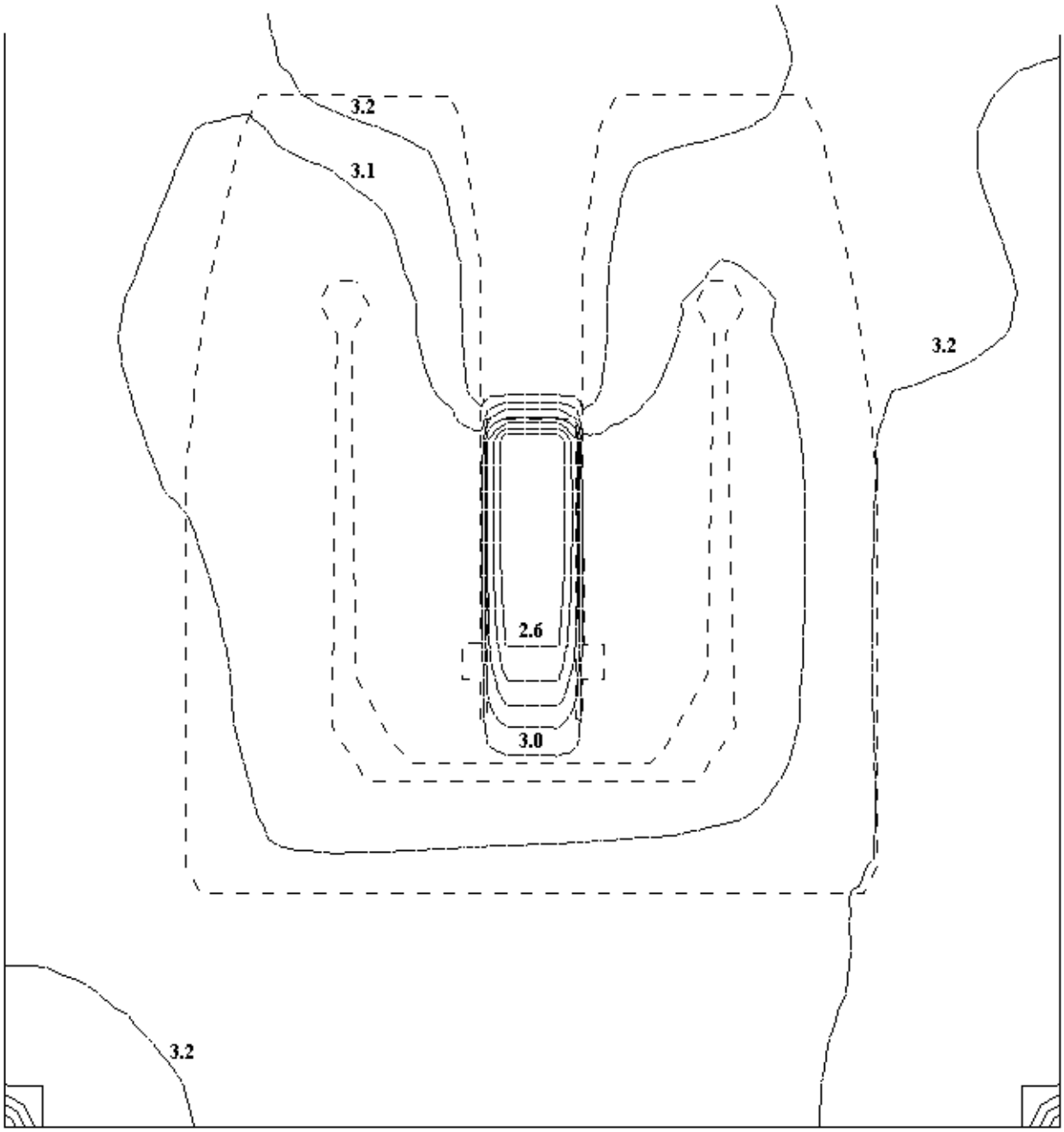

Figure 2-54
Stryker Creek Steam Pressures (in Hg) at Z = 6m (19.7 ft)

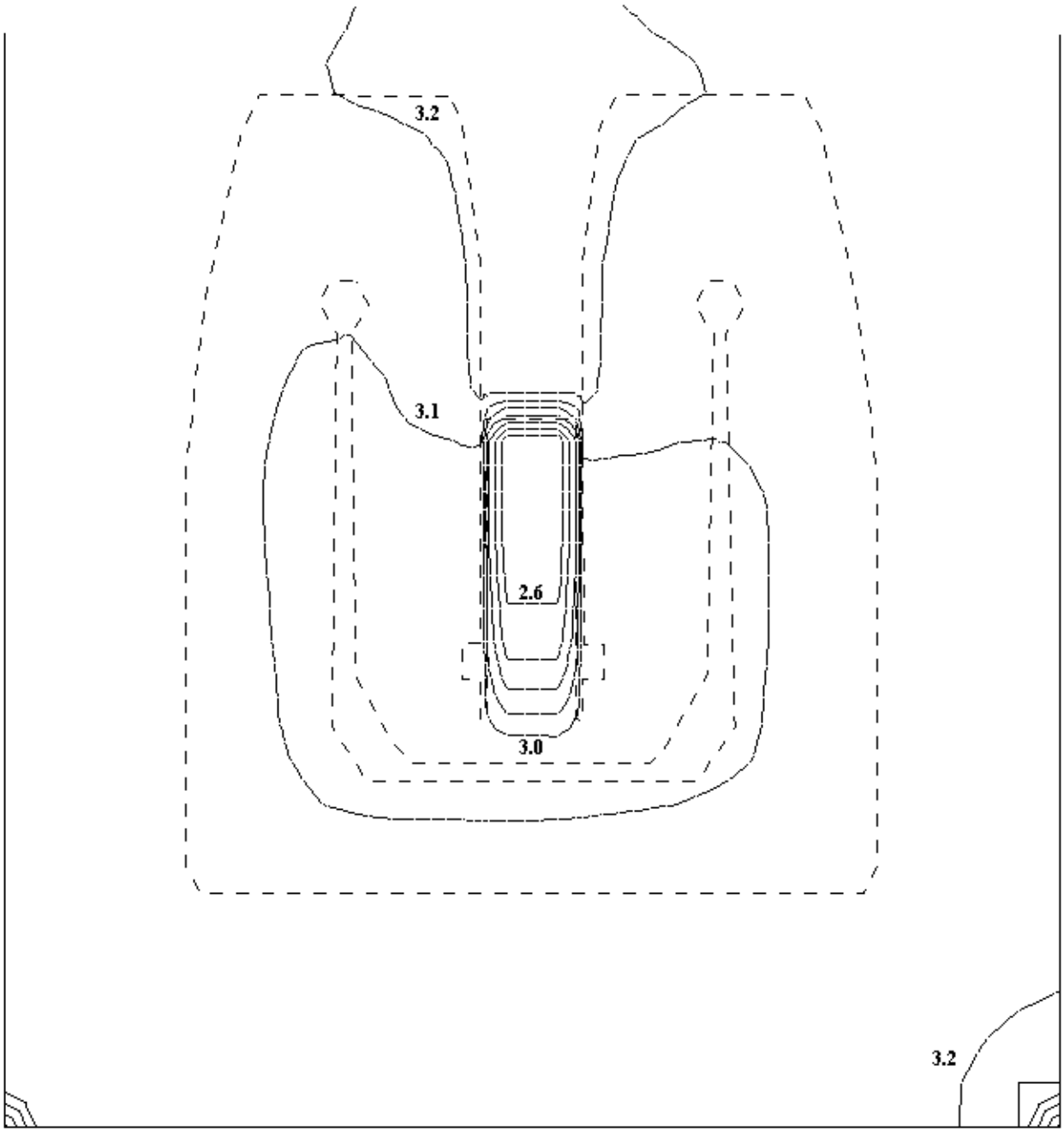

Figure 2-55
Stryker Creek Steam Pressures (in Hg) at Z = 9m (29.5 ft)

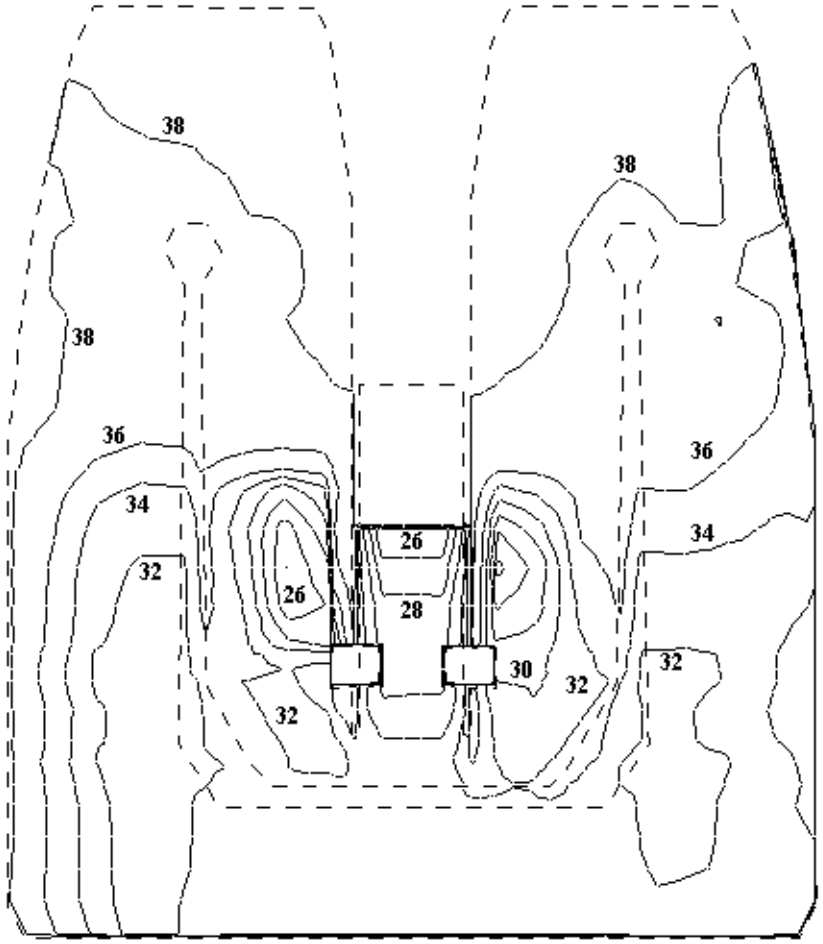

Figure 2-56
Stryker Creek Cooling Water Temperature Rise (°F) at Z = 11.5m (37.7 ft)

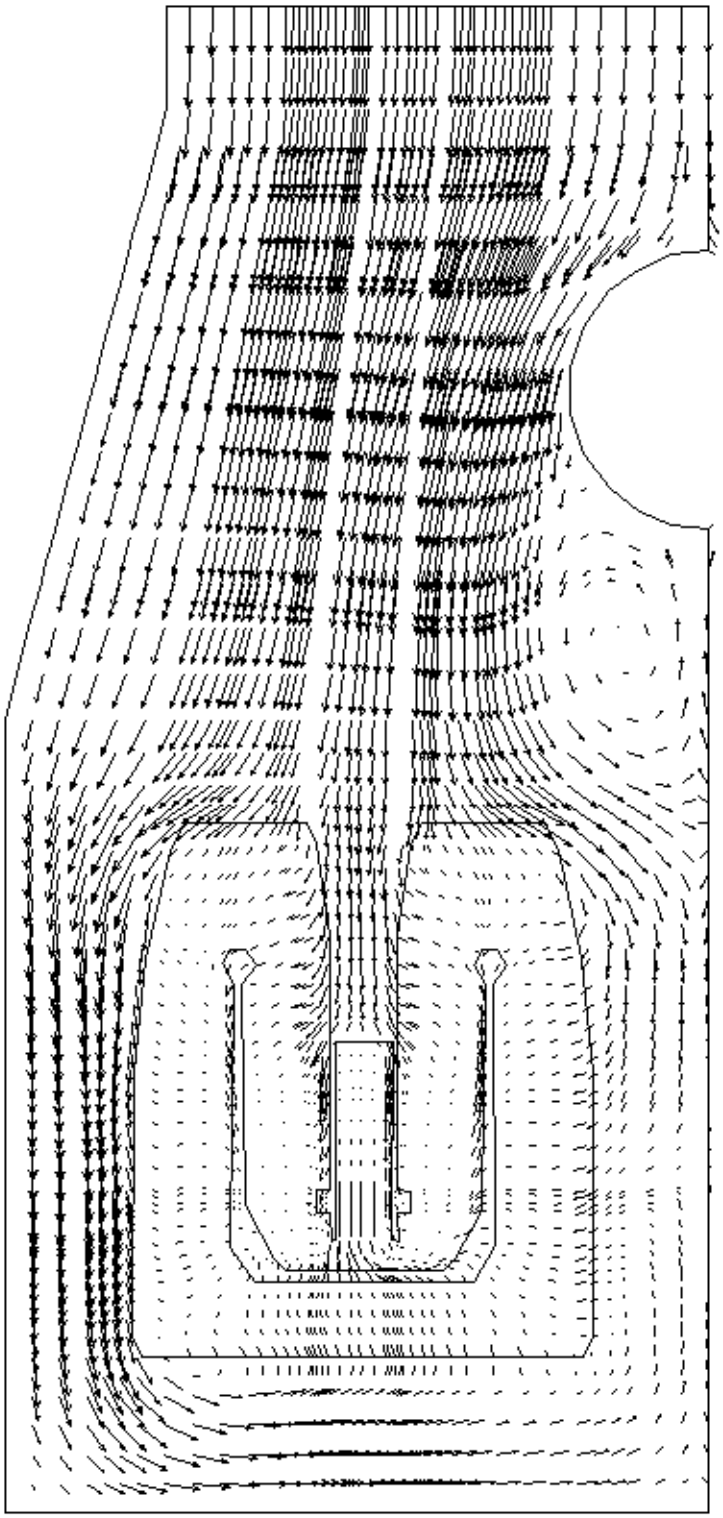

Figure 2-57
Stryker Creek Velocity Vectors at Z = 6m (19.7 ft)

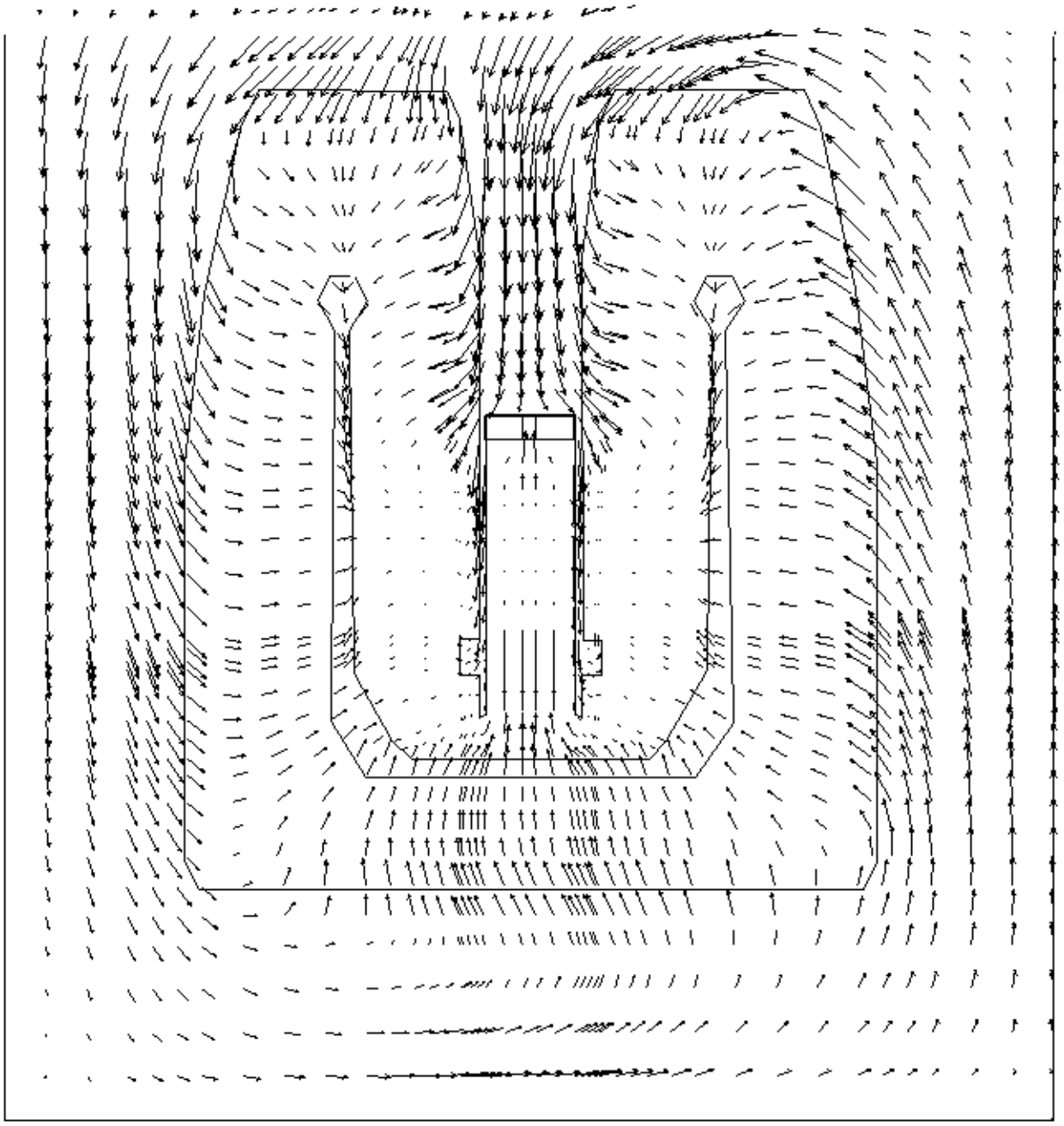

Figure 2-58
Stryker Creek Velocity Vectors at Air Offtake

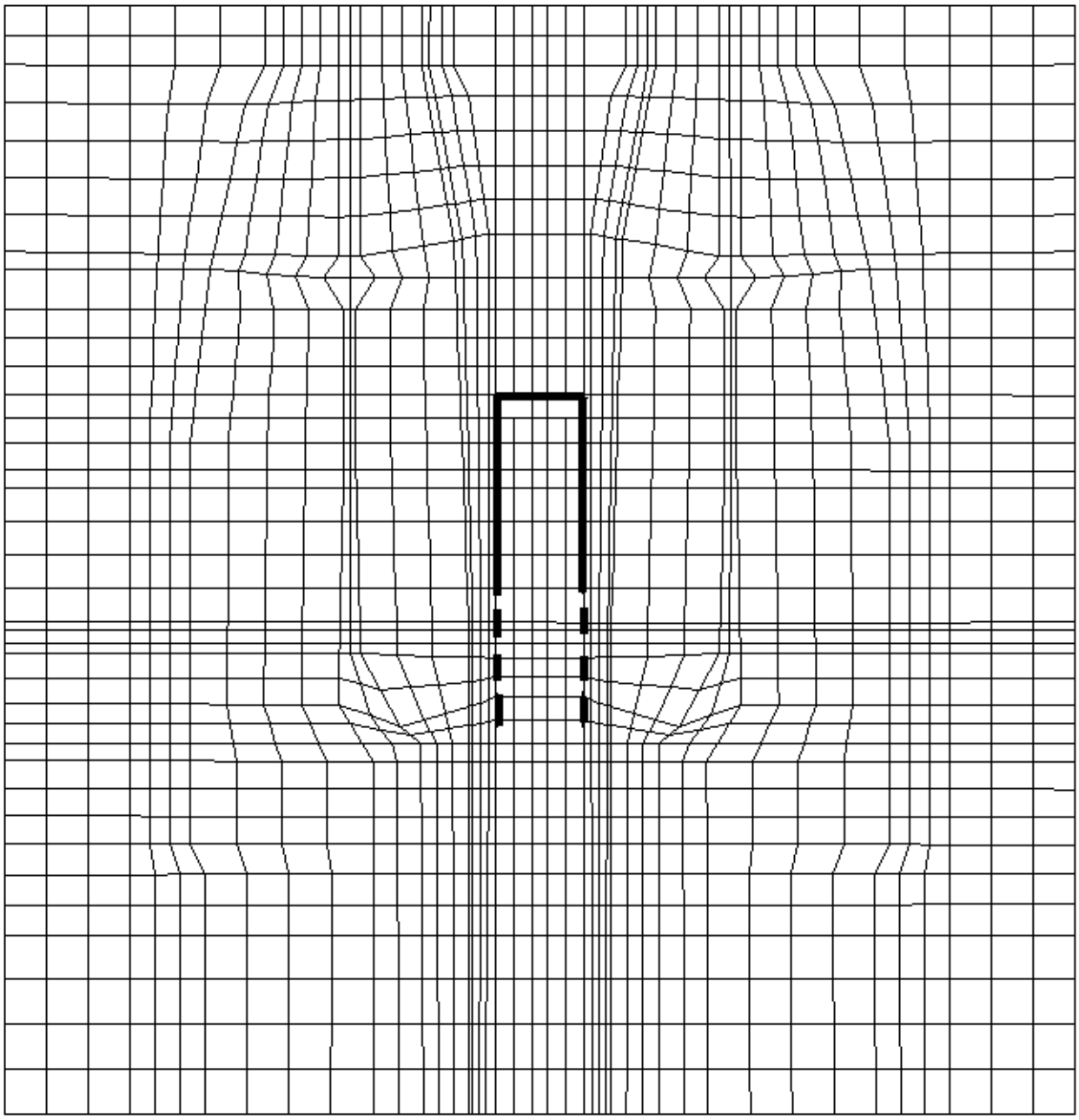

Figure 2-59
Stryker Creek Diagram of Cut Central Baffle Modification

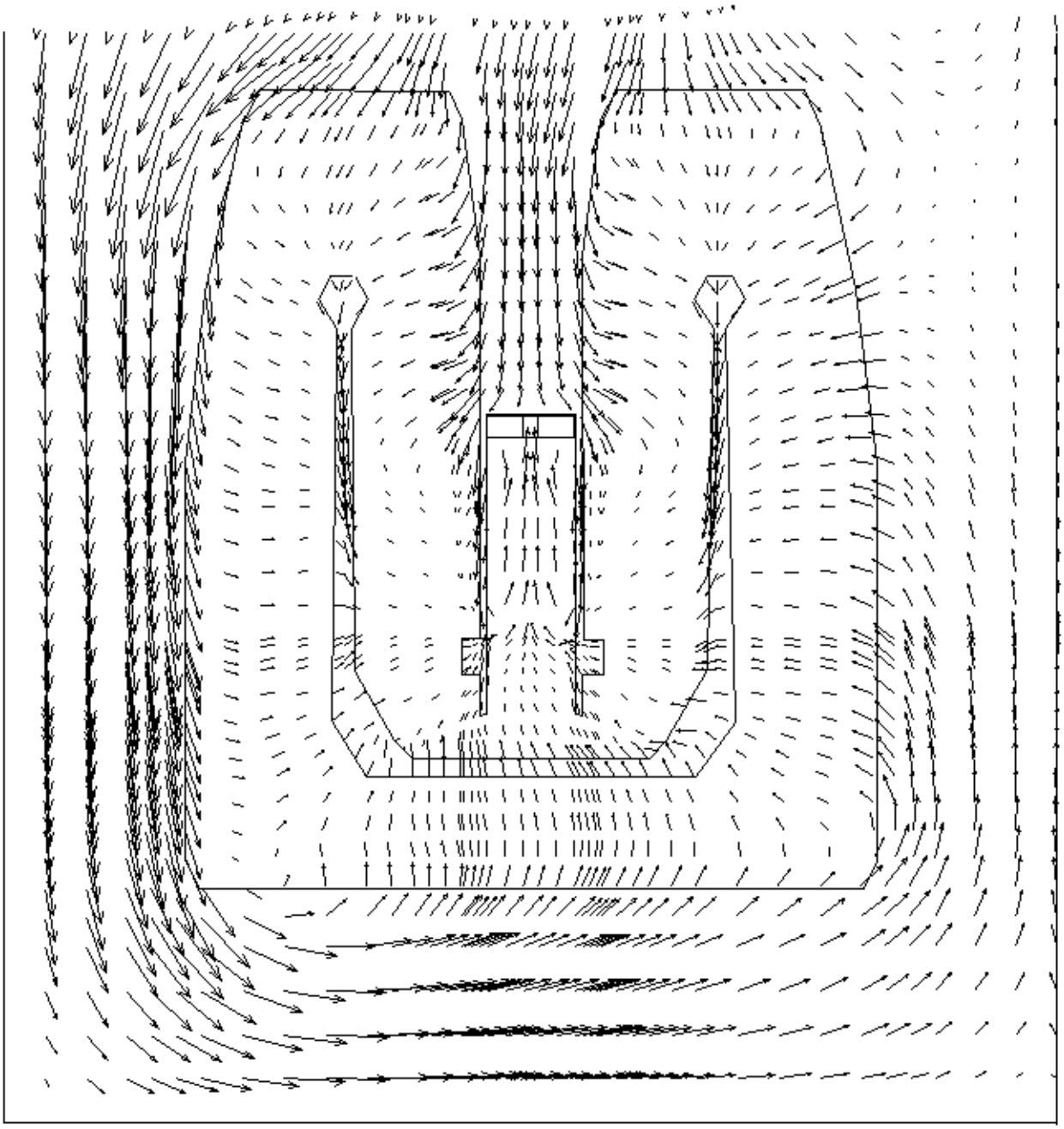

Figure 2-60
Stryker Creek Velocity Vectors for Cut Central Baffles

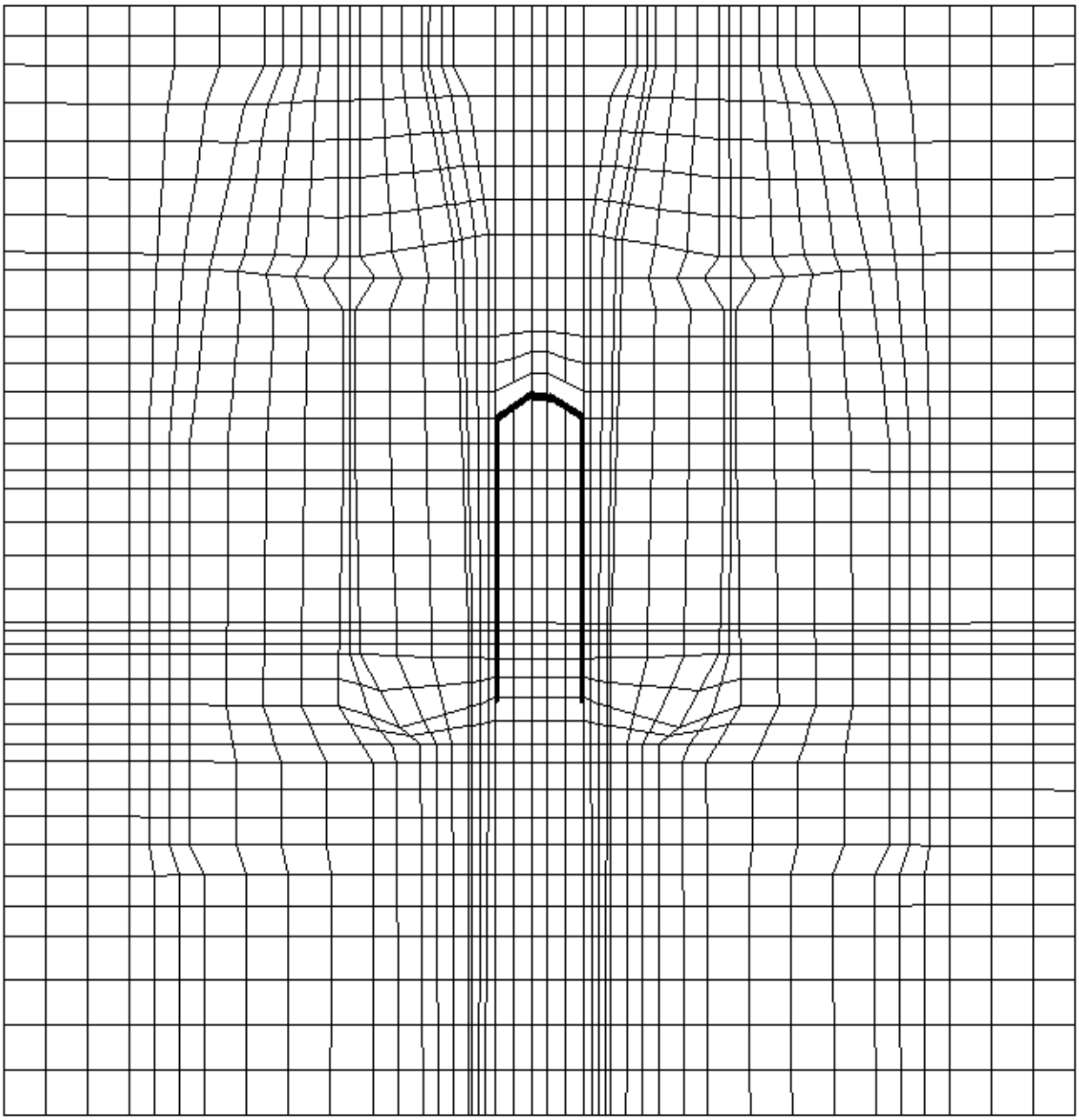

Figure 2-61
Stryker Creek Diagram of V-Shaped Central Baffle Modification

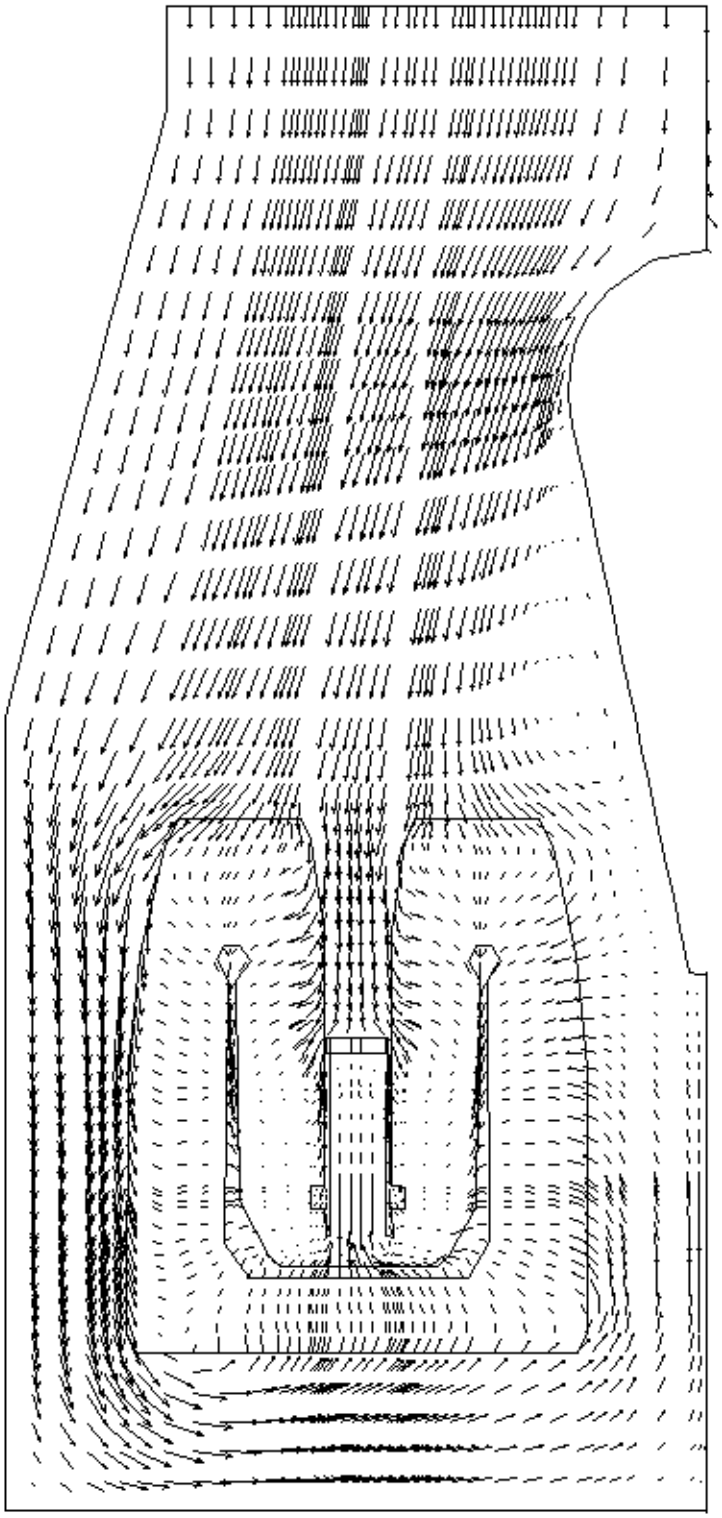

Figure 2-62
Stryker Creek Velocity Vectors with Heater Fairing

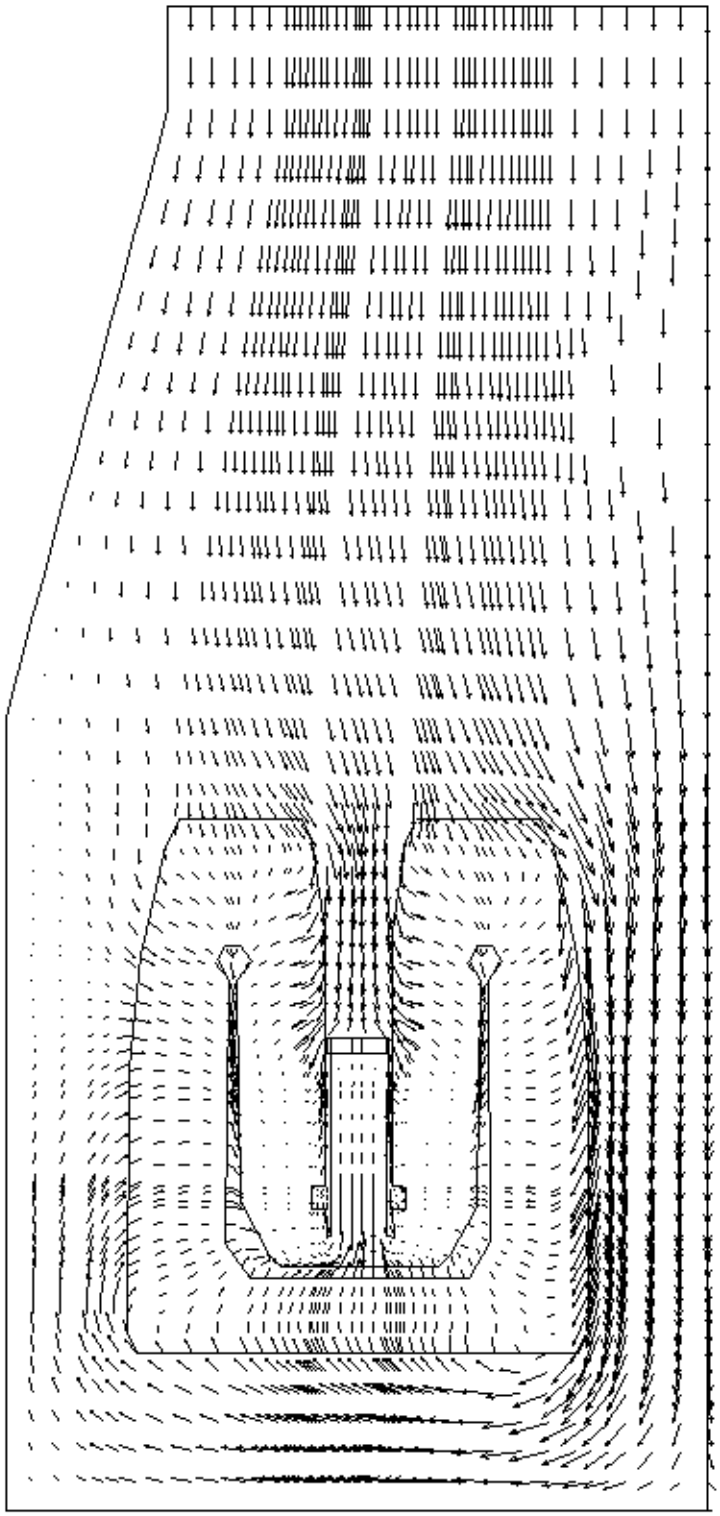

Figure 2-63
Stryker Creek Velocity Vectors without Heater Shell

3

MODIFICATION CASE EVALUATIONS

Monticello Unit 1

The simulations performed for the Monticello base case (summer conditions) revealed air bubbles forming to the left and right of the U-shaped hood and at the top of the center section of tubes near the air-offtake point. The total pressure drop across the bundle was predicted to be 30 mbar (0.9 in Hg), assuming an air-offtake pressure of 80 mbar (2.36 in Hg). Part of this drop will be due to tube bundle friction and part due to the condensation of the steam on the relatively cold surface of the tubes. In order to try and reduce the condenser pressure, a number of extra simulations were performed with parts of the tube bundle removed.

Modifications Evaluated

Tube Lanes Created on Left Side of Bundle

A number of tube lanes were modeled in the left side of the bundle by removing tubes from the model. Note that the heat transfer due to the tubes was retained and only the frictional pressure drop terms, due to the presence of the tubes, were removed.

The predicted improvement is tabulated below:

Normal Predicted Condenser Pressure	Predicted Condenser Pressure for Modification
120.04 mbar (3.54 in Hg)	119.86 mbar (3.54 in Hg)

The above table shows that hardly any improvement was obtained.

Tube Laning on Top of Bundle

Next, a number of tube lanes on the top of the bundle were created, about 20 rows deep. The effect is summarized below:

Normal Predicted Condenser Pressure	Predicted Condenser Pressure for Modification
120.04 mbar (3.54 in Hg)	118.22 mbar (3.49 in Hg)

The predicted improvement is about 1.8 mbar (0.05 in Hg). However, the removal of so many tubes would result in a large cut in the surface area available for condensation, thus having an adverse affect on the performance of the condenser.

Discussion of Results

It has been concluded that the Monticello condenser is operating well, and without having greater access to the condenser to add, remove or change other geometrical features (such as the baffles), it would be hard to improve performance. A check on the cooling water flow rate and operation of the pumps would ensure that the condenser reaches the best level of performance.

Martin Lake Unit 2

For the Martin Lake condenser, a good correspondence between the 2-D and 3-D simulations was obtained. The results indicated fairly large air bubbles appearing in the left and right-hand side bundles. A pressure drop across the bundle of about 12.6 mbar (0.37 in Hg) was implied by the results. Tests were performed using the 3-D and 2-D models to try and improve the pressure drop.

Modifications Evaluated

Air-Offtake Pipe moved away from Center of Condenser

A simulation was made with the air-offtake pipe moved from between the two tube bundles to underneath the feedwater heater shell. No significant difference in condenser pressure was predicted, indicating that the position of the feedwater heater shell has negligible effect.

Steam Lanes on Top of Bundles

Some studies were then performed to look at the effect of removing the frictional pressure drop due to the top rows of tubes in each bundle. About 15 rows of tubes were removed from the top of the left and right-hand bundles. The result was an increase in condenser pressure of about 1.5 mbar (0.04 in Hg). The removal of the tubes resulted in a steeper pressure gradient occurring over the remaining rows of tubes in the top areas of each bundle, with more of a pressure gradient occurring in the central sections of tubes towards the air-offtake. The central sections of each bundle do more work in steam condensation, compared with the normal flow case. The steam enters the gap above the central sections of tubes at a higher velocity, since it has not been retarded by as many rows of tubes and subsequently reaches the air-offtake at a higher velocity.

Discussion of Results

It is doubtful as to whether the creation of steam lanes in the bundles will lead to an improvement in performance since steam will find a quicker route to the gap around the central sections of tubes, i.e. an easier path directly to the air-offtake. In addition, any slight improvements in condenser pressure would be offset in part by the reduction in surface area available for condensation. It would be possible to examine the effect of adding extra baffling or removing baffles in the condenser, but for this study it would not be practical since there are no current plans for a re-tube of the condenser.

Stryker Creek Unit 2

Similar to Monticello, the base case simulations showed the presence of air bubbles forming on either side of the central baffles, although the Stryker Creek bubbles were smaller. There was a good correspondence between the 2-D and 3-D simulations, with very little difference in predicted condenser pressure. The results indicated a total pressure drop across the bundle of around 0.95 in Hg (32 mbar). A number of simulations were made to try and reduce the condenser pressure.

Modifications Evaluated

Central Vertical Baffles Cut by Half

First, it was thought that the condenser pressure could be reduced by cutting off the lower half of the central vertical baffles. This would allow steam to better penetrate into the air-bubble regions on the left and right side of the vertical baffles, consequently

reducing the pressure drop through the bundle. A simulation was performed with the lower half of the baffles removed. Figure 2-59 illustrates the modification.

A 1.4 mbar (0.04 in Hg) improvement was predicted, along with the removal of the air bubbles. The results are summarized below:

Normal Predicted Condenser Pressure	Predicted Condenser Pressure for Modification
107.6 mbar (3.18 in Hg)	106.2 mbar (3.14 in Hg)

The air-offtake pressure was 80 mbar (2.36 in Hg). However, the outlet steam concentration predicted for both simulations was very high (over 0.9), indicating that cutting the baffles leads to greater steam leakage to the air-offtake point. The improvement of 1 to 2 mbar (0.03 to 0.06 in Hg) that would be gained by cutting the baffles could be lost by the increased steam leakage. A high steam concentration cannot be tolerated by the extraction systems, and the steam pressure would rise until the offtake concentration was approximately 70%.

Velocity vectors at a cross-sectional plane in the center of the condenser are shown in Figure 2-60. In the air-offtake section, air bubbles form to the right and left of the central baffles. These bubbles get progressively smaller and vanish a small distance from the air-offtake in the region where the baffles have been cut.

Removal of all Baffles after 1st and 3rd Support plates

Another 3-D simulation was carried out with all the baffling removed after the 3rd support plate from the CW inlet end, allowing steam to enter directly into the central section of the bundle as well as both sides. The predicted improvement was about 1.2 mbar (0.04 in Hg), very similar to the previous 3-D simulation. The air-offtake concentration was also much lower (below 0.7), suggesting that this would be a feasible modification.

Finally, a 3-D simulation was undertaken for all the baffling removed after the air-offtake section (1st support plate) of the condenser. The improvement predicted was marginally greater than for all the baffling removed after the 3rd support plate.

Alteration to Top of Central Baffle

The top part of the central hood was then altered to an upside-down V-shape, rather than a flat top. A diagram of the modification is shown on Figure 2-61. A simulation indicated that there would be a slight increase in condenser pressure. It is therefore reasonable to expect that no improvement would be attainable by carrying out this modification.

Discussion of Results

An improvement in condenser performance would be gained by taking out all the baffling after the first support plate from the CW inlet end and sealing the hole at the top of the support plate. An improvement of up to about 1.5mbar (0.04 in Hg) was predicted by the model. Cutting off the lower half of the central vertical baffles from the first support plate down to the outlet end of the condenser could result in a larger drop in condenser pressure, but this would be offset by the increased by-passing of the steam directly to the air-offtake.

4

FEEDWATER HEATER FAIRING MODELING

Theoretical Calculation of Pressure Drop Across Feedwater Heater Shell

The feedwater heater shell acts as a flow obstruction in the exhaust neck of each condenser, impeding the movement of the flow down towards the tube bundles. Therefore, there is a pressure drop associated with the flow of steam around the heater shell. The theoretical pressure drop can be calculated by using the properties of the steam, together with the determination of the Reynolds Number (hence the drag coefficient), and the dimensions of the heater shell.

For very high Reynolds number flow around the heater shell, the flow is essentially turbulent in nature, with a turbulent wake appearing at the rear of the heater shell. The turbulent wake appears for Reynolds numbers above about 5 E+05. A determination of a typical value of Reynolds number for the condensers shows that the flow is undoubtedly turbulent in nature. The drag coefficient for flow around cylinders has been obtained by experiment, and for Reynolds numbers in the order of 1 E+06, C_D is approximately 0.7.

The drag force per unit length around a cylinder can be expressed as:

$$F_d = C_D \frac{\rho u^2 D}{2g} \qquad \text{(eq. 4-1)}$$

where u is the approach velocity, D is the diameter of the cylinder, ρ is the density of the fluid, and g is the acceleration due to gravity.

For the Monticello, Martin Lake, and Stryker Creek condensers, the theoretical pressure drop of the steam across the feedwater heater shell is in the order of 100 - 150 Pa (approximately 0.04 in Hg). Note that this calculation does not take into account the change in width of the exhaust opening.

Numerical Calculation of Pressure Drop

A number of 2-D simulations were performed to predict the pressure drop across the feedwater heater shell in the Martin Lake condenser. Tests were performed for the flow of steam over a cylinder having an identical radius to the feedwater heater shell in the absence of the tube nests.

The numerical result for the simulation is tabulated below:

Simulation	Pressure Drop
Condenser model	138.5 Pa (0.041 in Hg)

The simulation was carried out using the Martin Lake summer conditions, and the result was very similar to the estimate based on experimental data for flow around a cylinder.

Flow Prediction for Feedwater Heater Fairing

A 2-D simulation was undertaken for the Stryker Creek condenser, using the summer conditions. A fairing was attached to the feedwater heater shell, with the tip of the fairing one and a half heater shell diameters from the bottom of the heater shell.

The predicted improvement is shown in the following table:

Normal Predicted Condenser Pressure	Predicted Condenser Pressure for Modification
108.1mbar (3.19 in Hg)	107.8 mbar (3.18 in Hg)

A difference of only 0.25 mbar (0.01 in Hg) was predicted, therefore suggesting that no real improvement would be gained from this modification. A diagram of the velocity vectors is shown in Figure 2-62.

A small area of recirculation forms on the edge of the fairing. Another simulation carried out with the feedwater heater shell completely removed gave virtually the same

result. Although the flow pattern was different, the pressure drop was almost identical. A diagram of the velocity vectors for this case is shown in Figure 2-63.

5

CONCLUSIONS AND RECOMMENDATIONS

Monticello Unit 1

The Monticello tube bundle is fairly dense, with about 30 tube rows between the edge of the bundle and the central section of tubes. The performance is thus adversely affected by the frictional pressure drop across the tube bundle. Air bubbles form on both sides of the central section of the bundle. The bubbles will be difficult to remove without the ability to cut/remove or add baffling to the bundle. The removal of a large number of tubes from the top of the bundle has shown that it would be difficult to obtain any improvement by laning. A lot of tubes would need to be removed to make a considerable difference to the condenser pressure and increase the entrance of steam into the regions of air-blanketing, and any improvements that could be made would be offset by the reduction in surface area of the tubes. Thus, no changes are recommended to the condenser configuration.

Since the Monticello pressure drop across the bundle is the largest among all three condensers, it would be worthwhile checking the operation of the air-extraction equipment since the relatively high pressure drop requires an effective vacuum pump capability. The cooling water flow rate should also be confirmed as being at the highest achievable level.

Martin Lake Unit 2

This condenser tube bundle has not been designed quite as well as Monticello and Stryker Creek. The "church window" design has shown that it is difficult to ensure equal pressure drop paths from the exterior of the tube bundles to the air-offtake, especially in the central region of the condenser between the tube bundles. The pressure drop across the bundle is much lower than the Monticello bundle. Air bubbles form in both bundles with larger bubbles forming in the right-hand bundle.

It has been shown that repositioning the air-offtake pipe makes little difference to the predicted condenser pressure; in fact, the condenser pressure is slightly increased. There is a possibility of adding steam lanes, but the drawback is enabling steam to "break-through" into the air-offtake section. As a result, removing some of the tube-rows showed that the condenser pressure increased rather than decreased.

Without a re-tube, it would be difficult to obtain much improvement to the condenser pressure. A re-tube would allow other options to be considered, such as removing the small baffles above the central sections of the bundles, or shortening the side baffles. Therefore, no changes are recommended at this time.

Stryker Creek Unit 2

The Stryker Creek simulations also revealed the presence of air-bubbles on the right and left sides of the central cooler section. Since the Stryker Creek condenser will be undergoing a re-tube in the Spring of 1998, it was feasible to look at a number of possible modifications to try and improve the condenser performance.

Based on the CFD model results, no improvement in condenser pressure would be expected for installing a fairing underneath the feedwater heater shell. Additional runs made without the presence of the heater shell itself also showed very little variation in predicted condenser pressure.

Similarly, no improvement in condenser pressure was predicted by changing the top of the air offtake section to an upside-down V-shape rather than a flat top. The condenser pressure was actually slightly increased.

The CFD model does show that an improvement would be gained by taking out all the baffling after the first support plate from the CW inlet end and sealing the hole at the top of the support plate. An improvement of up to about 1.5mbar (0.04 in Hg) was predicted by the model. Cutting off the lower half of the central vertical baffles from the first support plate down to the outlet end of the condenser could result in a larger drop in condenser pressure, but this would be offset by the increased by-passing of the steam directly to the air-offtake.

The estimated cost to remove the baffling after the first support plate from the CW inlet end is estimated to be $2,500 if the modification is done while re-tubing the condenser. Utilizing the TU Electric heat balances (see Reference 5), a 50% capacity factor, and a value of $26 per megawatt, the yearly payback is approximately $228,000 for implementation of the modification.

6

REFERENCES

1. Al-Sanea S, Rhodes N, Tatchell T G and Wilkinson T S, "A Computer Model for Detailed Calculation of the Flow in Power Station Condensers", IMechE Symposium Series no. 75, pp 70-88 (1983).

2. Al-Sanea S, Rhodes N, and Wilkinson T S, "Mathematical Modelling of Two-Phase Condenser Flows". 2nd International Conference on Multi-Phase Flow, London (1985).

3. Chisholm, D, "Modern Developments in Marine Condensers: Non-condensable Gases: An Overview", Power Condenser Heat Transfer Technology, edited by Marto and Nunn, pub. by McGraw-Hill (1980).

4. Test run data used for the simulations (note that the summer case runs have been reported in this report):

Monticello Unit 1:	Summer Case: Test Run 2 data obtained on 06/04/91. Winter Case: Test Run 4 data obtained on 11/20/96. Design Case: Data given on design sheet.
Martin Lake Unit 2:	Summer Case: Test Data obtained on 09/25/97. Design Case: Data given on design sheet.
Stryker Creek Unit 2:	Summer Case: Test Run 13 data obtained on 05/14/97. Winter Case: Test Run 6 data obtained on 02/26/93. Design Case: Data given on design sheet.

5. Heat balances from TU Electric on 12/02/97.